The Use of Bipolar Electrochemistry in Nanoscience: Contact Free Methods for the Site Selective Modification of Nanostructured Carbon Materials

A Thesis

Submitted to the Faculty

of

Drexel University

by

Patrick Gathura Ndungu

in partial fulfillment of the

requirements for the degree

of

Doctor of Philosophy

March 2004

Dedications

I would not have managed to get as far as I did as a stranger in a strange land if not for my father, my family, and my friends. This thesis marks the end of my formal education and the beginning of a new journey in my life. This thesis is for my dad, my mom, my two brothers, my two sisters, the newest member of the family (my daughter Arielle), and all my friends who have enriched my life.

Acknowledgements

I would like to thank Dr Bradley for his patience, guidance and support through the years. Through him I have learnt the meaning of long days and longer nights, and the true meaning of innovation, hard work, and determination in research. Working in his research group I have realized my innate potential, and I have grown and developed from a naïve student to a man of science.

My thanks go to the Chemistry department at Drexel University for the financial support, to the professors who taught me chemistry is more than a bunch of chemicals; your efforts are much appreciated, and to the various people who helped me with various day to day details, Virginia, Edith, Ed, Tony, Bill, much thanks.

To Dr Wei, Dr Sohlberg, Dr Addison, Dr Gogotsi, Dr Johnson, and Dr Foley, the members of my committee I thank them for their patience and input.

A variety of individuals have contributed to my graduate school experience and I would like to thank them for their help, this list includes; that Indian character sometimes funky but always on point, Dr Babu. Fellow graduate students Hung, they call him "Mr Lee", we are still peons (Fifth floor forever!)! Houping I will be on time one day! Stephanie, Natalie, Melissa, Zhangfe, "Jim 2", Erb/Will/Bill, Alpa, Tyson, Pia, and Poonam, fellow graduate students in the struggle I still feel the shaft! Former graduate students: The Dr aka Jim Murray, Dr Jun Tian, Dr/Sister Rose, Dr Pascoe, Dr Prushan and Alex Falat I still remember all of you. To anyone I forgot to mention I am sorry and I owe you a drink!

Isabel I thank you. You have been an interesting experience and journey.

Finally but never the least, my friends, my peoples, those who have been there since day one, those who were always ready with a cold one at the end of the week (I still remember “La Hacienda”); Deućh (See you are listed first), JB, drago’n, E-hustle, Sarah (you are one of the boys), Curto, Kev-dawg, Eddy/Fisi, Steve, Sam, Murigi, Chico, and Ramon.

Table of Contents

List of Tables

List of Figures

Abstract

The Use of Bipolar Electrochemistry in Nanoscience: Contact Free Methods for the Site Selective Modification of Nanostructured Carbon Materials

Patrick Gathura Ndungu

Bipolar electrochemistry occurs when an isolated conductive substrate inside an electric field supports both oxidation and reduction reactions. The method requires no direct contact between the power supply and the substrate. In the following thesis bipolar electrochemistry has been used to deposit palladium onto isolated graphite platelets, carbon nanofibers (CNF), and carbon nanotubes (CNT), as well as, various metals, a semiconductor, and an electropolymer on CNTs.

Initial work used pulsed DC electric fields to deposit palladium onto isolated graphite platelets. Transmission electron microscopy (TEM) studies on the platelets found palladium metal on one area, indicative of a bipolar mechanism, and palladium deposits that varied from surface bound to highly ramified deposits. No correlation was found between the frequency used to prepare the deposits and the palladium metal dispersion.

The same field intensities and frequencies used on the graphite platelets were used to produce CNFs with palladium on one tip. The amount of palladium deposited on one tip of a CNF was controlled by adjusting how long the electric field was applied. Preliminary experiments to produce bulk quantities of CNFs with palladium bipolar electrodeposits used CNFs ball milled with silica, and CNFs suspended in tetrahydrofuran or methylene chloride. The palladium content, measured by atomic absorption spectroscopy, of the functionalized CNFs in silica showed no difference with increased CNF loading; however, TEM studies found a small number of functionalized CNFs with palladium on one tip. Work on CNFs suspended in THF and methylene

chloride used suspensions with high loadings of CNFs which led to small percentages of CNFs with bipolar electrodeposited palladium.

Finally CNTs obtained commercially and CNTs grown using chemical vapor deposition were successfully functionalized using bipolar electrodeposition. These experiments demonstrate a reliable and controlled method to modify nanostructured materials.

Chapter 1: Bipolar Electrochemistry

1.1 Summary Statement

A definition of bipolar electrochemistry as it relates to this thesis is outlined. The chapter presents examples describing bipolar electrochemistry in various applications. Finally the chapter ends with a synopsis on early work on bipolar electrochemistry in the Bradley research group.

Early work on bipolar electrochemistry uses substrates on the millimeter scale, and with the exception of one example, there are no examples of bipolar electrochemistry on the nanoscale or micrometer scale. It is the goal of this chapter to highlight the key literature on bipolar electrochemistry, and how this significantly differs from the unique application of bipolar electrochemistry in the Bradley research group.

1.2 Introduction to Bipolar Electrochemistry

Simply stated, bipolar electrochemistry occurs when an applied electrical field induces a cathode-anode pair on an isolated substrate.[1,2,3] The substrate can be any kind of material with sufficient conductivity, and in the literature these vary from various forms of carbon, metals, semiconductors or coated insulators. In this aspect, bipolar electrochemistry does not differ from conventional electrochemistry i.e. the substrate can be any shape or size but must be conductive; however, a significant difference is the substrate must have a higher conductivity than the surrounding medium. A fundamental difference between bipolar electrochemistry and conventional electrochemistry is that no physical connection is made between the substrate and the power source. Instead an electrical field applied

between two feeder electrodes provides the potential required to induce electrochemical reactions on the substrate. Literature descriptions of the various configurations that give rise to bipolar electrochemistry can be categorized into one of two arbitrary designations; these are, open bipolar electrochemistry and closed bipolar electrochemistry. Figure 1.1 illustrates the difference between the two designations. Open bipolar electrochemistry (Figure 1.1A) occurs on an electrically and physically isolated substrate that is completely immersed in a suitable electrolyte. In closed bipolar electrochemistry (Figure 1.1B) the substrate forms a barrier between the electrodes and separates the electrolyte into separate areas. The end result is the electrolyte acts as an electrolytic wire between the electrodes and the substrate. In closed bipolar electrochemistry the potential across the substrate is equal to the potential applied across the feeder electrodes, and electrochemistry will occur on the isolated substrate at relatively low field intensities[4]. In contrast in open bipolar electrochemistry the applied electrical field must reach a minimum value, which is relatively large, before the onset of bipolar electrochemistry on the isolated substrate. The minimum value in open bipolar electrochemistry depends upon the size of the substrate.[5,6,7,8] Thus in the open system there is a size dependant relationship between the applied field and the onset of bipolar electrochemistry, whereas in the closed system there is no size dependence.

Bipolar electrochemistry, like conventional electrochemistry, requires a solution that can support the separate oxidation and reduction reactions i.e. an electrolyte. The electrolyte composition affects the electrolyte's conductivity and the electrochemistry on the isolated substrate.

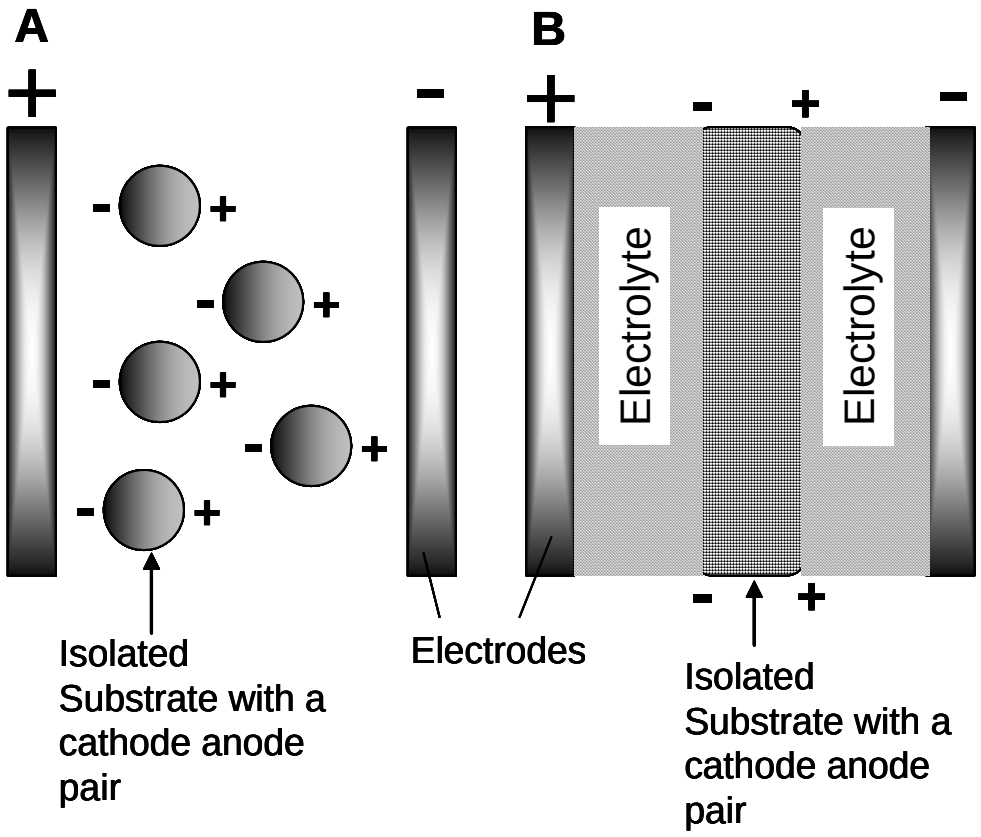

Figure 1.1. The various configurations described in the literature that give rise to bipolar electrochemistry can be categorized as open bipolar electrochemistry or closed bipolar electrochemistry. In Figure 1.1A the cathode anode pair is induced on isolated conductive particles that have been subjected to an electrical field from the two electrodes. This is an example of open bipolar electrochemistry, and the potential across the particles can be estimated using equation (1). Figure 1.1B is an example of closed bipolar electrochemistry. The cathode-anode pair is induced across an isolated substrate; however, the electrolyte is acting as an electrolytic wire connecting the electrodes to the substrate. In closed bipolar electrochemistry the potential difference across the substrate is essentially the same as the applied potential between the electrodes.

A concentrated electrolyte, one that has a large amount of free mobile ions, is too conductive to support the electric fields with the required magnitude to induce bipolar electrochemistry. A dilute electrolyte, one that has a low number of free or mobile ions, is a relatively poor conductor and can support the electric fields needed for bipolar electrochemistry. At these low concentrations the conductivity of the substrate is much higher than the solution. This difference in conductivity provides a driving force for the movement of current through the isolated substrates, and at sufficiently large enough potentials, electrochemistry occurs on the isolated substrates.[2,8]

The potential across an isolated spherical substrate (V) is related to the applied electrical field (E) and the radius (r) shown in equation (1)[1,9]

$$(1) \cdot E = V / 2r$$

This equation has been confirmed empirically.[6] This simple relationship between the applied electric field and the potential across the substrate illustrates the need for large electric fields on spherical substrates with small radii. For example a particle with a radius of 500nm needs an applied electrical field at 10kV/cm to produce a 1.0V potential difference across the particle. With a particle with a radius of 50nm the applied electrical field needs to be at least 100kV/cm.

1.3 Examples of Open Bipolar Electrochemistry

In order to observe open bipolar electrochemistry, any kind of isolated substrate that can support redox chemistry has to be in immersed in a suitable electrolyte and an electric field with the required magnitude must be applied. The isolated substrate need not be a metal and can take on any shape and size.

1.3.a Packed Bed Electrodes

Packed bed electrodes are early examples on the observations and applications of bipolar electrochemistry. Packed bed electrodes consist of two feeder electrodes and a large number of particles placed between the two electrodes, as illustrated in Figure 1.2. The particles are either all conductive or a mixture of conductive and non-conductive particles. The particles can either be a metal, a semi-conductor or some form of carbon. The orientation of the system can be horizontal or vertical. An electrolyte is usually flowed through the system, and the flow rate is optimized for the application. Applications of packed bed electrodes include electro-organic synthesis of propylene oxide[10,11], methoxylation of furan[12], methoxylation of p-terbutyltoluene,[13] trace metal recovery,[14] and potential use in phenol degradation[15]. One of the advantages of a packed bed electrode is its high surface area. In the packed bed electrode, the total surface area of the system includes the cathode feeder electrode, and the individual particles making up the packed bed. The larger surface area contributes to the electrodes large space time yields in electro-organic synthesis.[10-13] In metal recovery the large surface area makes it possible to remove trace metal impurities from solutions without the need to pre-concentrate the solution.[14] The ease of operation of the system is another advantage that is often cited in regards to the benefits of the packed bed electrode. Packed bed electrodes only need two electrodes connected to a power supply in order to function. In conventional monopolar systems multiple electrodes and connections are often needed.[16,17]

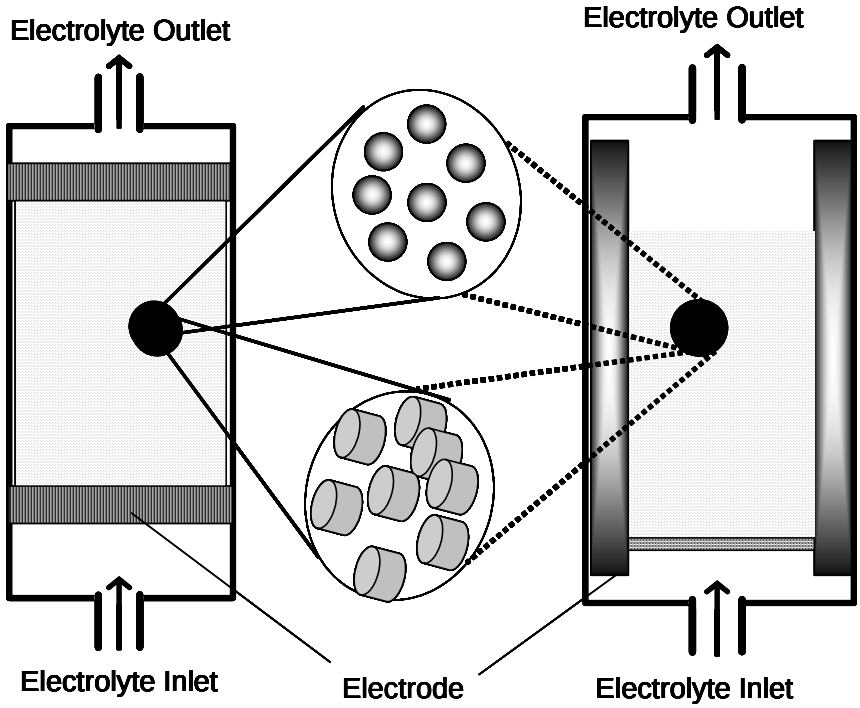

Figure 1.2. This is a simple illustration showing two possible configurations for a bipolar packed bed electrode. The electrodes can be arranged in a vertical or horizontal orientation. The particles in the bed can be either spherical or cylindrical. In the case of cylindrical particles the particles can be orientated in regular arrays (vertically or horizontally) or randomly. The particles in the packed bed can be separated from the feeder electrodes by non-conductive particles (e.g. glass beads) or inert spacers (e.g. plastic mesh). The particles can either be separated by non-conductive spacers, or the speed of the electrolyte can be used to keep the particles in intermittent contact.

Besides isolated particles rods have been used as bipolar electrodes for the electrolysis of sodium bromide. This example used rods as bipolar electrodes and was done as a model to study fluidized bed electrodes.[18]A significant amount of the theoretical work on bipolar electrochemistry comes from modeling and testing various hypotheses on packed bed electrodes. In these studies it has been necessary to measure the faradaic current across the isolated structures. The easiest and most common methods are to deposit a metal, such as copper, onto the substrate then recover and by some quantitative means determine the amount of deposited metal.[19,20]

Besides using packed bed electrodes, theoretical modeling using spherical particles,[5,7] diaphragm electrodes,[21] and, more recently, aluminum plates in electrokinetic cells[22] have been used as basis models on bipolar electrochemistry.

1.3.b Spherical Ultramicroelectrodes

Spherical ultra microelectrodes include loose micrometer sized metal particles or metal nano-particles encapsulated in a zeolite matrix. The hydrogen redox system and the oxygen redox system were studied using a suspension of platinum particles (2.5 μm diameter). This initial study proved catalytic processes could be affected by the application of an external electric field, and the system could be investigated using ultra microelectrodes.[23]

The use of metals such as platinum in a zeolite cage demonstrated that electrolysis could be accomplished using metals inside zeolite cages. The metals supported in zeolites could either be on the surface of the zeolite or inside. Thus it is possible to get

two types of electrochemical systems i.e. bipolar on isolated particles in the matrix, and conventional monopolar when the particles on the surface contact the feeder electrodes.[24]

In both examples described above there is no electron microscopy evidence to validate the claims that bipolar electrochemistry occurred on such a small scale. In the Pons et al paper[23] the electric field used, and the size of the particles (up to 1600 V/cm, and 2.5 μm diameter) used correspond to results obtained in the Bradley research lab (Figure 1.4C – 1.4F). In the second example the metal nanoparticles (1 - 2 nm) embedded in a zeolite matrix were exposed to electric fields on the order of hundreds of volts per centimeter.[24] This value for the applied field is below the value calculated using equation (1), and without any suitable microscopy evidence (electron or atomic force microscopy) it is unlikely this is a conclusive example of bipolar electrochemistry on the nanoscale.

1.4 Examples of Closed Bipolar Electrochemistry

Although a distinction between closed and open bipolar electrochemistry is not made in the literature, it is a significant categorization for the purposes of this thesis. The closed system is much simpler than the open system, and as will be seen in the following description it is the more technologically significant system.

1.4.a Characterization of Semi-conductors Using a Bipolar Electrolytic Cell Configuration

An alternative method to characterize semi-conductor wafers involves the use of suitable electrolytes in contact with the wafer and two feeder electrodes. The wafer separates two compartments that can be filled with the same or different electrolytes.

This configuration uses the electrolytes as a Schottky type connection to the two faces of the wafer. As a result the application of a potential across the feeder electrodes induces the same potential drop across the wafer. In contrast to bipolar electrochemistry on isolated particles, the potential across the wafer does not depend on the size of the wafer.

By choosing suitable electrolytes it is possible to etch and deposit on the wafer using bipolar conditions i.e. application of an electric field between the two feeder electrodes. Mott-Schottky plots, photocurrent/ potential curves, the photo-spectrum, and the minority carrier diffusion length can be determined using the bipolar cell configuration.[25,26]

Photoelectrochemical cells in a bipolar configuration do support redox reactions on a single substrate. This is induced by light and not an external electrical field and, by the definition outlined in this thesis; it is not an example of bipolar electrochemistry.[27]

1.4.b Bipolar Plate Electrodes

Bipolar plate electrodes are conductive plates placed between two feeder electrodes with a suitable electrolyte. Bipolar plate electrodes have been used in electrolytic cells[16, 28], batteries[29] and fuel cells[30].

In electrolytic cells bipolar electrodes have been used for the electrolysis of aluminum, and magnesium in molten salts[16], zinc from zinc chloride melts[28], and the defluoridation of water.[31] The bipolar plates have been arranged in various configurations which include vertical, horizontal and slanted at an angle. The conditions in bipolar cells used for electrolysis follow similar patterns found in the pack bed electrodes. Some configurations of the bipolar cells in electrolysis do suffer from by-pass or current leakage phenomena i.e. application of a small potential between the two feeder

electrodes does not induce bipolar electrochemistry on the bipolar plates.[5] In this regard this system does follow the bipolar electrochemical phenomena seen in open bipolar electrochemistry, unlike the previous example that describes the characterization of semi-conductor wafers.

Although the oxidation and reduction processes occur on the opposite sides of a single substrate in a fuel cell[30] and some types of batteries[29], the bipolar plates are not under the influence of an externally applied electrical field. This does not fit the definition of bipolar electrochemistry used in this thesis.

1.4.c Bipolar Membranes

Two compartments with electrolyte solutions are separated by a conductive membrane. The membrane can be a porous metal[32] or a polymer.[4] Application of the potential between the two feeder electrodes produces a similar potential drop across the membrane. This set-up is similar to that seen with the characterization of semi-conductor wafers i.e. the electrolyte is a 'wire' that connects the membrane directly to the feeder electrodes. This example of bipolar electrochemistry differs from the type presented in this thesis because the potential across the substrate does not differ with the length or radius of the substrate. Figure 1.1B gives an illustration of the simplest configuration for bipolar membranes. The application of the potential across a bipolar membrane has been used to recover acids and bases from salt solutions[33], adjusting the pH of various fluids, separation of soy proteins and water electrolysis.[34]

1.5 Bradley Research Group's Early Work with Bipolar Electrochemistry

The Bradley research group adapted the concepts of bipolar electrochemistry to develop a contact free method known as Spatially Coupled Bipolar Electrochemistry (SCBE) that connects isolated metal substrates. In SCBE an applied electrical field induces redox reactions on isolated metal substrates. The oxidation reaction provides metal ions in the system which are preferentially driven towards the nearest metal substrate by the distorted electrical field and various (electro-, and gravitic-) convective forces. When the concentration of the ions reaches a sufficient value, electrodeposition occurs on the opposing isolated metal substrate (Figure 1.3). The first published work involved using two isolated copper beads measuring approximately 900 μm in diameter. The copper beads were placed in an aqueous solution containing sulfuric acid and a surfactant (Figure 1.4). Application of an electrical field (any value between 15-75V/cm) across the isolated copper beads resulted in the growth of copper dendrites between two isolated copper beads. Growth of the dendrites continued until it contacted the opposing copper bead. Dendrite growth was initiated by the reduction of copper ions that had been generated by the electrodissolution of copper. Under the applied electrical field, copper ions were produced by the oxidation of copper on one face of the copper bead. The concentration of copper ions between the two beads continued to increase until sufficient for the electrodeposition of copper on the opposite bead. The distortion of the electrical field between the two beads and the electroconvective forces helped to ensure the dendrite growth followed the shortest path between both beads. This initial work demonstrated it was possible to contact isolated micrometer-size structures using electrical fields and no additional metal salt.[35]

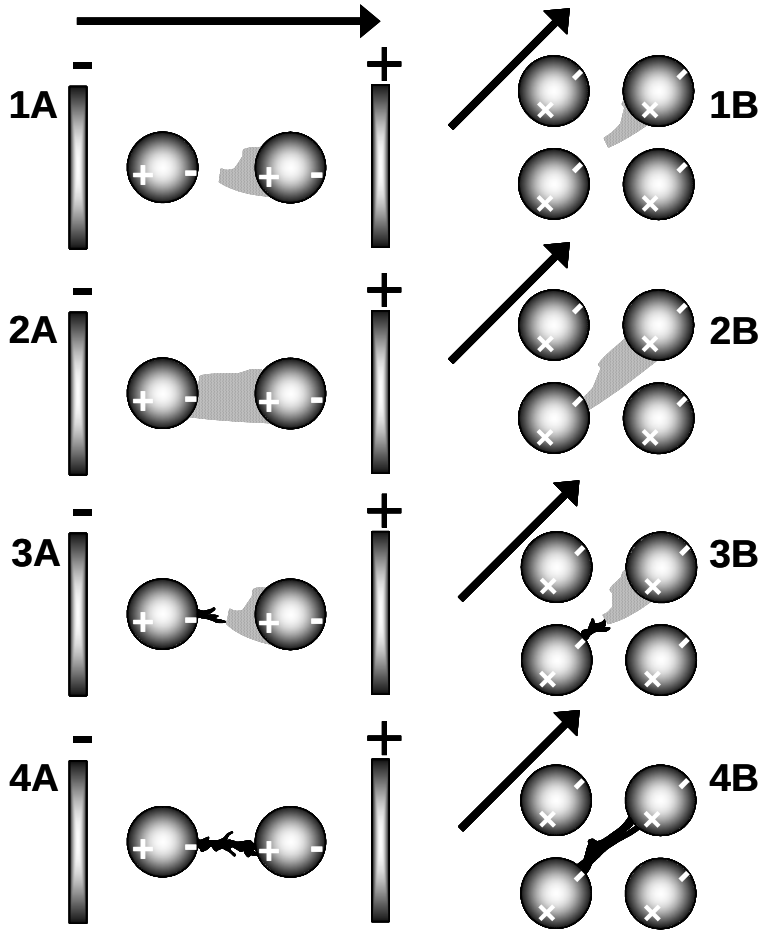

Figure 1.3. 1A: Two copper particles are placed in a suitable electrolyte with no supporting metal salt. Application of an electrical field (of sufficient magnitude) induces oxidation on one particle. The release of copper ions by oxidation is represented by the shaded region.

2A: When the copper ion concentration near the opposite particles reaches a sufficient value electrodeposition occurs, and a wire grows towards the opposing particle.

3A: Electrodeposition will preferentially occur on the tip where the cathodic polarization is expected to be the highest.

4A: When the wire contacts the opposite particle an electrical contact is made, and the potential difference between both particles drops to zero. Electrochemical processes in the region between the particles stops and no further growth is seen.

2A - 2B illustrate how the same process can be used to selectively grow a wire between particles in an array.

The method was refined, and connections between isolated copper structures and a light emitting diode were established. In order to light up the diode the electrical conductivity of the copper dendrites was enhanced by the electroless plating of copper onto the dendrites.[36] When a toluene/acetonitrile (60/40) solution was used, the deposits were thick and highly ramified, multiple deposits could be grown between two isolated copper structures, higher fields could be used, and arrays of copper structures could be connected in multiple directions (Figure 1.5). The plating time had been reduced from a typical 48 hours, when the dendrites were grown in aqueous solutions, to 2 hours when ramified deposits were grown in organic solvents.[37]

Besides growing wires between copper substrates, the copper wires were grown between n-type silicon squares (1.0 x 1.0 millimeter) and copper rings. The resulting Schottky junctions displayed rectifying behavior.[38]

Besides growing metallic wires between copper beads, there were successful attempts to grow polymer wire connections between isolated gold particles. The polymer chosen was polypyrrole, and the sizes of the gold particles were on the order of a few millimeters. The polymer wires were ramified; however, the electrical properties of the resulting polymer wires were not elucidated.[39]

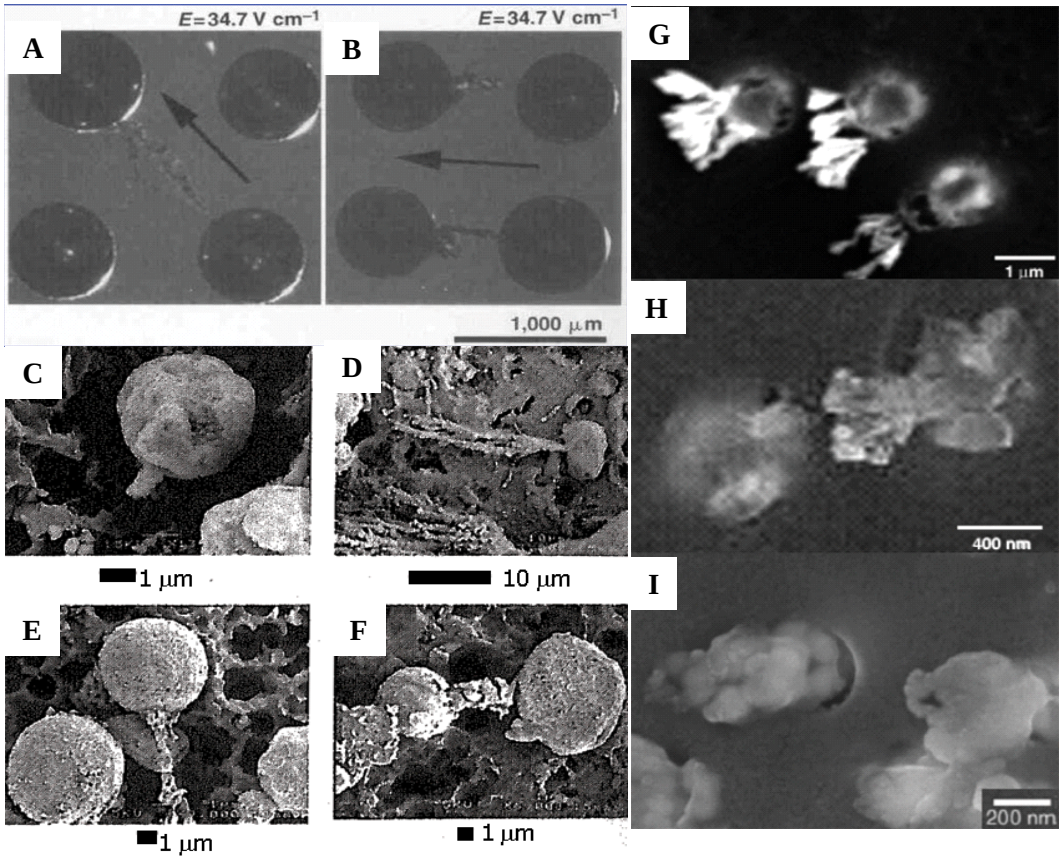

Figure 1.4. Optical micrographs in images (A) and (B) show the control of wire growth within a 4 x 4 particle array. In (A) the applied electric field was along the diagonal of the copper particle array (indicated by the arrow) generating a single wire in the expected location. The other two particles were left unaffected. In image (B) the applied electric field vector was parallel to the side of the particle array (arrow) generating two parallel wires. The electrolyte consisted of 0.1 mM H_2SO_4 and 0.01% Nonidet-P40, and the feeder electrodes were made of two parallel 1-mm-diameter Pt wires. The SEM micrographs in (C) – (F) show wire growth between copper particles less than 10 μm in length. The copper particles were dispersed on demetalized commercial circuit boards. The copper particles in (C) were exposed to a 2.5kV/cm field for 5 minutes, in (D) particles were exposed to a 2.5 kV/cm field for 10 minutes, in (E) the copper particles were exposed to a 5.0 kV/cm field for 5 minutes, and in (F) the particles were exposed to a 3.5 kV/cm for 5 minutes. The electrolyte consisted of 1:1 toluene/acetonitrile, and the copper particles were immobilized on a commercial circuit board (metal removed with 50% nitric acid). Images (G) – (I) show SEM micrographs of silver cylinders immobilized in the pores of polycarbonate membrane. In (G) the pores are 1 μm and the silver cylinders were exposed for 180s at 4.0 kV/cm. In image (H) the pores are 400nm and the silver cylinders were exposed for 120s at 4.0 kV/cm. In (I) the silver cylinders are in 200nm pores and were exposed to a 6.0 kV/cm field for 90s.

The initial studies used copper beads that were hundreds of micrometers in diameter and were in aqueous solutions. The next step successfully demonstrated that copper wires with sub-micrometer (hundreds of nanometers) diameters could be grown to connect isolated copper particles. In these studies the copper particles used were approximately 10 μm in diameter and spherical. The transition to much smaller dimensions resulted in ramified deposits instead of the dendrites seen earlier, necessitated the use of electrical fields two orders of magnitude greater than before, and the use of acetonitrile toluene mixtures (Figures 1.4C - F).[40]

SCBE was then studied on the nanoscale. For these studies gold and silver nanocrystals on glass microscope slides, and silver rods in nuclear track etched membranes were used. The silver and gold nanocrystals investigations were inconclusive. Gold, an inert metal in SCBE, did not show any effect as expected; however, silver showed an effect that could not be explained conclusively by electrochemical or electrorheological effects. The experiments on silver nano-rods (nanowires) in the nuclear track etched membranes did show SCBE-like behavior. The nano-rods were orientated perpendicular to the applied field and only a small portion of the top part of the nano-rod was exposed to the field thus forming a disc. In the earlier copper experiments there was a focusing effect i.e. wire growth was directed from one copper bead to the adjacent bead even when the copper bead was slightly offset relative to the adjacent bead. With the nanoscale silver discs this was not seen, instead wide branched deposits that grew in the direction of the applied field were seen (Figure 1.4G - I). This observation was attributed to a possible loss of convective forces on this scale, and a greater diffusion of silver ions relative to the disc size.[41]

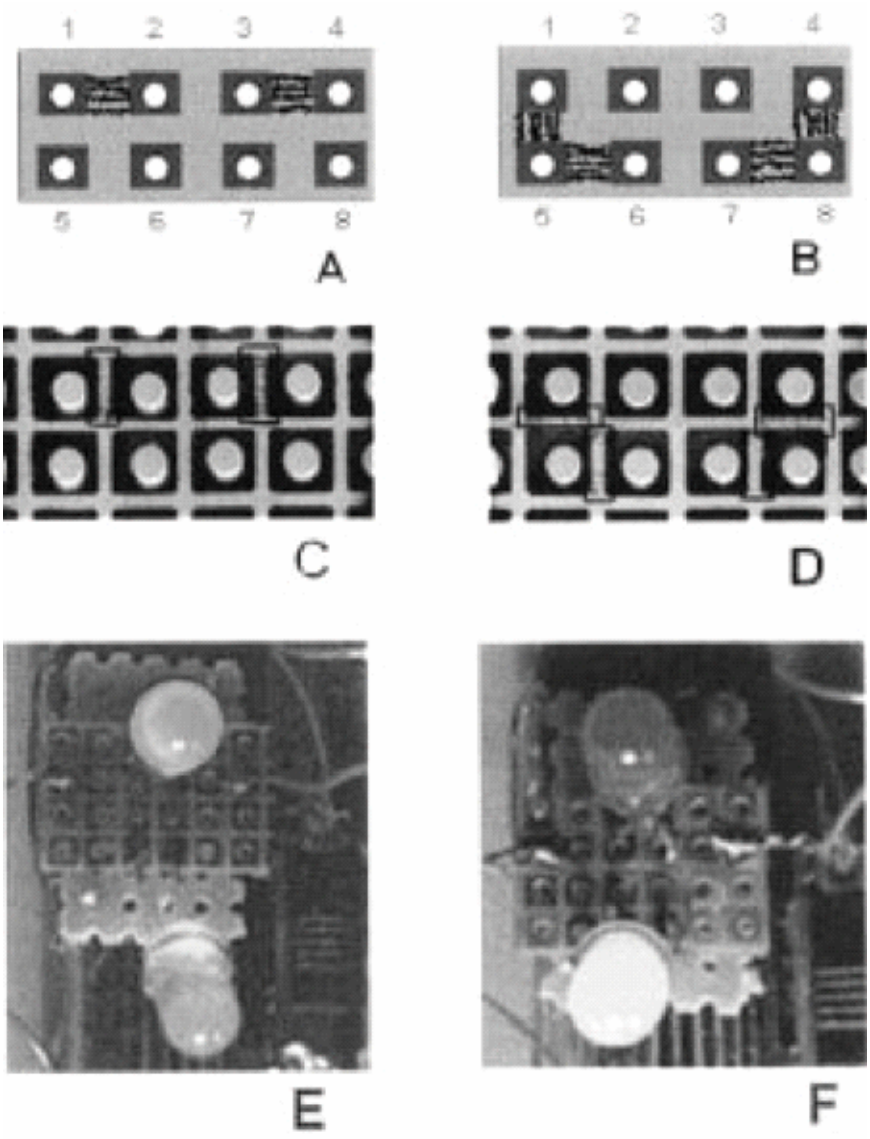

Figure 1.5. Selective circuit formation. Schematic diagram of pattern 1 (A) and pattern 2 (B) formed by the activation of selected positions shown within an eight-pin array. Examples of micrographs after growth of pattern 1 (C) and pattern 2 (D) using conditions of Fig 3C. Examples of selective circuit construction form an initially identical component configuration of presoldered leads at positions 1 and 4 and two diodes across positions 2-3 and 6-7, respectively. In (E), the growth of pattern 1 leads to the lighting of the top diode whereas in (F) the growth of pattern 2 leads to the lighting of the lower diode. To grow the wires the solvent used was 60:40 toluene/acetonitrile and the field was applied for 30 seconds in one direction at 2kV/cm, and then the field was reversed and applied for 30 seconds at 2kV/cm. To improve the electrical conductivity of the resulting wires a 2 hour electroless plating (copper) step was done.

Using a combined empirical and theoretical approach on the process of SCBE Molina et al., determined that SCBE growth can be divided into two main parts. In the first part the movement of copper ions is due to gravitoconvective fluid motion, and in the second part the growth of the copper wires is similar to processes observed in thin layer electrochemical deposition.[42]

Exploiting the redox chemistry in bipolar electrochemistry the Bradley research group demonstrated bipolar electrochemistry can be used to grow interconnects between isolated substrates without the addition of any metal salt. In contrast to this method bipolar electrodeposited catalyst (BEC) uses a metal salt in the electrolyte to deposit a metal onto one area of an isolated conductive substrate. Palladium metal was deposited onto one area of isolated graphite particles to form BECs. The resulting BECs were catalytically active in the reduction of crotonaldehyde to butyraldehyde.[43]

1.6 Conclusions

The concept of open bipolar electrochemistry and closed bipolar electrochemistry is a distinction that is not commented on in the literature. In open bipolar electrochemistry there is diameter dependant relationship between the applied electric field and the induced potential on the substrate (equation 1). There is no such relationship in closed bipolar electrochemistry.

An examination of the literature finds that bipolar electrochemistry is used in a variety of applications; which include, molten salt electrolysis, trace metal recovery, electro-organic synthesis, electroanalysis, water electrolysis, soy protein separation, recovery of acids and bases from salt solutions, adjusting the pH of various fluids, and

the characterization of semiconductor wafers. With the exception of the electroanalysis example, that uses spherical ultramicroelectrodes, there are no examples of open bipolar electrochemistry on the micrometer scale (below 10 μm) or on the nanometer scale. On further examination there are no examples of bipolar electrochemistry used to construct devices, functional circuit paths or catalytic material. In this respect the work done by the Bradley research lab is unique. It is the goal of this thesis to present work that continues to build upon the foundation of innovation and cutting edge research conducted in the Bradley research group.

References

1. Eardley, D.C.; Handley, D.; Andrew, S. P. S. Bipolar Electrolysis with Intra Phase Conduction in Two Phase Media. *Electrochim. Acta.* **1973,** *18,* 839-848.

2. Goodridge, F. Some Recent Developments of Monopolar and Bipolar Fluidized Bed Electrodes. *Electrochim. Acta.* **1977,** *22,* 929-933.

3. Kusakabe, K.; Morooka, S.; Kato Y. Current Paths and Electrolysis Efficiency in Bipolar Packed Bed Electrodes. *J. Chem. Eng. Jpn.* **1982,** *15,* 45-50.

4. Pourcelly, G. Electrodialysis with Bipolar Membranes: Principles Optimization, and Applications. *Russ. J. Electrochem.* (*Engl. Transl.*) **2002,** *38,* 919-926.

5. Keh, H. J.; Li, W. J. Interactions among Bipolar Spheres in an Electrolytic Cell. *J. Electrochem. Soc.* **1994,** *141,* 3103-3114.

6. Goodridge F.; King, C. J. H.; Wright, A. R. Performance Studies on a Bipolar Fluidised Bed Electrode. *Electrochim. Acta.* **1977,** *22,* 1087-1091.

7. Yen, S.-C.; Yao, C.-Y. The Bipolar Analysis of a Single Sphere in an Electrolytic Cell, *J. Electrochem. Soc.* **1991,** *138,* 2697-2703.

8. Yang, J.; Zhang, Q.; Wang, H.; Liu,Y. Establishment and Verification of Mathematical Model for Current Leakage in Bipolar Multi-Compartment Cell. *Trans. Nonferrous Met. Soc. China* **1995**, *5*, 29-35.

9. Fleischmann, M.; Oldfield, J. W.; Tennakoon, C. L. K. *The Electrochemical Bipolar Particulate Cell,* Symposium on Electrochemical Engineering, 1971; Thornton, J. D., Eds.; Inst. Chem. Eng, 1973: London; 53-69.

10. Ellis, K. G.; Jansson, R. E. W. Further Studies on the Epoxidation of Propylene in a Bipolar Trickle Bed. *J. Appl. Electrochem.* **1981,** *11,* 531-535.

11. Manji, A.; Oloman, C. W.; Electrosynthesis of Propylene Oxide in a Bipolar Trickle-Bed Reactor. *J. Appl. Electrochem.* **1987,** *17,* 532-544.

12. Kusakabe, K.; Morooka, S.; Kato, Y. Equivalent Resistances of Current Pathways in a Bipolar Packed-Bed Electrode. *J. Chem. Eng. Jpn*. **1986,** *19,* 43-47.

13. Kim, H. J.; Kusakabe, K.; Hokazono, S.; Morooka, S.; Kato, J. Electro-Oxidation Rate of p-tert-butyltoluene in a Bipolar Packed-Bed Electrode Cell. *J. Appl. Electrochem.* **1987,** *17,* 1213-1222.

14. Plimley, R. E.; Wright, A. R. A Bipolar Mechanism for Charge Transfer in a Fluidised Bed Electrode. *Chem. Eng. Sci.* **1984,** *39,* 395-405.

15. Sudoh, M.; Kodera, T.; Hino, H.; Shimamura, H. Effect of Anodic and Cathodic Reactions on Oxidative Degradation of Phenol in an Undivided Bipolar Electrolyzer. *J. Chem. Eng. Jpn.* **1988,** *21,* 198-203.

16. Beck, T. R.; Rousar, I.; Thonstad, J. Energy Efficiency Considerations on Monopolar vs Bipolar Fused Salt Electrolysis Cells. *Metall. Mater. Trans. B* **1994,** *25B,* 661-668.

17. Zhao, G.; Inman, D. Electrowinning Zinc From Chloride Melts In Bipolar Cell, *Trans. Nonferrous Met. Soc. China* **1995,** *5,* 45-48.

18. King, C. J. H.; Wright, A. R. Current Distribution in a Thin Film Bipolar Electrode System. *Electrochim. Acta.* **1977,** *22,* 1135-1139.

19. Lee, J. K.; Shemilt, L. W.; Chun, H. S. Studies of Bipolarity in Fluidized Bed Electrodes, *J. Appl. Electrochem.* **1989,** *19,* 877-881.

20. Kusakabe, K.; Kimura, T.; Morooka, S.; Kato, Y. Recirculating Feed Operation of Bipolar Packed-Bed and Trickle-Bed Electrode Cells Equipped with Mesh Spacers. *J. Appl. Electrochem.* **1987,** *17,* 724-730.

21. Alkire, R. A Threoretical Study of Bipolar Porous Electrodes, *J. Electrochem. Soc.* **1973,** *120,* 900-905.

22. Duval, J.; Kleijn, J. M.; van Leeuwen, H. P. Bipolar Electrode Behaviour of the Aluminium Surface in a Lateral Electric Field. *J. Electroanal. Chem.* **2001,** *505,* 1-11.

23. Fleischmann, M.; Ghoroghchian, J.; Rolison, D.; Pons, S. Electrochemical Behavior of Dispersions of Spherical Ultramicroelectrodes. *J. Phys. Chem.* **1986,** *90,* 6392-6400.

24. Rolison, D. Zeolite-Modified Electrodes and Electrode-Modified Zeolites. *Chem. Rev.* **1990,** *90,* 867-878.

25. Cattarin, S.; Musiani, M. M. Characterization and Processing of Bipolar Semiconductor Electrodes in a Dual Electrolyte Cell, *J. Electrochem. Soc.* **1995,** *142,* 3786-3792.

26. Cattarin, S.; Peter L. M. Determination of Minority Carrier Diffusion Length in Silicon Wafers by a Dual Electrolyte Cell. *J. Phys. Chem. B.* **1997,** *101,* 3961-3967.

27. Licht, S.; Khaselev, O.; Soga, T.; Umenob, M. Multiple Bandgap Photoelectrochemistry: Energetic Configurations for Solar Energy Conversion. *Electrochem. Solid-State Lett.* **1998,** *1,* 20-23.

28. Guangwen, Z.; Inman, D. Electrowinning Zinc from Chloride Melts in Bipolar Cell. *Trans. Nonferrous Met. Soc. China* **1995,** *5,* 45-48.

29. Wiesener, K.; Ohms, D.; Benczur-Urmossy, G.; Berthold, M.; Haschka, F. High Power Metal Hydride Bipolar Battery. *J. Power Sources* **1999,** *84,* 248-258.

30. Mehta, V.; Cooper, J. S. Review and Analysis of PEM Fuel Cell Desiegn and Manufacturing. *J. Power Sources* **2003,** *114,* 32-53.

31. Mameri, N.; Lounici, H.; Belhocine, D.; Grib, H.; Piron, D.L.; Yahiat, Y Defluoridation of Sahara Water by Small Plant Electrocoagulation Using Bipolar Aluminium Electrodes. *Sep. Purif. Technol.* **2001,** *24,* 113-119.

32. Alkire, R. A Theoretical Study of Bipolar Porous Electrodes. *J. Electrochem. Soc*. **1973,** *120,* 900-905.

33. Mafe, S.; Ramirez, P.; Manzanares, J. A. How Does a Transition Zone Affect the Electric Field Enhanced Water Dissociation in Bipolar Membranes. *Ber. Bunsen-Ges. Phys. Chem.* **1994,** *98,* 202-205.

34. Bazinet, L.; Lamarche, F.; Ippersiel, D. Bipolar-Membrane Electrodialysis: Applications of Electrodialysis in the Food Industry. *Trends Food Sci. Technol.* **1998,** *9,* 107-113.

35. Bradley, J.-C.; Chen, H.-M.; Crawford, J.; Eckert, J; Ernazarova, K.; Kurzeja, T.; Lin, M.; McGee, M.; Nadler, W.; Stephens, S.G. Creating Electrical Contacts Between Metal Particles Using Directed Electrochemical Growth. *Nature* **1997,** *389,* 268-271.

36. Bradley, J.-C.; Crawford, J.; Ernazarova, K.; McGee, M.; Stephens, S. G. Wire Formation on Circuit Boards Using Spatially Coupled Bipolar Electrochemistry, *Adv. Mater.* **1997,** *9,* 1168-1171.

37. Bradley, J.-C.; Ma, Z.; Clark, E.; Crawford, J.; Stephens, S. G. Programmable Hard-Wiring of Circuitry Using Spatially Coupled Bipolar Electrochemistry. *J. Electrochem. Soc.* **1999,** *146,* 194-198.

38. Bradley, J.-C.; Ma, Z.; Stephens, S. G. Electric Field Directed Construction of Diodes Using Free-standing Three-dimensional Components. *Adv. Mater.* **1999,** *11,* 374-378.

39. Bradley, J.-C.; Ma, Z.; Christaffer, S.; Crawford, J.; Ernazarova, K.; Stephens, S. G. The Construction of Circuitry Using Spatially Coupled Bipolar Electrochemistry. In *Semiconductive Polymers: Applications, Properties, and Synthesis*; Hseih, B. R., Wei, Y., Eds.; ACS Symposium Series 735; American Chemical Society: Washington, DC, 1999; pp 429-439.

40. Bradley, J.-C.; Crawford, J.; McGee, M.; Stephens, S.G. A Contactless Method for the Directed Formation of Submicrometer Copper Wires. *J. Electrochem. Soc.* **1998,** *145,* L45-L47.

41. Bradley, J.-C.; Babu, S.; Carroll, B.; Mittal, A. A Study of Spatially Coupled Bipolar Electrochemistry on the Sub-Micrometer Scale: Colloidal Particles on Surfaces and Cylinders in Nuclear-Track Etched Membranes, *J. Electroanal. Chem.* **2002,** *522,* 75-85.

42. Bradley, J.-C.; Dengra, S.; Gonzalez, G. A.; Marshall, G.; Molina, F. V. Ion Transport and Deposit Growth in Spatially Coupled Bipolar Electrochemistry. *J. Electroanal. Chem.* **1999,** *478,* 128-139.

43. Bradley, J.-C.; Ma, Z. Contactless Electrodeposition of Palladium Catalysts. *Angew. Chem. Int. Ed*. **1999,** *38,* 1663-1666.

Chapter 2: Bipolar Electrodeposition of Palladium onto Graphite Platelets Using Pulsed dc Electrical Fields

2.1 Summary Statement

This chapter describes the continuation of earlier work on the synthesis of bipolar electrodeposited catalysts (BECs). The initial purpose of the project was to study the effect of frequency on the catalytic and morphological properties of the synthesized BECs. Further work on the project led to the development of a technique to study the graphite platelets with the minimum amount of perturbation to the platelets after bipolar electrodeposition.

2.2 Introduction

Palladium supported on carbon (Pd/C) is a very versatile catalyst. It is widely used in various research laboratories around the world, and in a wide range of industrial processes.[1, 2, 3] Carbon is extensively used as a support for palladium (as well as other metals) catalysts due to carbon's several distinct advantages. These advantages include a large surface area, chemical stability, the ability of the carbon support to keep the palladium in a highly stable and dispersed state, and carbon supports are cheap and easy to produce.[1, 2, 3, 4]

A review of the methods used to synthesize Pd/C catalysts is beyond the scope of this thesis; however, brief descriptions on various synthetic approaches are presented. There are various methods used to produce Pd/C and the common feature with these methods is the carbon is placed in contact with a suitable precursor salt for a certain period of time, and then the precursor salt is reduced to the zero valent metal. The various methods

include deposition precipitation, deposition reduction, impregnation and drying, colloid deposition, electroless plating, and electrodeposition. [1,2,3] In deposition precipitation the palladium salt in a suitable solvent is precipitated (often as a hydroxide) onto the carbon support, the precipitate is then reduced to the zero valent metal using a suitable reducing agent (e.g. hydrazine, formaldehyde, etc). [1,2,3] With the deposition reduction method the aqueous metal salt is directly reduced to the metal onto the carbon support. [1,2,3] Impregnation and drying, also known as the incipient wetness method, consists of leaving the carbon support in contact with the palladium salt solution, drying the carbon support and then reducing the absorbed metal ions to the metal under a hydrogen stream at high temperatures. [1,2,3] Colloidal dispersion simply deposits the metal colloid onto the carbon support straight from colloidal solutions. [1,2,3] Electroless plating relies on the fact that the carbon surface can be pretreated to induce reduction of the metal ion to the zero valent metal without the application of a current or reducing agent. [1,2,3] The method used, the type of carbon support used, the surface chemistry of the carbon support, and the precursor salt solution used to produce the Pd/C catalyst can affect the resulting catalysts activity, selectivity, and lifetime.[1,2,3]

Electrodeposition of palladium onto carbon is one of the many methods that have been used to prepare Pd/C catalysts.[5] Unlike electroless plating; a current source and a direct contact between the substrate and the power source is required. In general, the use of electrodeposition has been shown to affect the size and morphology of the deposit as well as the dispersion of the deposit.[6, 7, 8, 9] Electrodeposition is not limited to Pd/C catalysts, and it has been used to prepare various other metal catalysts on carbon, metal, polymer, or conductive oxides.[10, 11]

The Bradley research group recently introduced a non-contact method to electrodeposit palladium onto isolated graphite platelets. The method takes advantage of bipolar electrochemistry and as a result offers several key advantages over conventional electrochemical preparative methods. These advantages include no direct contact between the power source and the substrate, homogenous electrodeposition within large volumes, and the ability to control where the deposition occurs. The catalytic particles that are produced using bipolar electrochemistry are called bipolar electrodeposited catalysts (BECs). BECs require a current during synthesis only; this is in stark contrast to conventional electro-catalysts that require a current for the catalytic activity. [12, 13]

There are other non-contact electrochemical methods to prepare catalysts. These include electroless plating, and photo-electrochemical deposition. Electroless plating requires extensive pretreatment of the carbon substrate but does allow for the synthesis of industrial amounts of catalyst. In photo-electrochemical deposition the substrate used is a semi-conductor. The redox process responsible for the deposition of metal onto the substrate is driven by electrons excited into the valence band by the appropriate wavelength of light. This method suffers from the inability to deposit homogenously in large volumes.

2.3 Bipolar Electrodeposited Catalysts

Bipolar electrodeposited catalysts (BEC) were first introduced by the Bradley research group in 1999. This initial work showed that palladium can be electrodeposited onto isolated dispersed graphite platelets, the toposelective nature of the deposition, the catalytic activity of the resulting deposits, and the bipolar nature of the deposition.[12, 13]

Pulsed electrical fields were used to synthesize the BECs in order to determine whether the dispersion, the selectivity, and the catalytic activity of the BEC could be modified and controlled.

Using conventional methods of electrodeposition, the particle size and morphology of the electrodeposits has been controlled by modulating such parameters as applied potential[6], and pulsed[7,8] or reversed currents[6]. Palladium catalysts have been prepared using conventional electrodeposition methods on various carbon supports. Controlling the magnitude and the duration of the potential used modifies the catalytic activity and particle size of the palladium particles.

2.3.a Experimental

Graphite powder with an average diameter of 1–2 μm (Fisher, BET surface area 200m^2) was suspended in acetone. The graphite suspension was then nebulized onto 60 μm thick cellulose paper (Kimwipe). For some samples the graphite suspension was sonicated in a Branson Bath sonicator for 10 hours before nebulization onto the cellulose paper. The cellulose paper was then cut and stacked to a height of 0.3cm between two flat graphite electrodes measuring 2 x 2cm. The graphite electrodes were then immersed in a solution of 1mM palladium chloride (Aldrich) in 1:1 acetonitrile/toluene (dried over calcium hydride). Under a nitrogen atmosphere the electric field was applied (Figure 2.1). The electric field was applied as either a pulse with a 50% duty cycle or as a DC electric field. For DC field experiments the field duration was 7.5 minutes, and for pulsed field experiments the field duration was 15 minutes. Four different electrical field intensities were used; these were 0.5 kV/cm, 1.0 kV/cm, 2.0 kV/cm, and 3 kV/cm.

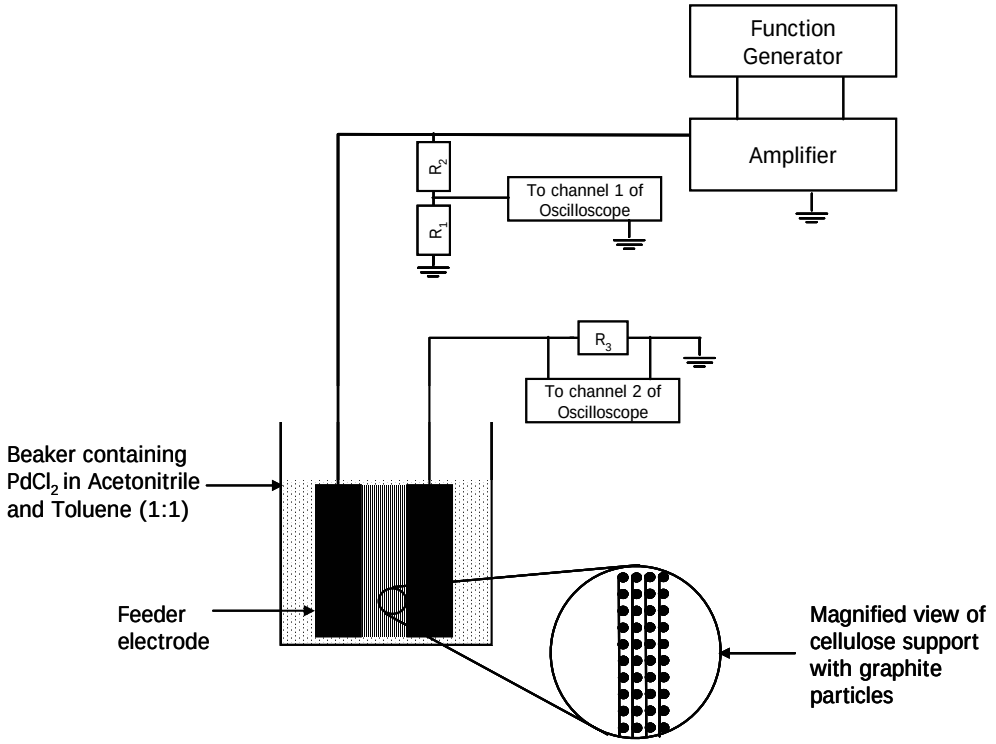

Figure 2.1. Experimental set up used to electrodeposit palladium onto graphite platelets. Channel 1 on the oscilloscope measured the voltage across a potential divider with resistances of 30 MΩ (R1), 300kΩ (R2), and channel 2 measured the current across a 100Ω resistor (R3).

The pulsed electrical fields were used with the following frequencies of 0.5 kHz, 1.0 kHz, 2.0 kHz, 5.0 kHz, 10 kHz, and 20.0 kHz. For pulsed field experiments the voltage signal was generated as a square waveform with a 50% duty cycle by an HP 33120A function generator. The voltage signal was amplified by a Trek P0674 high voltage amplifier before it was applied across the graphite electrodes. The current and voltage traces were monitored on an HP 54602B oscilloscope. The function generator and the oscilloscope were controlled by Labview. The experimental parameters (current and voltage data) were passed to and from Labview though Internet Explorer 5.0, and stored in a custom built laboratory management system (Standard Modulator Integrated Research Protocols, SMIRP[14]). After the field application the stacked cellulose paper was rinsed with large amounts of acetone, dried, and characterized

2.3.b Characterization

The amount of palladium on the samples was determined by atomic absorption spectroscopy (AAS). To prepare the samples for AAS a sample of the cellulose paper was digested in aqua regia (3:1 by volume concentrated hydrochloric acid: concentrated nitric acid) and diluted, using distilled water, to a total volume of 10.0 mL. A series of standard solutions were prepared from a stock solution of palladium atomic absorption solution (Aldrich). The solutions were then run through a Varian AA-1275 atomic absorption spectrophotometer. The palladium content was then determined from the calibration curve obtained and converted to percentage palladium per gram of sample.

In order to study the morphology of the deposits, BECs were examined on a transmission electron microscope (TEM). The graphite platelets were removed from the

cellulose paper by vigorously shaking a sample of the paper in acetone, and then drop drying the resulting suspension onto copper grids (200 mesh, SPI Supplies Inc) with a holey carbon membrane support. The samples were then examined on a JEOL 2010 F TEM with an accelerating voltage of 200 kV.

The surface area of the samples was studied using two model reactions. The first reaction used was the hydrogenation of crotonaldehyde, and the second was the reduction of methylene blue. The hydrogenation of crotonaldehyde to butyraldehyde followed methods used in an earlier paper.[12] A 60 micromolar solution of crotonaldehyde in ethanol and in 1.0 atm of hydrogen were used for the hydrogenation of crotonaldehyde to butyraldehyde. The amount of BEC used depended on the percentage of palladium (determined by AAS) on the sample. For each run the amount of BEC i.e. the number of cellulose paper was adjusted to keep the total amount of palladium constant for each run. Conversion was monitored by taking aliquots at time intervals of 0-, 0.5-, 1-, 2-, and 4-hrs. Each aliquot was run through a gas chromatography unit with a flame ionization detector. Reduction of methylene blue was done using methods adapted from experiments by Jana and Pal.[15] In this method two pieces of cellulose papers with the electrodeposited catalyst were immersed in 15.0 mL of an aqueous solution of 69.7 micromolar methylene blue in an approximately 15 millimolar $NaHCO_3$ /Na_2CO_3 buffer solution (pH 9.5). Initially a 0.4 mL aliquot was removed from this starting solution and then a freshly prepared aqueous solution of sodium borohydride (~107 mL, 0.53 mM) was added. 0.4 mL aliquots were removed every 60 seconds for 300 seconds. The 0.4mL aliquots were diluted by adding the aliquots to approximately 4.56 mL $NaHCO_3$ /Na_2CO_3 buffer (pH 9.5). These diluted aliquots were then monitored at a wavelength of 620 nm

with a Perkin Elmer Lambda 2 UV-visible spectrophotometer. Calibration data was obtained by using palladium with a known surface area. The palladium used was in the form of wire with a 1.0 mm diameter that had been cut into approximately 1.0 cm lengths. A plot of surface area versus the first order rate constant for the first 300s of the reduction of methylene blue was used as a calibration curve

2.3.c Results

Figure 2.2 shows the percentage palladium on the platelets for all parameter spaces explored. The figure shows a strong correlation between field intensity and percentage palladium (%Pd) especially between 2000V/cm and 3000V/cm. There is no correlation between frequency and %Pd for all parameters explored. The sonication of samples prior to nebulization did not cause a significant affect on the %Pd. The palladium dispersion did not correlate with frequency (Figure 2.3). The dispersion did increase for sonicated samples, and there seemed to be a slight trend for samples at higher frequencies.

Figure 2.4 and Figure 2.5 present TEM micrographs of samples prepared at 3000V/cm at various frequencies. The TEM studies revealed that generally there were three types of palladium deposits: ramified deposit, amorphous deposits, or as surface bound deposits. High resolution images of the deposits revealed that the ramified growths consisted of aggregates of spherical deposits on the order of 25-50 nm diameters. These aggregates were decorated with smaller structures on the order of a few nanometers. In addition to these larger deposits, for both DC and pulsed samples, surface-bound deposits approximately 5 nm in size were also identified.

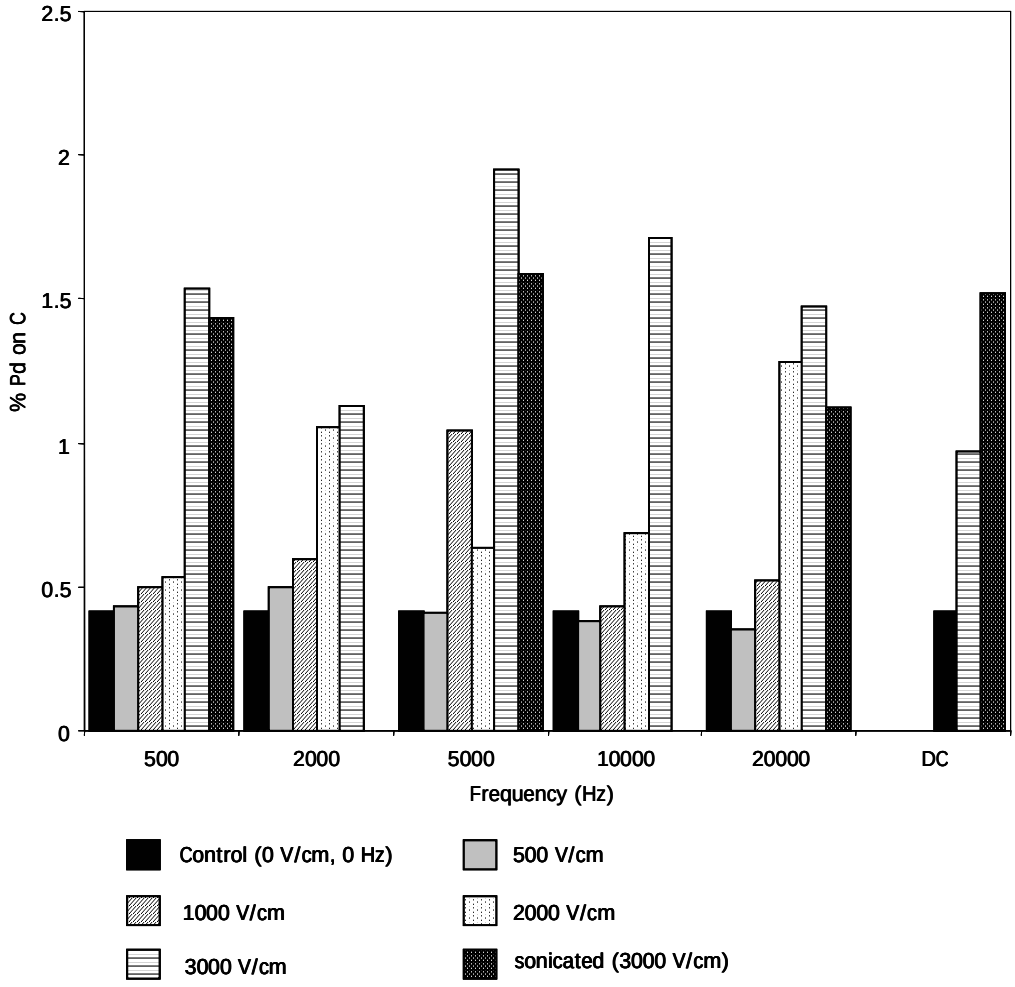

Figure 2.2. Amount of palladium deposited, expressed as a percentage, at all field intensities and frequency regimes explored.

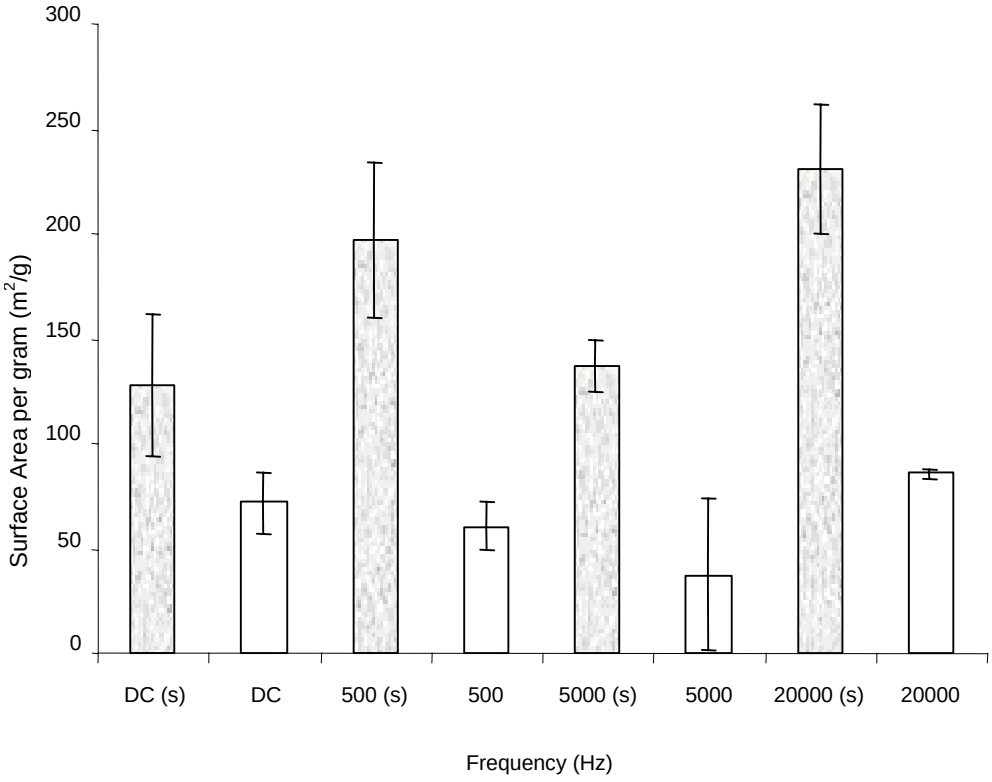

Figure 2.3. The average surface area per gram of palladium vs. frequency at 3 kV/cm. Entries marked with a (s) were sonicated for 10 hours prior to nebulization onto the cellulose support.

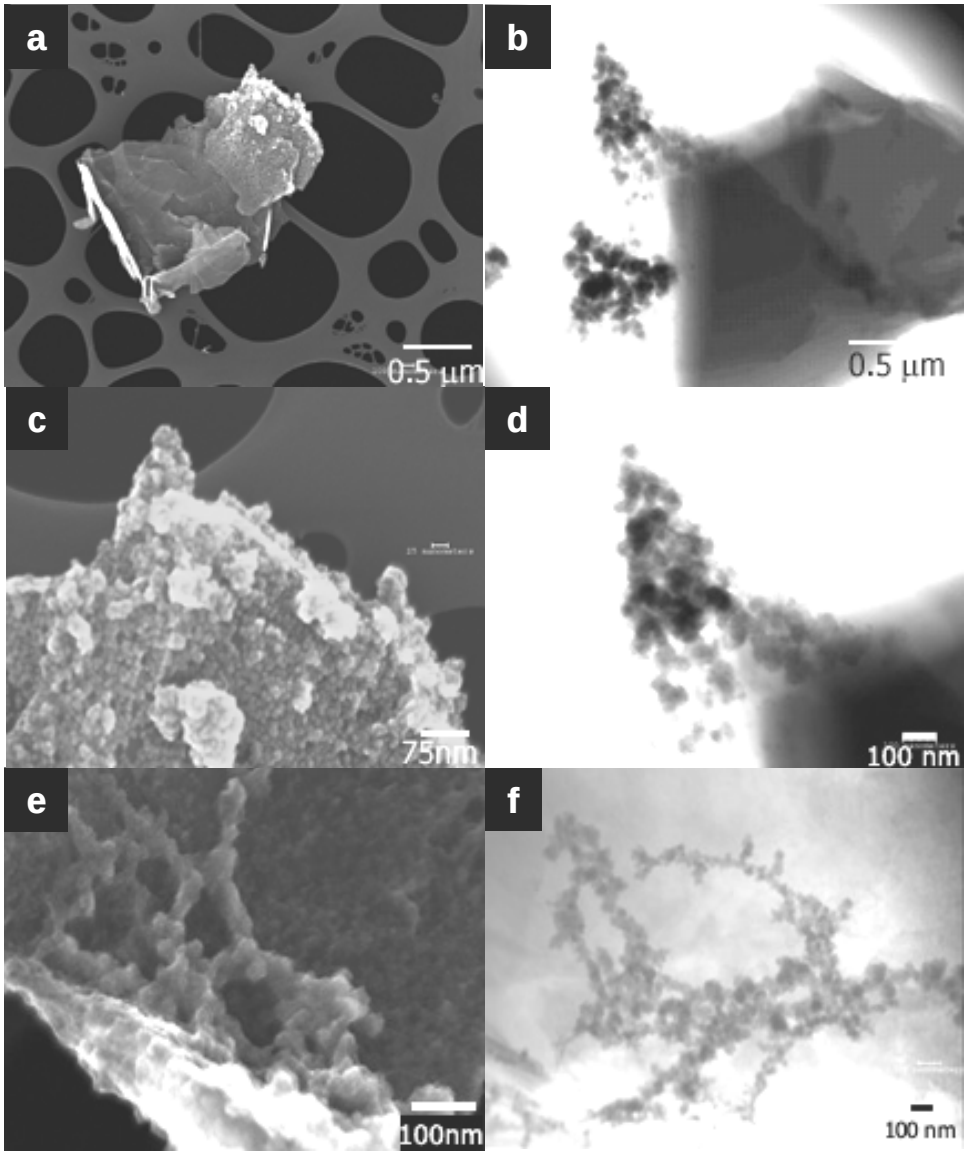

Figure 2.4. Electron micrographs of samples prepared at 3000 V/cm and at various frequencies. (a) DC toposelective electrodeposition of palladium onto right side of a graphite particle. (b) 5 kHz, toposelective deposition; (c) DC deposit magnified view of amorphous deposit in (a); (d) 5 kHz, magnified view of ramified deposit in (b); (e) 500 Hz, ramified deposit; and (f) 3 kHz, extended ramified deposit.

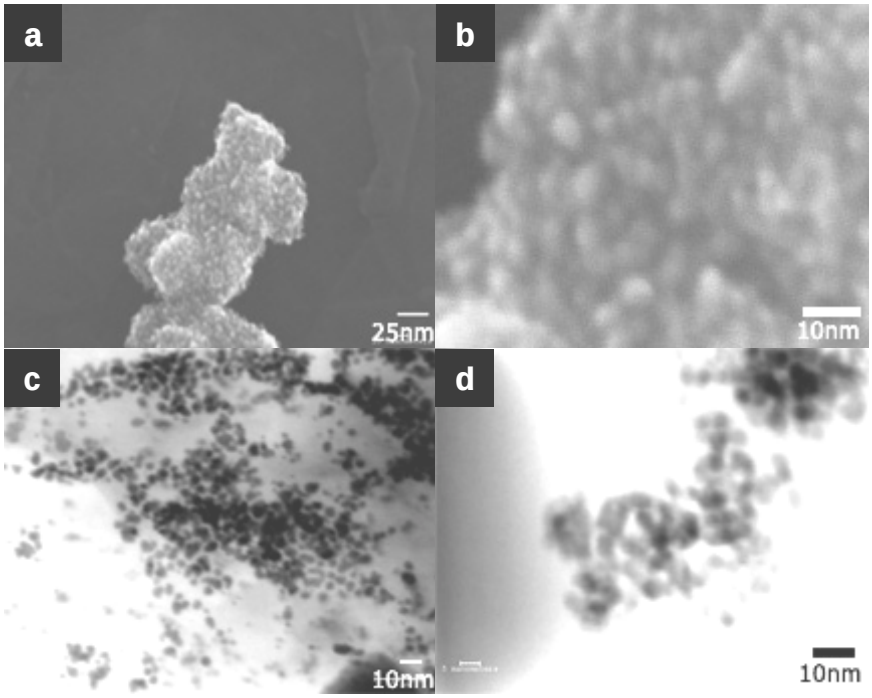

Figure 2.5. High-magnification view of different deposit types at various frequencies for samples prepared at 3 kV/cm: (a) 5 kHz, ramified deposit; (b) further magnified view of (a) showing decoration of ramified deposits; (c) dc surface-bound deposits on graphite; and (d) 20 kHz, surface-bound deposits on graphite.

2.3.d Discussion

There is a non linear increase in the amount of palladium deposited, expressed as percent of palladium on graphite, with an increase in the field intensity. The relationship, however, is not linear, with the palladium content exhibiting a sharp increase at about 2-3 kV/cm. This transition is very similar to that observed in an earlier study.[12] In bipolar electrochemistry, the potential (η) at a point (X) on a spherical particle can be calculated from the electric field (E), the radius of the particle (r) and the angle (θ) by using the following equation[16, 17, 12, 13] illustrated in Figure 2.6.

$$(1)\cdot \eta_X = 2Er\cos\theta$$

For the case of the graphite particles, if we assume point X is in line with the electrical field, then the potential drop across the graphite particle can be estimated from the following second equation:

$$(2)\cdot \Delta V = 2Er$$

From the second equation it is possible to estimate the potential across a graphite particle. For example the graphite platelet in Figure 2.4a is approximately 2 μm, thus the potential drop experienced by the platelet in the electric field will be 0.6V. This value is consistent with the magnitude of the potential needed to induce deposition of palladium. A more accurate value for the potential cannot be easily determined due to bipolar electrodeposition being a contact-less method, thus the exact nature of the redox processes can not be ascertained.

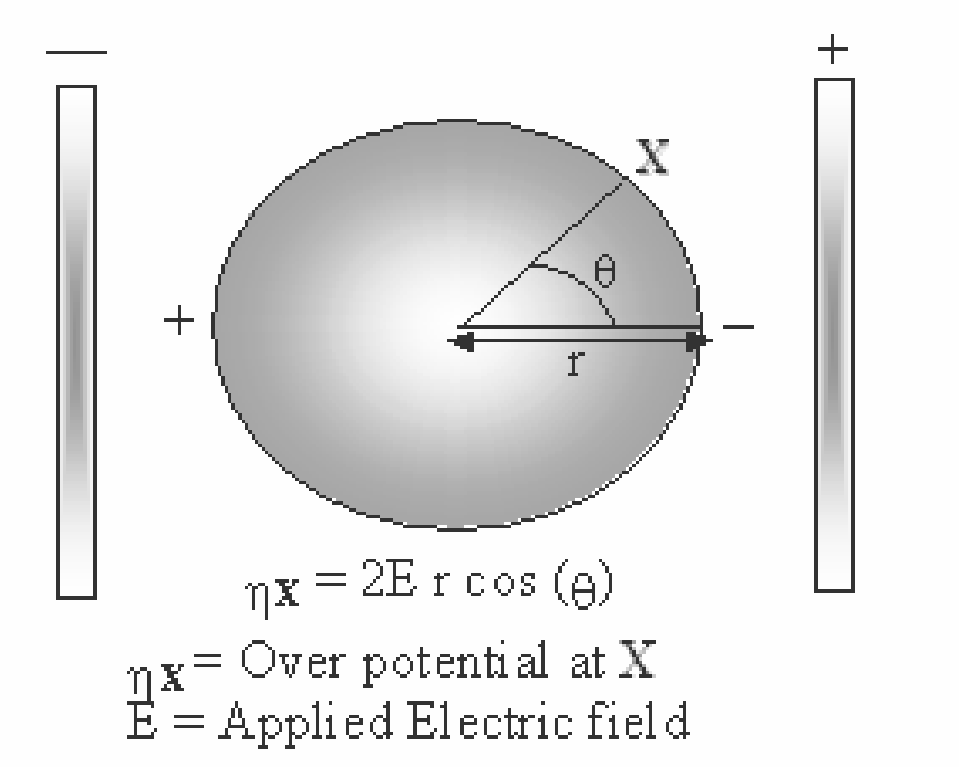

Figure 2.6. Illustration of the relationship between the overpotential at a point on a sphere immersed in an electrolyte, and the applied electric field.

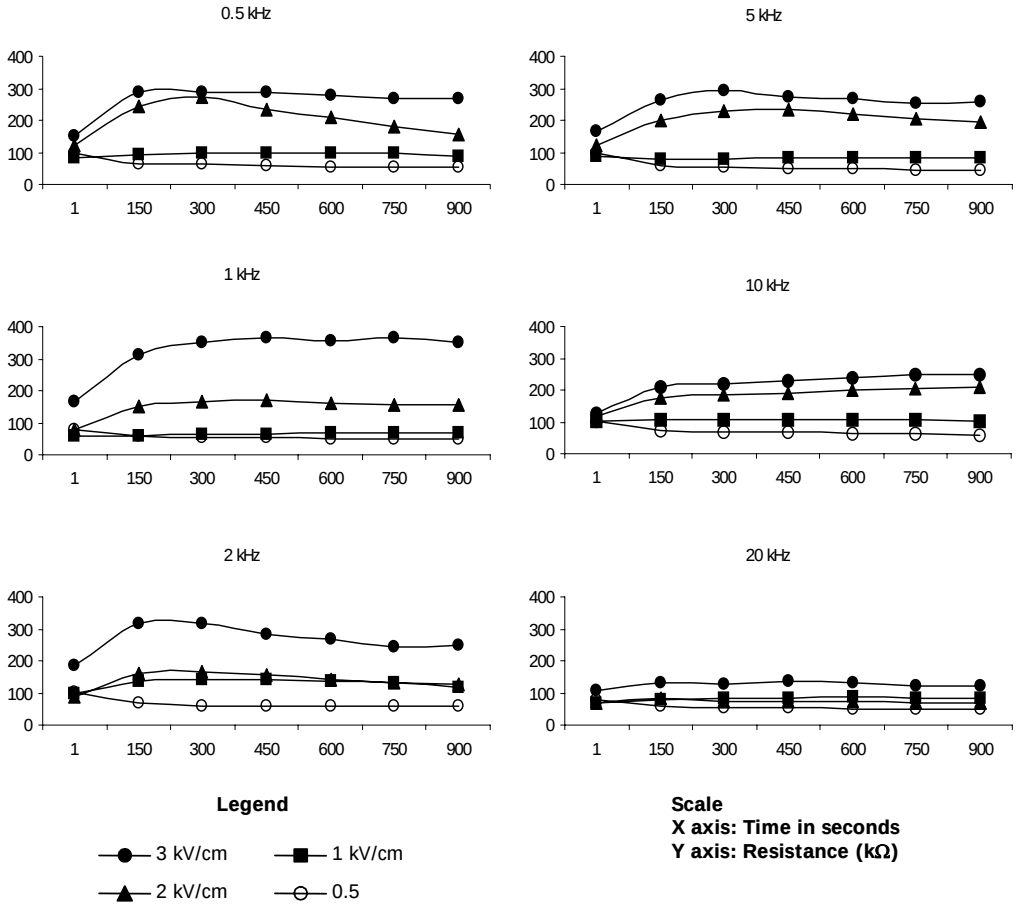

Figure 2.7. Changes in resistance during the course of the experimental run for all field intensities and frequencies. Data points are averages of triplicate experiments.

Figure 2.2 shows that there was no trend in the percentage palladium and the frequency, however there was a frequency dependant behavior of the cell resistance as shown in Figure 2.7. Possible reasons for this trend can be attributed to a quick depletion of palladium ions near the electrodes at high potentials and lower frequencies. This quick depletion results in a decrease in the current and hence an increase in cell resistance, whilst at higher frequencies there may be some mixing of the solution near the electrodes. This trend can be used in the design of bipolar electrochemical cells, where the optimal configuration is the highest cell resistance that will still enable electrochemistry on the dispersed conductive phase. An examination of the frequency and the current showed no discernible trend (Figure 2.8). Due to the nature of bipolar electrochemistry these current readings cannot be used to interpret any of the processes that may be occurring on the platelets, but only on the feeder electrodes.

Ideally for morphological studies the graphite platelets should be imaged directly on the cellulose support using SEM. Attempts to do this were unsuccessful due to the nature of the cellulose support, thus the graphite platelets were removed from the support and imaged using TEM. This process of removing the platelets and preparing them for TEM lead to the breakage and loss of the various deposits, and as a result the TEM studies did not give a complete picture of the true nature of the deposits or for the case of the ramified deposits the degree of ramification. Generally the various samples of platelets examined showed coverage of palladium that was limited to one general area of the platelet as seen in Figure 2.4a. The exact area of the platelet that is covered by palladium depends on the platelets orientation in the electric field.

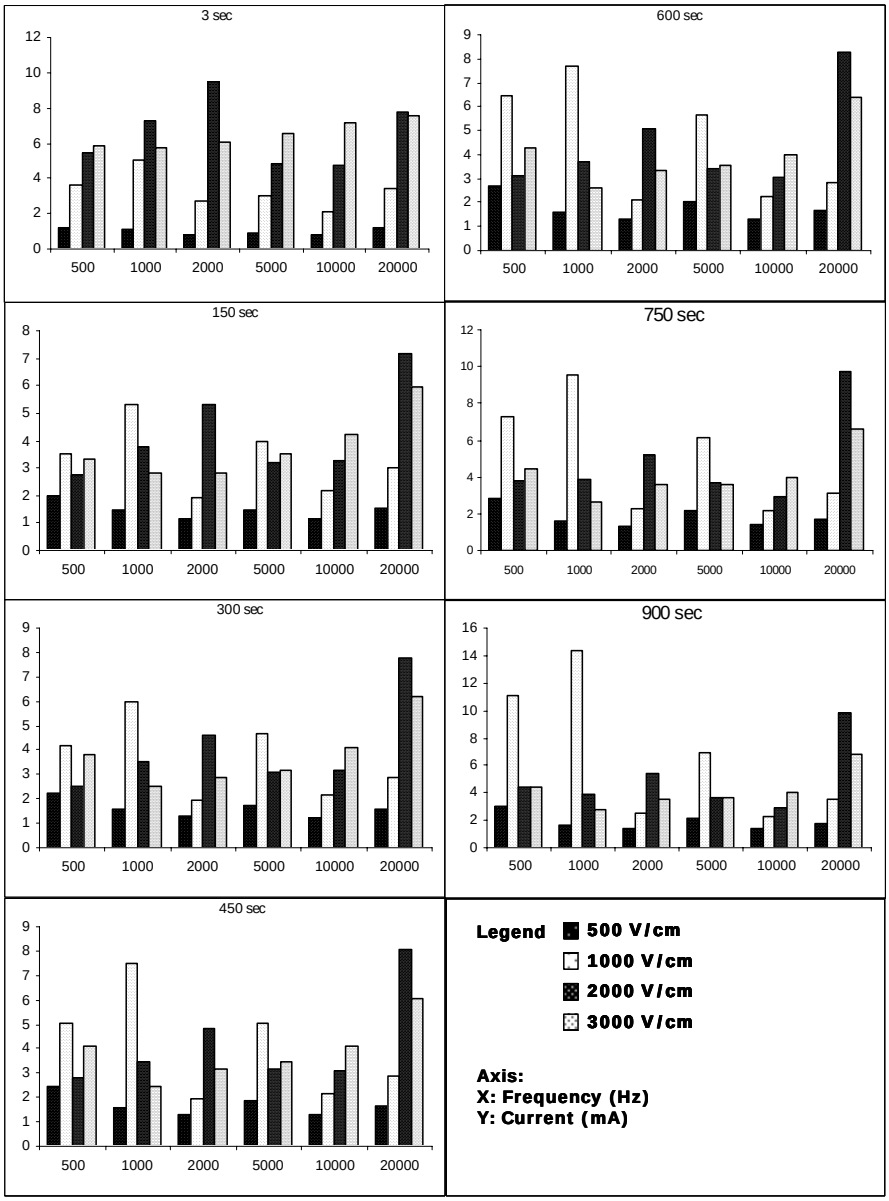

Figure 2.8. Changes in the current during the course of the experimental run for all field intensities and frequencies**.**

The TEM studies revealed three distinct types of deposits; these were, amorphous, surface-bound, and ramified. It was not uncommon to find deposits that extended for several micrometers as seen in Figure 2.4f; however, it was more common to find the types of amorphous deposits seen in Figures 2.4a and 2.4c, as well as, the short aggregates seen in 2.4b and 2.4d. The ramified deposits, as seen in Figure 2.5a, consisted of collections of spherical structures that were 25-50 nm in diameter. Higher magnification images (Figure 2.5b) of the spherical structures revealed that these were decorated by smaller deposits only a few nanometers in diameter. Surface bound deposits of palladium (Figure 2.5c and 2.5d) were found to be of the order of a few nanometers; this result suggests that a significant reduction of the deposition time by a few orders of magnitude could result in highly dispersed deposits of palladium 5 nm or less in size on the surface of the graphite platelets. The long deposition times used in this study did result in micrometer-long chains with diameters of 50 nm that extended off the platelet surface (Figure 2.4f); which does suggest a method for the growth of nanowires.

The process of preparing the TEM samples resulted in a great deal of loss of the palladium deposits, and thus it is not possible to correlate any significant TEM data with the various field parameters used. As a result, surface area measurements were determined by using a colorimetric technique based on the reduction of methylene blue catalyzed by palladium. The main advantage of this method was it allowed the direct use of the BEC supported on the cellulose paper. This minimized the loss of palladium deposit, and thus the data was more inclusive. Results revealed little difference between palladium dispersion from frequency to frequency, however, there was a significant difference between sonicated and non-sonicated samples (Figure 2.3). These differences

can be explained by considering the nature of the distribution of the platelets on the cellulose support when the platelets are not sonicated before nebulization and when the platelets are sonicated before nebulization. Without sonication a fraction of the platelets are nebulized onto the cellulose support as aggregates. When exposed to the electric field the aggregates behave as one particle and the palladium deposits onto a small area of the aggregate. When the platelets are sonicated the aggregates are broken into smaller aggregates or individual platelets, and when nebulized onto the cellulose support this resulted in a larger total surface area of graphite platelets for the deposition of palladium. This resulted in a larger dispersion of palladium.

2.4 Bipolar Electrodeposition of Palladium onto Graphite Platelets Immobilized on a Glass Substrate

2.4.a Introduction

The initial study of BEC synthesized on a cellulose support revealed that there was a detrimental loss of information when transferring platelets from the cellulose support to the TEM grids for electron microscopy study. In order to address this issue, a method needed to be devised that would avoid the problem encountered in the earlier TEM investigations. The new method had to have the platelets prepared on a substrate that would allow the direct examination of the platelets by electron microscopy with the minimum amount of disruption of the platelets after deposition of palladium. This study was designed to address this issue specifically and to determine and confirm the nature of the palladium deposits on the platelets.

Several possibilities to address this issue were considered. A suspension of the platelets in a suitable solution that was then directly exposed to an electric field, spin coating of epoxy and subsequent dispersal of the platelets onto the epoxy layer, or simple direct dispersal of the platelets onto a suitable substrate using electrostatic interactions. The main disadvantage of the suspension method is that the platelets still needed to go through a fairly rigorous process to prepare the platelets for electron microscopy. Such a rigorous process would include a method to remove excess reagents and a way to disperse the platelets on a suitable substrate. The end result would be a sample that had still undergone a process as rigorous as the earlier methods with cellulose paper, and which still resulted in a loss of palladium deposits. The spin coating method required longer processing times when compared to the direct dispersal method.

2.4.b Experimental Methods

Microscope cover glass slides (Fisher Scientific) were cut into square pieces measuring 5 mm by 5 mm. Less than 1 milligram of graphite powder (Fisher, BET surface area 200 m^2) was placed on a separate uncut cover glass slide. A 5 mm by 5 mm piece was then placed on top of the graphite powder. By pressing down on the glass piece and gently moving the 5 mm by 5 mm piece in a circular motion the graphite platelets were immobilized on the glass piece. Excess platelets were washed off the surface using a few milliliters of acetone. The glass slide was then set up for field application (Figure 2.9). Electrolyte used consisted of 1.0 mM palladium chloride in a 1:1 mixture of acetonitrile: toluene. For all experiments the field applied was 3000 V/cm.

In this study DC fields were compared to pulsed fields which had frequencies of 500 Hz and 50% duty cycle.

After field application the slides were placed in 100 mL HPLC grade acetonitrile for 5 minutes to wash away excess salts. Samples were then allowed to air dry and prepared for characterization on a scanning electron microscope (SEM). For SEM preparation samples were mounted on SEM stubs and coated with either gold or gold palladium. Samples were then examined on an AMRAY 1830, or a JEOL 6300.

2.4.c Results

Palladium deposits were found on one area of the platelets and an area on the platelets opposite to the deposit was devoid of any metal deposit (Figure 2.10). Various numbers of separate platelets combined to form agglomerated structures. The platelet agglomerates had metal deposit on one general area and no deposit anywhere else on the agglomerate (Figure 2.10). The metal deposits varied from large ramified deposits seen on separate platelets (Figure 2.10c, and 2.10d), to large deposits that covered one general area of an agglomerate of platelets (Figure 2.10a, 2.10b, and 2.11b). A low magnification image of a few agglomerates shows the deposits growing off one end to be aligned (Figure 2.11b). There was no significant difference between the pulsed samples and the DC field samples. High magnification image (Figure 2.11a) revealed the palladium deposits consist of spherical clusters. The clusters build up to form larger spherical clusters. When examining isolated single platelets surrounding the agglomerates; typically the isolated single platelets near the agglomerates did not have any palladium deposit (Figure 2.10a).

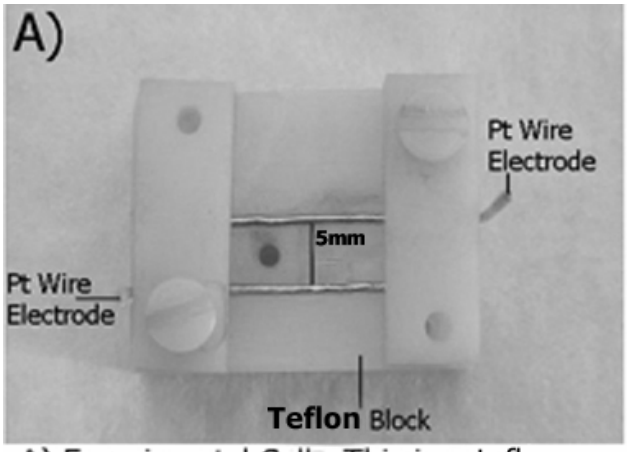

A) Experimental Cell. This is a teflon block that has been machined to hold a sample in a small depression in the center and two Pt wire electrodes.

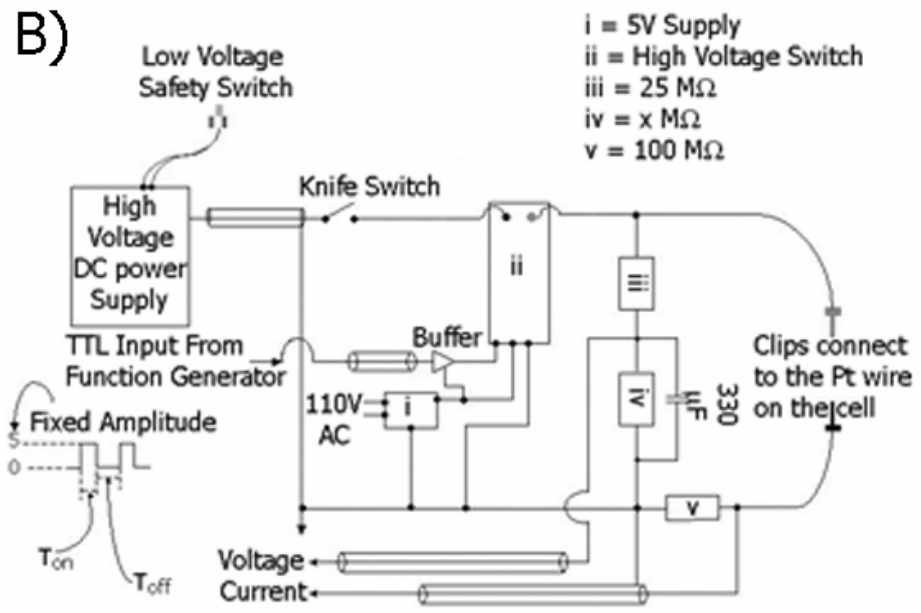

B) Schematic showing the setup for the power supply function generator, and the high voltage switch.

Figure 2.9. Picture of the experimental cell used to hold the glass pieces, and a schematic showing the field application set up.

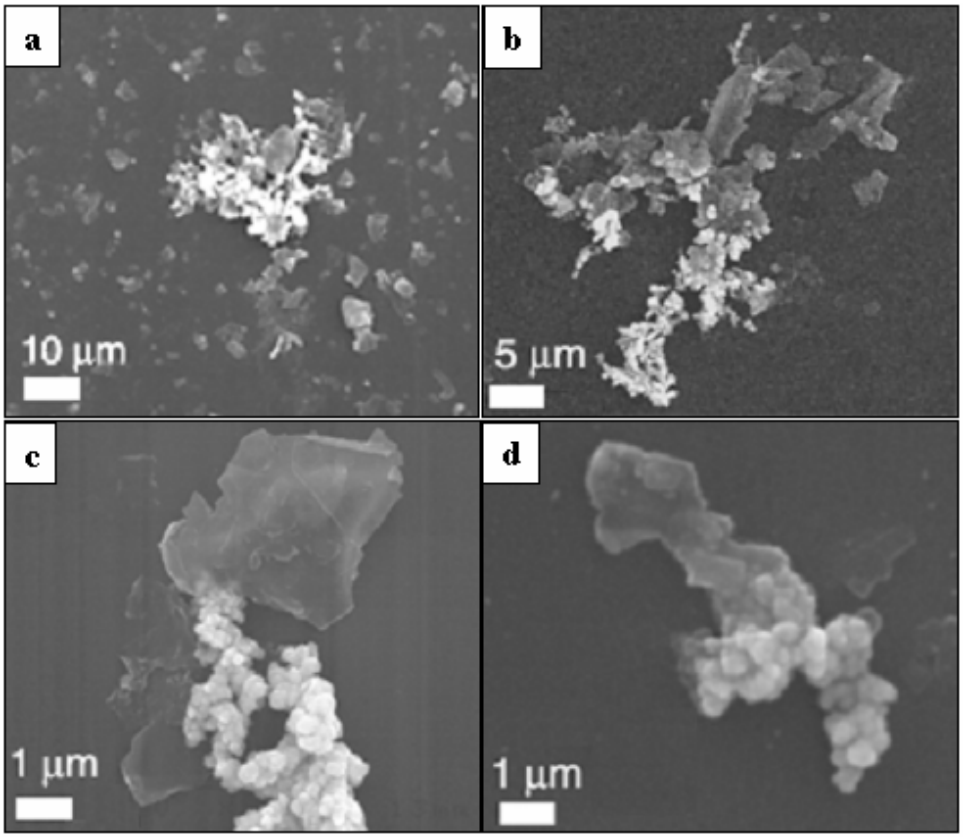

Figure 2.10. These are SEM micrographs of the graphite platelets immobilized on glass microscope slides. Electric field = 3000 V/cm. Image (a) and (c) were exposed for 300s, (b) was exposed for 450s, and (d) was exposed for 900s. In (d) the field was applied as a series of square wave pulses at a frequency of 500Hz and with a duty cycle of 50%.

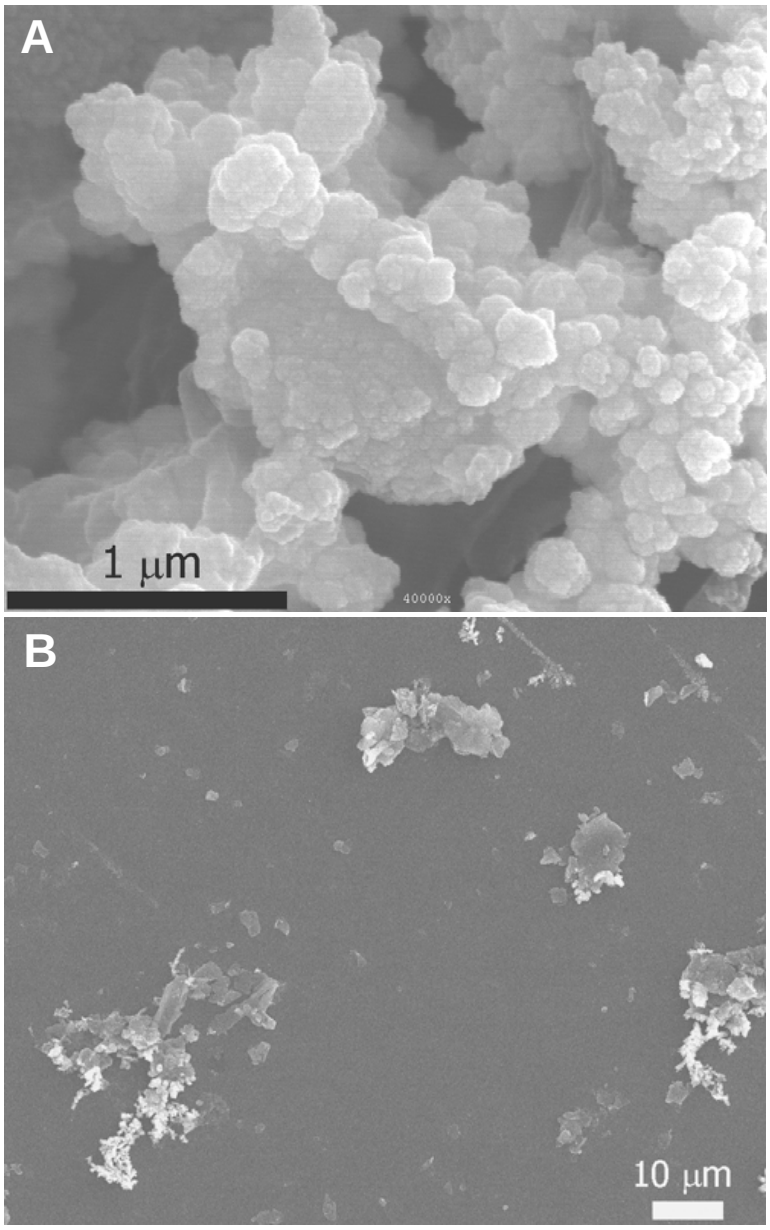

Figure 2.11. A is a high magnification of palladium deposit off of graphite platelets. B is an unrelated low magnification image showing palladium deposit on one area of various platelet agglomerates. For both samples a dc electric field at 3000V/cm was applied for 450seconds.

2.4.d Discussion

One important advantage of the SEM study of the platelets was the ability to image the platelets after deposition with the minimum amount of processing. With little processing from electrodeposition to SEM examination certain conclusions could be drawn. First, the SEM studies revealed the agglomeration of the graphite platelets. This confirmed earlier conclusions with the experiments with methylene blue. The methylene blue experiments showed sonication increased the total surface area of the graphite available for palladium deposition. This increase was attributed to the breaking up of agglomerates by the sonication; however, agglomerates were never found with the TEM studies.

The agglomeration of the platelets dominates the system. Agglomerates act as one large particle, and in bipolar electrochemistry larger particles in the applied electrical field will have a larger potential across their diameter when compared to smaller particles.[12,13,16,17] The larger potential on the agglomerates will result in preferential nucleation and subsequent growth of palladium deposit on the agglomerate, and depletion of the palladium ions in the vicinity of the agglomerate. In conventional electrochemistry the nucleation density increases with the applied potential. In the current system a similar observation is expected and the large agglomerates will have a much higher nucleation density of palladium metal than the smaller isolated platelets. Continual deposition of metal occurs preferentially on metal deposits already present such as nucleated deposits. This favors growth of palladium on the areas were there is a greater density of nucleation sites i.e. the agglomerates. The depletion of palladium ions in the

vicinity of the agglomerate will be aided by electroconvective forces. Such forces were observed in experiments involving spatially coupled bipolar electrochemistry (SCBE).[18]

An alternative explanation is that the platelets surrounding the agglomerate are not large enough for the induction of the minimum potential required for palladium electrodeposition. This alternative explanation is unlikely because a number of the isolated platelets surrounding the agglomerate in the image (Figure 2.10a) are above 2 μm. The length of 2 μm is significant because in earlier experiments this was the length of the smallest platelet found with palladium deposit (Figure 2.4a). In terms of the synthesis of BEC this result suggests that for the bipolar electrodeposition of palladium onto graphite platelets the agglomeration of platelets has to be broken up. This is in line with the earlier results obtained when the platelets were sonicated before dispersion.

In spite of the agglomerates deposition did occur on the separate platelets. SEM micrographs were obtained (Figure 2.10c and Figure 2.10d) that did show palladium deposits growing off the ends of isolated graphite platelets. From SEM studies no significant differences could be seen between pulsed samples and DC electric field. On the separate platelets, the long deposition times resulted in large long ramified deposits off one end of the graphite platelets. These long deposits were not seen in the earlier TEM studies, and asserted the earlier conclusion that the larger deposits were falling off the graphite platelets when processed for TEM. For the synthesis of BECs much shorter deposition times would be needed. The long deposition times however could be used for the growth of nanowires between isolated conductive micrometer sized structures.

The SEM studies revealed that the graphite platelets were a very inhomogeneous substrate; specifically, the platelets were all different shapes and sizes. The shape and

size differences did not hinder electrodeposition onto the platelets. The differences in size and shape however did make direct comparison between platelets difficult and necessitated the need for a more uniform substrate.

2.4.e Conclusions

By applying a 3000 V/cm electrical field bipolar electrochemistry can be used to deposit palladium from a 1.0 mM solution of palladium (II) chloride (1:1 acetonitrile: toluene) onto isolated graphite platelets. The electrical field can be applied as a series of square wave pulses (50% duty cycle, 500–20000 Hz) or as a DC electrical field. Under these conditions the average lengths, of the platelets modified, varied from 2–10 μm. When examined under TEM, the palladium deposits consisted of 2–5 nm nanocrystals, which were, either surface bound to the platelets or were part of highly ramified structures. Catalytic methods (reduction of methylene blue) used to determine the palladium dispersion on the platelets found no significant differences between the dispersion and the frequency used to prepare the samples; however, sonication of the platelets before field application did increase the palladium dispersion.

Experiments using platelets on a glass substrate conclusively demonstrated that the platelets were agglomerating, the agglomeration resulted in the majority of the palladium depositing as large ramified structures on the agglomerated platelets, and when deposition did occur on the individual platelets it was in the form of long and highly ramified structures. In light of these results, for the synthesis of BECs much shorter deposition times are needed and it is imperative the platelet agglomerates are separated

into individual platelets. The separation can be achieved by the sonication of the platelets before deposition.

Possible additional work in this area would be to synthesize the BECs using different pulsing regimes, for example, very short on-times (less than 1 millisecond) with long off-times (20 times greater than the on-time used). In addition to the modified pulsing regime, short deposition times should be used. A recommended time scale for the short deposition times would include 20 seconds or less (compared to 900 seconds used). Once the ideal parameters have been established for palladium other metals should be explored, examples include, but should not be limited to, gold or nickel. Then the deposition of two different metals on opposite areas of the platelets and on the same area can be compared in the appropriate catalytic reactions.

References

1. Auer, E.; Freund, A.; Pietsch, J.; Tacke, T. Carbons as Supports for Industrial Precious Metal Catalysts. *Appl. Catal. A.* **1998,** *173,* 259-271..

2. Rodriguez-Reinoso, F. The Role of Carbon Materials in Heterogeneous Catalysis. *Carbon* **1998,** *36,* 159-175.

3. Toebes, M. L.; Van Dillen, J. A.; De Jong, K. P. Synthesis of Supported Palladium Catalysts. *J. Mol. Catal. A: Chem.* **2001,** *173,* 75-98.

4. Blaser, H.-U.; Indolese, A.; Schnyder, A.; Steiner, H.; Studer, M. Supported Palladium Catalysts for Fine Chemical Synthesis. *J. Mol. Catal. A: Chem*. **2001,** *173,* 3-18.

5. Li, F.; Zhang, B.; Dong, S.; Wang, E. A Novel Method of Electrodepositing Highly Dispersed Nano Palladium Particles on Glassy Carbon Electrode. *Electrochimica. Acta* **1997,** *42,* 2563-2568.

6. Popov, K.I.; Pavlovic, M.G. Electrodeposition of Metal Powders With Controlled Particle Grain Size and Morphology. In *Modern Aspects of Electrochemistry*; Conway, B. E., Bockris, J. O. M., White, R. E., Eds.; 24; Plenum: New York, 1993, pp 299-391.

7. Natter, H.; Hempelmann, R. Nanocrystalline Copper by Pulsed Electrodeposition: The Effects of Organic Additives, Bath Temperature, and pH. *J. Phys. Chem.* **1996,** *100,* 19525-19532.

8. Penner, R. M. Mesoscopic Metal Particles and Wires by Electrodeposition. *J. Phys. Chem. B* **2002,** *106,* 3339-3353.

9. Lu, D.-L.; Tanaka, K.-I. Au, Cu, Ag, Ni, and Pd Particles Grown in Solution at Different Electrode Potentials. *J. Phys. Chem. B* **1997,** *101,* 4030-4034.

10. Kost, K. M.; Bartak, D. E.; Kazee, B.; Kuwana, T. Electrodeposition of Palladium, Iridium, Ruthenium, and Platinum in Poly(4-vinylpyridine) Films for Electrocatalysis. *Anal. Chem.* **1990,** *62,* 151-157.

11. Maksimov, Y. M.; Kolyadko, E. A.; Shishlova, A. V.; Podlovchenko, B. I. Electrocatalytic Behavior of a Palladium–Polyaniline System Obtained by Electrodepositing Palladium into a Preliminarily Formed Polyaniline Film. *Russ. J. Electrochem.* (*Engl. Transl.*) **2001,** *37,* 777-781.

12. Bradley, J.-C.; Ma, Z. Contactless Electrodeposition of Palladium Catalysts. *Angew. Chem. Int. Ed*. **1999,** *38,* 1663-1666.

13. Bradley, J.-C.; Babu, S.; Mittal, A.; Ndungu, P.; Carroll, B.; Samuel, B. Pulsed Bipolar Electrodeposition of Palladium onto Graphite Powder. *J. Electrochem. Soc*. **2001,** *148,* C647-C651.

14. Bradley, J.-C.; Samuel, B. SMIRP-A Systems Approach to Laboratory Automation. *JALA* **2000,** *5,* 48-53.

15. Jana N. R.; Pal, T. Redox Catalytic Property of Still-Growing and Final Palladium Particles: A Comparative Study. *Langmuir* **1999,** *15,* 3458-3463.

16. Goodridge, F. Some Recent developments of Monopolar and Bipolar Fluidized Bed Electrodes. *Electrochim. Acta.* **1977,** *22,* 929-933.

17. Fleischmann, M.; Ghoroghchian, J.; Rolison, D.; Pons, S. Electrochemical Behavior of Dispersions of Spherical Ultramicroelectrodes. *J. Phys. Chem.* **1986,** *90,* 6392-6400.

18. Bradley, J.-C.; Dengra, S.; Gonzalez, G. A.; Marshall, G.; Molina, F. V. Ion Transport and Deposit Growth in Spatially Coupled Bipolar Electrochemistry. *J. Electroanal. Chem.* **1999,** *478,* 128-139.

Chapter 3: Development of Bipolar Electrodeposition as a Tool for Nanotechnology: Part 1 from Platelets to Nanofibers

3.1 Summary Statement

The original goal of the work presented in this chapter, was to deposit palladium metal onto the ends of carbon nanofibers (CNFs) using bipolar electrochemistry. After establishing the ideal parameters needed for the deposition of palladium metal, the next step in the project was to develop an experimental technique that could produce milligram quantities of the functionalized CNFs.

3.2 Introduction

Bipolar electrodeposition is a unique method that can be used to modify isolated micrometer sized structures.[1,2,3] Practical application of bipolar electrodeposition on the micrometer scale was successfully demonstrated with the synthesis of palladium supported on carbon catalysts. The resulting catalysts, called bipolar electrodeposited catalysts (BECs), were shown to be catalytically active in two different reduction reactions.[2,3]

One of the underlying problems encountered during the studies on the synthesis of BECs was the graphite platelets. As a substrate for the synthesis of BECs graphite platelets are a non-ideal substrate, and the reason for this is the non-uniform shapes and sizes of the graphite platelets. To address this issue a more uniform substrate was selected and the substrate chosen was carbon nanofibers. Although the impetus for the original work was to synthesize BECs, it was immediately realized that this initial transition to carbon nanofibers expanded on the capabilities of bipolar electrodeposition.

3.3 Carbon Nanofibers

Carbon nanofibers are a unique tubular form of carbon with diameters that vary from tens to hundreds of nanometers and lengths ranging from a few to hundreds of micrometers. Although there is a large amount of size overlap between carbon nanotubes and carbon nanofibers, there are significant structural differences. Carbon nanofibers consist of graphitic layers that stack either at an angle, perpendicular or parallel to the tube axis (Figure 3.1).[4,5,6,7,8] A carbon nanotubes' wall consists of continuous graphitic layers composed of carbon atoms that are arranged in an ordered repeating pattern with no defects. This inherent feature of carbon nanotubes has been used to describe carbon nanotubes as single crystals. In contrast the wall of a carbon nanofiber has numerous defects and, because of this, it is not a single crystal.[8] A simpler way to distinguish between carbon nanofibers and carbon nanotubes is to define nanotubes as graphitic layers of carbon arranged around a hollow central core, and carbon nanofibers as graphitic layers arranged around a filled central core.[7]

Due to the unique characteristics of carbon nanofibers there is a wide range of applications for carbon nanofibers. The thermal and chemical stability, high surface area, low ohmic resistance, and the surface properties are the unique qualities that are exploited when carbon nanofibers are used as catalytic support materials.[4,6,7,9,10] As an additive in polymers carbon nanofibers have been shown to increase the thermal, mechanical, and electrical properties of a variety of polymer matrices.[11]

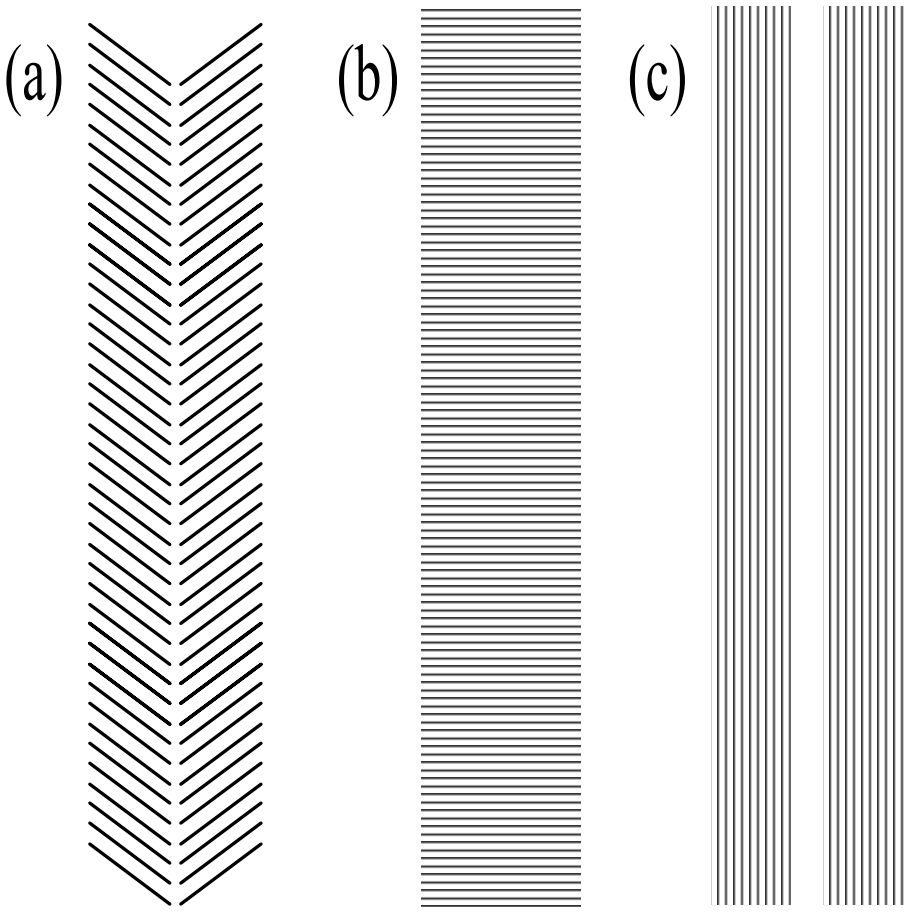

Figure 3.1. The graphitic layers in carbon nanofibers can adopt different configurations. In part (a) the graphitic layers are arranged at an angle to the tube axis in the herring bone configuration. In (b) the graphitic layers are stacked perpendicular to the tube axis. In (c) the graphitic layers are arranged parallel to the tube axis. The gap in (c) can be filled with amorphous carbon or more layers.[4 – 7]

The surface at the tip of a carbon nanofiber possesses a large amount of exposed edges due to the arrangement of the graphitic layers. This, along with carbon nanofiber's good electrical conductivity, may provide a good pathway for the emission of electrons from the nanofiber. As a result carbon nanofibers have been investigated as components in electron field emitting devices.[12,,13,14]

Another highly active area of research, and sometimes controversial, is the use of carbon nanofibers as hydrogen storage materials.[4,5,15]

In general carbon, in various forms, has been used as an electrode material due to its stability at positive potentials, wide potential window in various systems (aqueous and non-aqueous), good response in stripping voltammetry applications, low cost, and low background current. Carbon nanofibers could prove to be much better electrode materials (once the cost of manufacture is reduced) due to the greater conductivity, larger surface area, and increased stability.[16] The combination of these properties is why carbon nanofibers have been explored as electrode materials for a technologically important specialized device i.e. fuel cells[6,17]

Carbon nanofibers have been investigated as electrode materials for various electrochemical based applications. Bessel et al. and Lukehart et al. studied the use of platinum and platinum-ruthenium supported on carbon nanofibers as electrocatalysts for methanol oxidation.[6,17] In both cases the authors prepared the electrocatalysts using standard wet chemical techniques.[6,17] Using cyclic voltammetry, Chen et al. deposited platinum onto carbon nanofibers and demonstrated good electro-catalytic activity towards methanol oxidation at low platinum loading.[18] Cyclic voltammetry experiments have been conducted to study whether carbon nanofibers can be used for the effective

electrochemical storage of hydrogen. These studies revealed modest storage capacities below the required capacity set by the US department of energy.[19,20] In sonoelectrochemistry carbon nanofibers were grown on a ceramic backbone and used as electrodes. The electrodes were found to have an increased contact time with the redox active species in the system.[21] Applications involving the use of carbon nanofibers as potential electro-analytical electrodes have been pursued.[22,23,24,25]

The work presented in this thesis is not the first example of metal deposition on carbon nanofibers. Zinc and lead have been electrodeposited onto carbon nanofibers. [16,22] In these examples the carbon nanofibers were used as a web of material supported on various substrates that provided support and a direct connection between the nanofibers and the power supply. These studies were done to access the feasibility of using carbon nanofibers as electrodes for stripping voltammetry.[16,22] Another example of metal deposition on carbon nanofibers is the deposition of gold onto individual carbon nanofibers. Using extensive micro-fabrication techniques direct contact to the individual nanofibers was achieved. Unlike previous work this study was able to use individual carbon nanofibers as the electrodes in various voltammetry experiments as well as in the deposition of gold. At the time of the writing of this thesis (besides the work presented in this thesis) this is the only example where individual carbon nanofibers have been electrochemically modified by the deposition of a metal.[24]

From a survey of the literature, there is only one example[24] where individual carbon nanofibers are addressed and modified using any kind of electrochemistry. There are no examples where bipolar electrochemistry has been used to modify carbon nanofibers. The immediate goal of the project in this chapter is to functionalize one tip of a carbon

nanofiber with palladium metal. The long term goal of the project in this chapter is to produce milligram quantities of the functionalized carbon nanofibers. This project developed from the original BEC project and thus the carbon nanofibers were initially investigated as a substrate for the synthesis of BECs.

3.4 Bipolar Electrodeposition onto Carbon Nanofibers Immobilized on a Glass Substrate

3.4.a Theoretical Considerations

A 3000 V/cm electric field was used to electrodeposit palladium on graphite platelets immobilized on the glass substrate (chapter 2). One of the conclusions from these initial experiments was that palladium could be deposited onto platelets that were 2-10 μm in length. Theoretically bipolar electrochemistry can be used to modify any isolated conductive substrate, and therefore bipolar electrodeposition of palladium can be done on substrates other than graphite platelets that are 2-10 μm in length i.e. the carbon nanofibers. This assertion is supported by examining the relationship between applied electric field and the potential difference across a sphere, an irregularly shaped object and a cylindrical object (Figure 3.2). Substrates in line with the electric field with the same overall length will have the same potential difference across the length of the substrate. Even though the nanofibers have diameters well below a micrometer the only factor to consider in modifying the nanofibers is the length of the nanofiber that is in line with the applied electrical field. Thus a carbon nanofiber with a length of 10.0 μm in a 3000 V/cm electrical field will have a potential of 3.0 V.

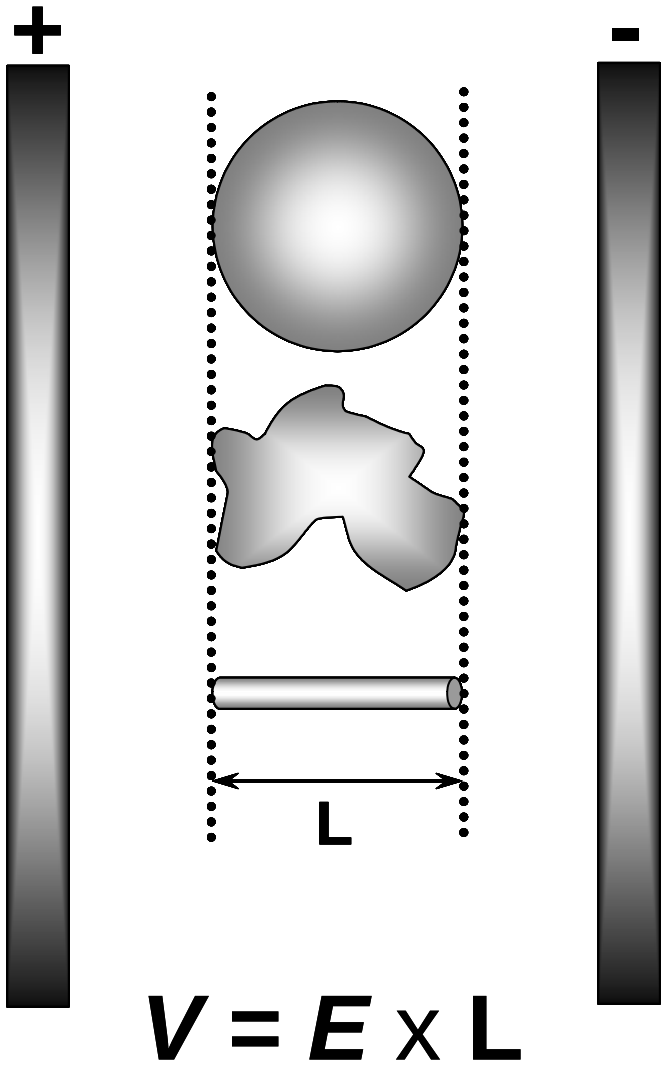

Figure 3.2. Different shaped particles with the same lengths in line with an applied electrical field (*E*) will have the same potential (*V*) across the length (L) of the particle.

From earlier experiments on graphite platelets[1,2] this is greater than the required potential for palladium deposition.

3.4.b Experimental Methods

All carbon nanofibers used were obtained from Applied Sciences Inc. Nanofibers were used without any additional purification steps. Glass cover slips (Fisher Scientific) were cut into 3 mm by 3 mm pieces. Carbon nanofibers were immobilized onto the glass substrates using simple frictional methods. This was done by placing a small amount (less than 1.0 mg) of the nanofibers on an uncut glass cover slip. The small amount of carbon nanofibers was then covered with a 3 mm by 3 mm piece of glass cover slip. By gently pressing down on the 3 mm by 3 mm piece and moving the 3 mm by 3 mm piece in a circular motion, the nanofibers were immobilized on the 3 mm by 3 mm glass piece. Excess and loose nanofibers were removed by rinsing the glass pieces with a few milliliters of acetone. Once dry the glass piece with the carbon nanofibers was placed in an experimental cell and set up for field application (Figure 3.3).

For all electrical field applications used the electrical field used was 3000 V/cm. The electrolyte used was 1.0 mM palladium chloride in 1: 1 (v/v) acetonitrile/toluene (both dried over calcium hydride). Initial experiments used DC electrical fields, which were applied by bypassing the high voltage switch (Figure 3.3). In these initial experiments the electrical field was applied for 120-, 240-, and 480 seconds. Comparative experiments were done with a pulsing (500 Hz, 50% duty cycle) DC electrical field. The pulsed DC electrical fields were applied using the high voltage switch for either 240 seconds or 480 seconds. Experiments with shorter field times were done with 10-, 20-,

40-, and 80second dc fields. The shorter timed DC electrical fields were applied using a single pulse from the function generator. The on-time from the single pulse from the function generator controlled the amount of time the voltage, through the high voltage switch, was applied across the electrodes.

To remove excess reagents after field application the experimental cell was placed in 100mL of HPLC grade acetonitrile for five minutes. After the acetonitrile rinse the cell was allowed to air dry and the glass piece was mounted on a scanning electron microscopy (SEM) stub for SEM characterization. SEM work was done on either an Amray 1830 at Drexel University, or a JEOL 6300F at Lehigh University.

For some samples (10-, 20- and 40 seconds) the nanofibers were removed from the glass surface and mounted on a 200 mesh copper transmission electron microscopy (TEM) grids (Holey carbon membrane support, obtained from SPI, Inc). Removal of the nanofibers was accomplished by placing the glass piece in a 2.0 mL glass vial and then adding 0.5 mL of acetone. The nanofibers were removed from the surface by scratching the glass piece with the tip of a Pasteur pipette. Both surfaces of the glass piece were repeatedly scratched with the pipette to ensure that the nanofibers were gathered from the correct surface. Using a 10.0 microliter syringe 50 to 100 microliters of the suspension was drop dried onto a TEM grid. Preliminary TEM examination was done on a JEOL 100CX2 at Drexel university, and follow up TEM examinations were done on a JEOL 2000FX at Lehigh university.

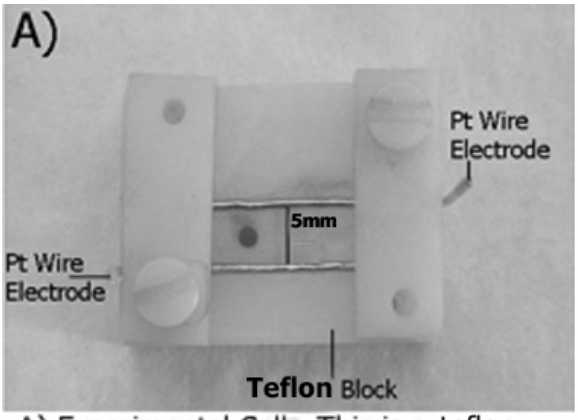

A) Experimental Cell. This is a teflon block that has been machined to hold a sample in a small depression in the center and two Pt wire electrodes.

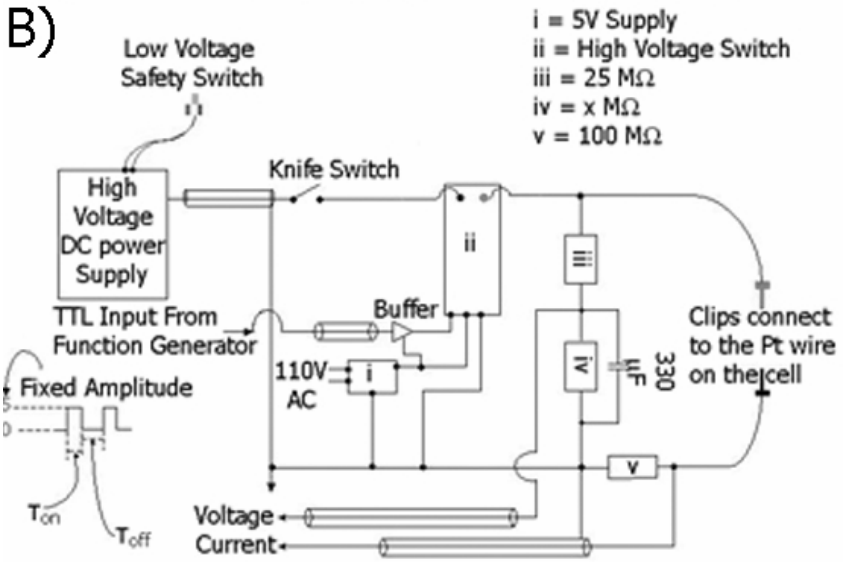

B) Schematic showing the setup for the power supply function generator, and the high voltage switch.

Figure 3.3. Picture and schematic of the experimental apparatus used for electrical field application.

3.4.c Results

Carbon nanofibers with palladium on one tip were found on all samples at the different regimes attempted. After removing the carbon nanofibers from the glass piece, nanofibers with palladium deposit on one tip were found. Figure 3.4 presents such an example. The carbon nanofiber is approximately 15.0 μm in length, with the palladium deposit extending for a total length of 4.0 μm. The deposit covers the tip of the nanofiber and extends back along the length of the carbon nanofiber, leaving about 11.0 μm of the nanofiber uncovered. Note that the opposite tip is clear of deposit.

Figure 3.5 is a combination of TEM and SEM micrographs which illustrate the increase in the amount of palladium with the increase in the electrical field time. The SEM images (Figure 3.5 E - H) clearly show palladium deposits on only one tip of the carbon nanofibers. The TEM micrograph of the nanofiber with no deposit on the tip shows a separate film-like structure with numerous bubbles; the film is located inside the nanofiber (Figure 3.5A).

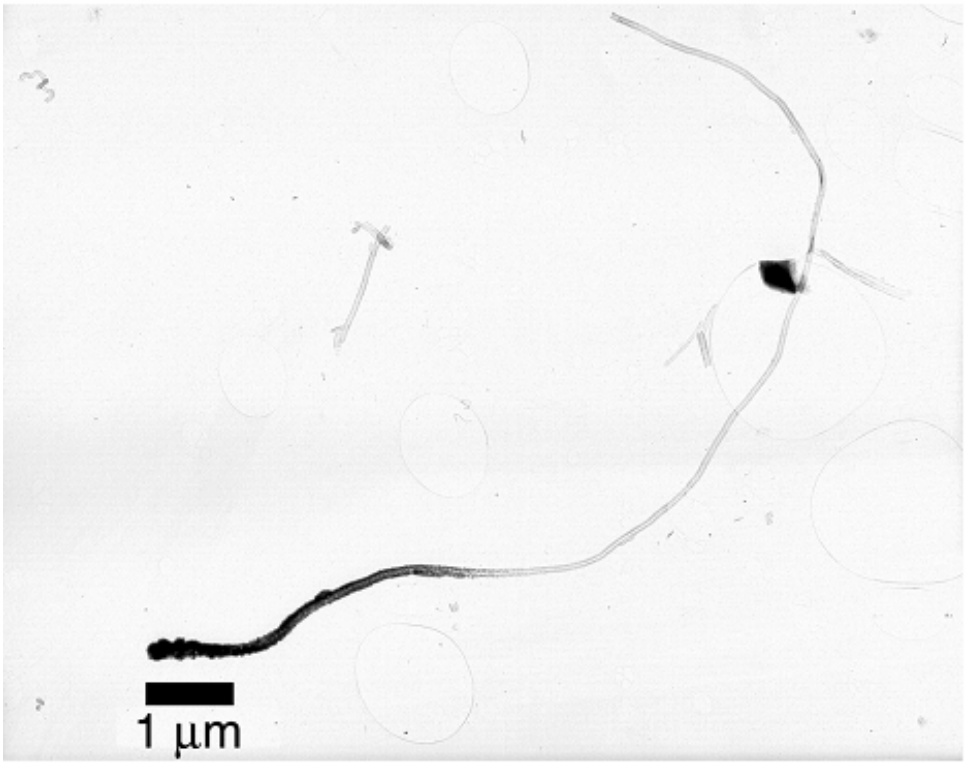

Figure 3.4. A TEM micrograph of a carbon nanofiber with a deposit of palladium on one tip of the carbon nanofiber. A 3000V/cm dc electrical field was applied for 40seconds, and the solution used was 1.0 mM palladium (II) chloride in a solvent mixture of 1: 1 acetonitrile/toluene (v/v, both dried over calcium hydride). TEM examination was done on a JEOL 2000 FX with an accelerating voltage of 200 kV.

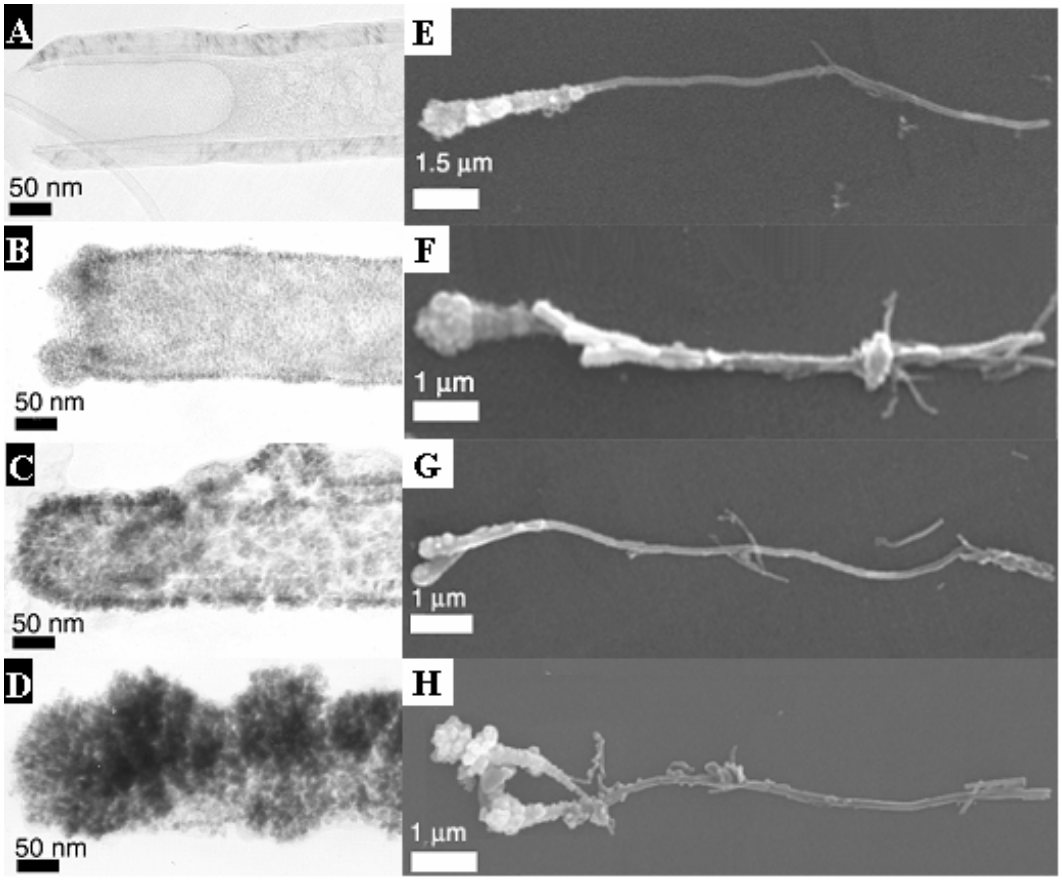

Figure 3.5. A series of TEM and SEM micrographs of carbon nanofibers with palladium deposit on one tip. For all samples shown the electrical field was 3000 V/cm, and the electrolyte used was 1.0 mM palladium (II) chloride in a mixture of 1: 1 (v/v) acetonitrile: toluene (dried over calcium hydride). The electrical field application time for the samples in TEM micrographs A – D was 0-, 10-, 20- and 40seconds. The time for the samples presented in SEM micrographs E – H was 80-, 120-, 240-, and 480seconds. TEM images were obtained on a JEOL 2000FX with an accelerating voltage of 200 kV. SEM images E and H were obtained on an Amray 1830, and SEM images G and H were obtained on a JEOL 6300F. For all SEM imaging the samples were coated with gold.

Figure 3.6 is an example of nanofibers that were not modified while a nanofiber in the vicinity was modified with palladium deposit on one tip. The nanofiber with deposit has an approximate length of 8 μm, and the two unmodified nanofibers have lengths of 4-, and 5 μm. The two unmodified nanofibers are almost perpendicular to the nanofiber with palladium deposit.

3.4.d Discussion

When a carbon nanofiber is immersed in a suitable electrolyte and is exposed to an electrical field with sufficient magnitude, a cathode-anode pair is induced on the isolated carbon nanofiber. As a result the palladium will deposit on the cathode of the isolated carbon nanofiber and thus on only one tip of the carbon nanofiber. This is characteristic of bipolar electrodeposition and it is why palladium found on one tip of a carbon nanofiber is indicative of a bipolar mechanism for electrodeposition, as seen in the various SEM and TEM images (Figures 3.4 -3.6).

The change in potential across a carbon nanofiber, in line with the applied electrical field, can be estimated by using the simple relationship between the length of the carbon nanofiber and the applied electrical field (Figure 3.2). A 15 μm carbon nanofiber (Figure 3.4) in a 3000 V/cm field will have a potential drop of 4.5 V across its length. In a similar system, the measured reduction potential for palladium ions in 1: 4 acetonitrile/toluene was 700 mV vs Ag/AgCl in acetonitrile.[26] A direct comparison between the literature value and the calculated value on the nanofiber cannot be made; however, if we assume the oxidation reaction on the nanofiber is Cl^-/Cl_2, then it is likely that the potential at the cathode-end of the nanofiber lies above a similar range.

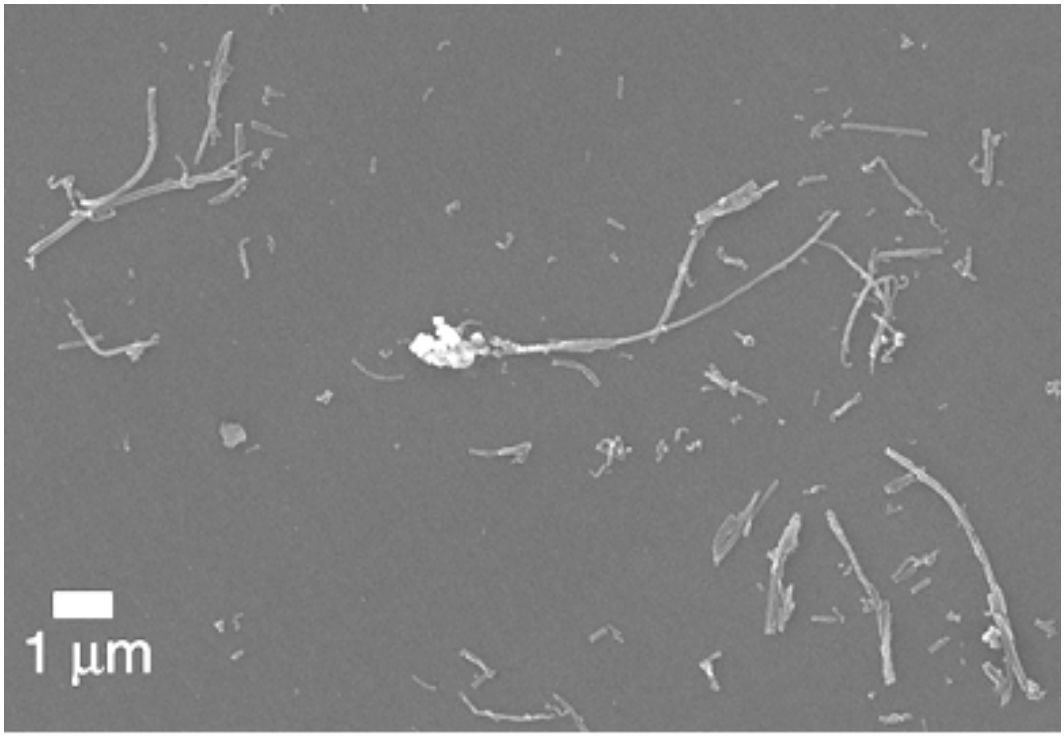

Figure 3.6. A SEM micrograph of a sample that was exposed to a pulsed dc electrical field (3000V/cm, 500Hz, 50% duty cycle) for 480seconds in a 1.0 mM palladium (II) chloride solution in 1: 1 acetonitrile: toluene (v/v, both dried over calcium hydride). The sample was gold coated and the SEM analysis was done on a JEOL 6300F.

It is also possible to estimate the minimum length a carbon nanofiber has to be in order to be modified (i.e. palladium on one tip) in the current system. Before making this estimate a reasonable value for the potential required to deposit palladium from the electrolyte used is needed. In earlier work on the synthesis of bipolar electrodeposited catalysts the smallest graphite platelet with metal deposit was 1.5 μm across.[1,2] A length of 1.5 μm corresponded to a potential of 0.45 V across the platelet. From this empirical data the expected minimum length for the modification of a carbon nanofiber is estimated to be 1.5 μm.

Using a 3000 V/cm pulsed DC electrical field with a 1.0 mM palladium chloride solution, the amount of palladium deposited on the tip of a carbon nanofiber can be controlled by varying the time of the applied electric field. Figure 3.5 shows the increase in the amount of palladium deposit on the tips of carbon nanotubes. The increase stops after 80 seconds. This maximum length of the palladium deposits, under these conditions, is a result of the depletion of palladium ions in the surrounding electrolyte. The main source of the depletion is the cathode feeder electrode. On the macro-scale, the Bradley research group was able to grow copper wires off isolated copper beads. In this example of bipolar electrochemistry, the deposit stopped growing once it contacted the opposite electrode. The micrometer sized wires grown by this method kept growing due to a continual supply of metal ions from the dissolution of the copper beads.[27] In the current system there is no replenishment of the palladium; however, the results on the macro-scale suggest that longer structures grown off of the carbon nanofibers could be achieved with a continuous supply of palladium ions. Application of a DC electrical field for 10 seconds gives a thin uniform layer of palladium nanoparticles on the nanofiber

(Figure 3.5B). This suggests that for any further exploration on the synthesis of bipolar electrodeposited catalysts using carbon nanofibers as a substrate; a 3000 V/cm field for a period of 10 seconds or shorter should be used. The palladium nucleates along the carbon nanofiber on areas were the potential is equal to or greater than the minimum potential required for palladium ions to reduce. Growth then continues preferentially on the nucleation sites (seen as coverage over the body of the nanofiber in Figure 3.5B) and more-so on areas with higher potentials (seen as 'horns' of palladium off the tip of the nanofiber in Figure 3.5B). This is why palladium deposit is seen back along the nanofibers. The point with the highest potential is at the tip of the nanofiber, and it is the area in which palladium deposition will occur most favorably. The result is the palladium will grow off the tip of the nanofiber. A secondary effect that will favor the continued growth off the tip is as the length of the nanofiber increases the potential drop across the nanofiber increases with a maximum at the growing tip.

At set electrical field strength, the potential drop across a carbon nanofiber depends on the length of the carbon nanofiber. As a result only carbon nanofibers with a specific minimum length, 1.5 μm for palladium deposition, will have palladium deposit on one tip. This size selective deposition of a metal onto the tip of a carbon nanofiber introduces a secondary facet to bipolar electrodeposition. Another characteristic feature of bipolar electrodeposition is the dependence of the angle of the carbon nanofiber to the applied electric field. Palladium deposits only on carbon nanofibers aligned with the applied electrical field. In Figure 3.6 the palladium deposits only on the 7 μm nanofiber that is aligned with the applied field. The two nanofibers that are perpendicular to the modified nanofiber do not have any deposit. These two nanofibers are 4 and 5 micrometers in

length, which is above the minimum length required to induce the requisite potential drop for palladium electrodeposition. This demonstrates the dependence of the nanofibers orientation with the applied field for the deposition of palladium on the tip.

At the time of the study SEM imaging of samples that had been exposed to an electrical field for 40 seconds and below did not show any clear deposits (Figure 3.7). This necessitated the development of a method to remove the nanofibers from the glass and mount them on a TEM grid. The process of removing the nanofibers from the glass does not seem to remove a significant amount of the deposit from the tip. The TEM micrographs, at various magnifications, do not show any evidence of the deposits falling off the nanofibers (Figure 3.8). Any such evidence would appear as noticeable gaps in the deposits on the nanofibers. This shows how well the palladium deposits have adhered to the surface of the nanofibers. This is an encouraging result and suggests loss of precious metal in catalytic applications from carbon nanofiber supports would be low.

A high resolution image of a carbon nanofiber after a 10 second electrical field exposure reveals a uniform coverage of palladium nanocrystals. The palladium nanocrystals are 3-5nm in diameter (Figure 3.5B and Figure 3.8A). After 20 seconds there is an increase in the amount of palladium deposit on the tips of the nanofibers. The size of the deposits has increased slightly from 3-5 nm to 8-12 nm. After 40 seconds the palladium deposits are starting to form larger spherical clusters, at this stage of deposition the nanocrystals have grown to between 12- and 18 nm. By 80 seconds the deposits resemble the large ramified spherical clusters seen growing off the graphite platelets. After 80 seconds little change in the deposit is seen.

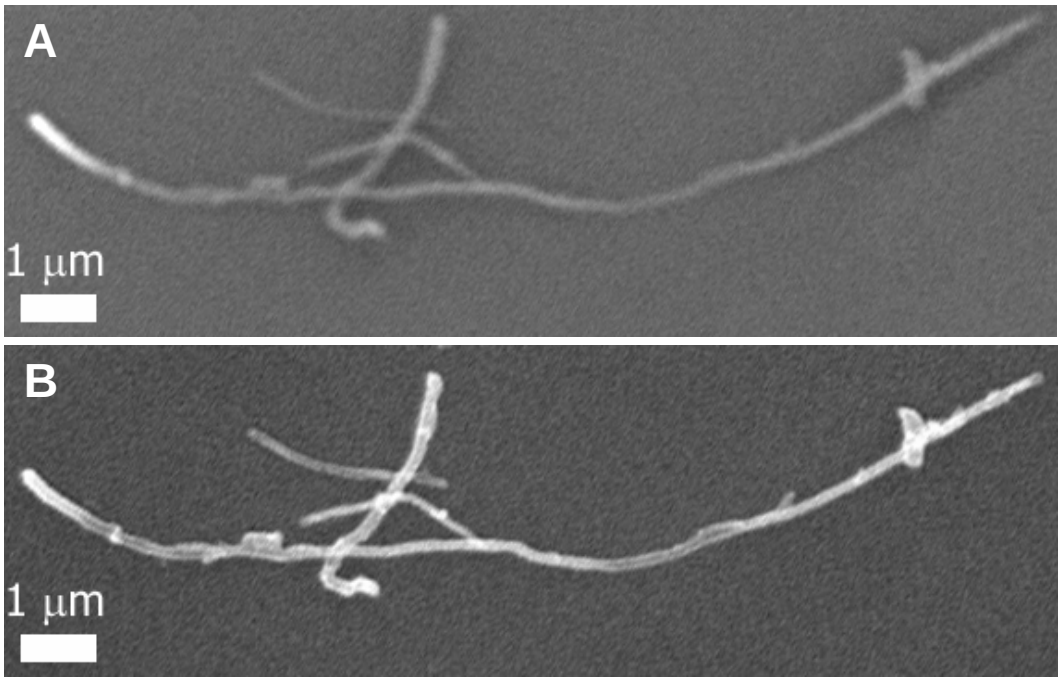

Figure 3.7. The sample was exposed to a 3000 V/cm dc electrical field for 40 seconds (1.0 mM palladium chloride, 1: 1 acetonitrile: toluene (v/v)). Image (A) was taken in backscattering mode. The bright structure at the tip in (A) is the palladium deposit. SEM micrographs were obtained on an Amray 1830. The sample was coated with gold.

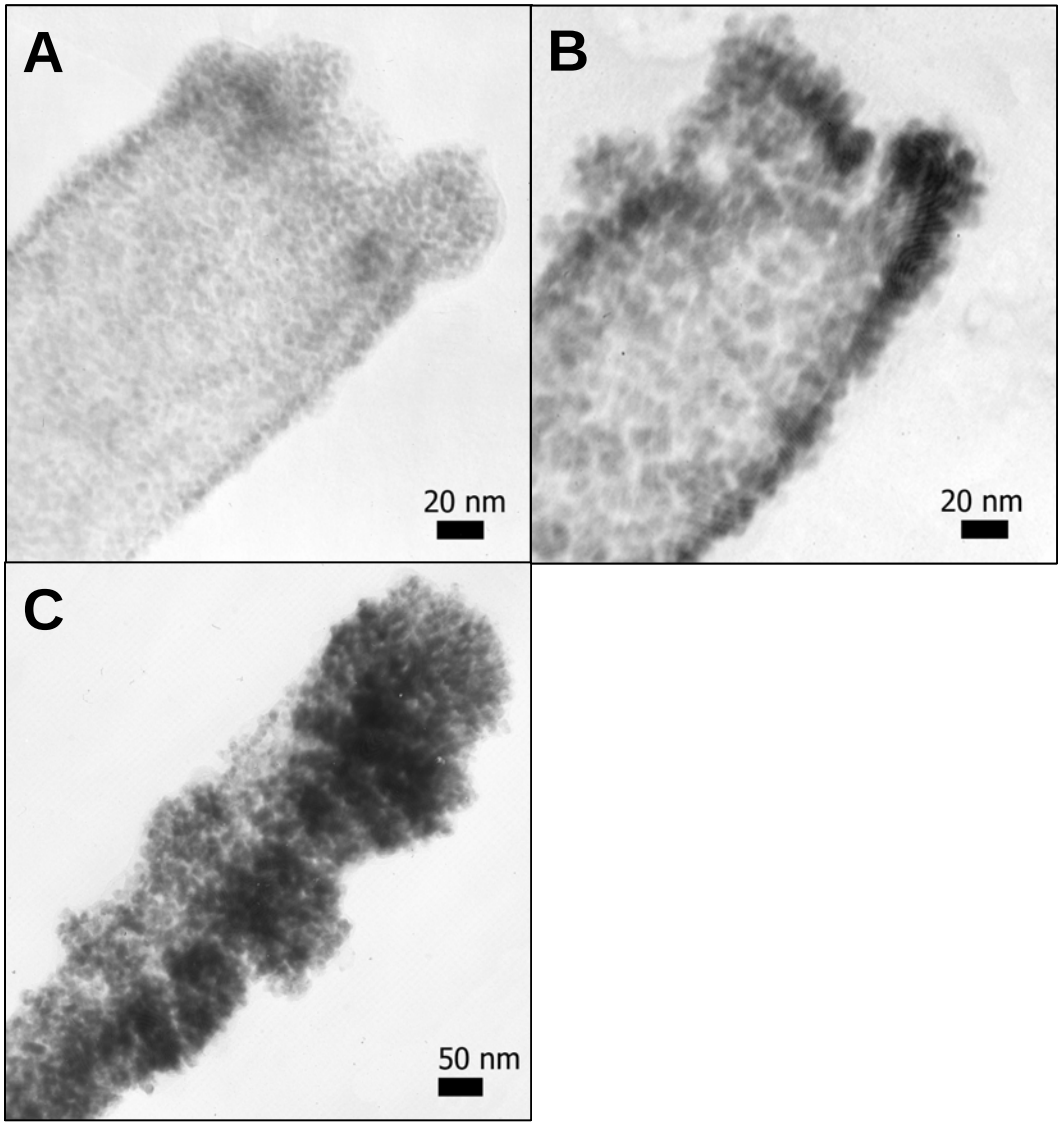

Figure 3.8. High magnification TEM images of palladium deposits on the tips of carbon nanofibers. For all samples a dc electrical field with an intensity of 3000V/cm was applied. The electrolyte consisted of 1.0 mM Palladium chloride in 1: 1 acetonitrile: toluene (v/v). The electrical field had been applied for 10-, 20-, and 40seconds for the samples in micrographs (A), (B), and (C) respectively. The TEM used was a JEOL 2000 FX with an accelerating voltage of 200kV.

Although the nanofibers differ in length, and as a result the potential across each nanofiber will differ slightly, a general pattern in the palladium deposition can be inferred from the data. After initial nucleation palladium growth occurs on the initial nucleation sites to produce the 3-5nm nanocrystals seen. By increasing the duration of the applied electrical field larger clusters of palladium nanocrystals grow and eventually develop into the ramified spherical clusters.

Another interesting feature observed on the carbon nanofibers are nanofibers that have contacted together to make one nanostructure with two cathodes and one anode. An example is seen in Figure 3.5G and H. The deposit grows on each nanofiber and does not favor the longer or shorter nanofiber.

3.5 Bipolar electrodeposition of Pd onto carbon nanofibers in a silica matrix

The next step in the synthesis of carbon nanofibers (CNF) with palladium on one tip was to try and scale up the production from a simple demonstration model (carbon nanofibers on glass) to a bulk model. One option would be to apply the earlier techniques using cellulose (Kimwipe) papers as a support. This was not attempted because nebulization of the CNF would result in the nanofibers landing parallel to the Kimwipe surface. Then when the Kimwipe papers are stacked between the electrodes the CNF would be perpendicular to the applied electrical field, and the tips would not be aligned with the electrical field for deposition onto the tips. Silica was chosen as an alternative support because it is non conductive, easily processed, inexpensive, and offered the possibility of easy separation from the carbon nanofibers.

3.5.a Experimental methods

The first step was to obtain a uniform mixture of nanofibers and silica. Simply stirring a mixture composed of toluene, silica and nanofibers did not produce a good uniform mixture. The nanofibers in such mixtures formed aggregates that could be seen with the naked eye. Instead a modified ball milling procedure was developed. The carbon nanofibers (Applied Sciences Inc.) were weighed out and mixed with 10 grams of silica. The silica and nanofibers were placed in a wide mouth glass jar (height approximately 11 cm, diameter approximately 4 cm). Approximately 130 grams of steel balls (1/4 inch diameter) were added to the jar. The glass jar was sealed and placed on a wrist action shaker (Burrell Model 75). The wrist action shaker was set at the maximum tilt angle, and the sample was left shaking for 2 hours. Using a cylindrical sieve the mixture of carbon nanofibers and silica (CNF/silica) was separated from the steel balls.

To prepare the sample for electric field application, 2.0 grams of the CNF/Silica mixture was combined with 30 mL of toluene (dried over calcium hydride) to make a slurry. Two graphite electrodes were then placed in a Gooch type filtering crucible with a fritted glass disc (porosity = coarse). The crucible was then filled with blank silica slurry (10 grams silica: 100 mL toluene dried over calcium hydride). The crucible was connected to a line vacuum via a filtering flask, and the vacuum was applied to compact the silica by removing the toluene. The compacted silica between the electrodes was removed and replaced with the CNF/silica slurry. Using a burette, toluene was slowly dripped onto the CNF/silica slurry, and a ‘gentle’ vacuum was applied. The CNF/silica slurry was then washed with 50 mL of 1.0 mM palladium chloride (1: 1 (v/v) toluene/acetonitrile both dried over calcium hydride). Care was taken to avoid air bubbles in the CNF/silica slurry between the electrodes. This was done by ensuring there

was always a small layer of liquid at the top of the slurry at all times. The crucible was then set up for field application. A 6000 V/cm pulsed dc electrical field was applied for a total on-time of 20 seconds. The electrical field was applied as a series of square wave pulses with 1.0 millisecond on-time and 8milliseconds off-time. The field was generated by passing the output from a high voltage dc power supply through a high voltage switch (Behlke HTS 651-03-LC) controlled by a HP33120A function generator. After field application the funnel was connected to a line vacuum and the slurry was washed with 50.0 mL of a 1:1 toluene/acetonitrile mixture, 50.0 mL of 2.5% sodium nitrate solution (1:1 acetone/water), and finally 50.0 mL of acetone. Once dry, the samples of the CNF/silica mixture were used for atomic absorption spectroscopy (AAS), or extraction experiments, or a combination of both. After the CNFs had been extracted from the silica, the nanofibers were examined on various transmission electron microscopes (TEMs).

For AAS, a 1.5 gram sample was digested with 5.0 mL of aqua regia (1: 4 (v/v) nitric acid/hydrochloric acid). This mixture was filtered through a glass funnel with a fritted glass disc (porosity medium) to remove the silica. A total of eight 1.0 mL aliquots of warm concentrated nitric acid were used to wash the silica. Using distilled water the resulting filtrate was made up to 25.0 mL and used for AAS.

The carbon nanofibers were extracted from the CNF/silica mixture using solvent extraction methods. In a separatory funnel the CNF/silica mixture was mixed with approximately 325 mL of toluene and an initial 600 mL of distilled water. This mixture was shaken vigorously and after settling for a few minutes the aqueous layer was removed and the process repeated. Each subsequent cycle used approximately 300 mL of

distilled water. The separated CNF were collected in a glass funnel with a fritted disc (porosity = fine), washed with acetone, and dried.

For TEM characterization, a small sample was suspended in acetone, and drop dried on a 400 mesh Holey carbon copper grid.

3.5.b Results and Discussion

Initial AAS experiments on the CNF/silica samples showed no significant difference between the samples that had been exposed to an electric field and samples that had not been exposed. This lack of difference was attributed to the strong adsorption of palladium ions onto silica surfaces. A quick search of the literature found that silica is used and is investigated as a support for palladium metal catalysts. The primary method of synthesis involves the adsorption of palladium ions onto the silica surfaces.[28,29] To remove as much adsorbed palladium as possible, a multi-step washing process was developed. The steps involved first removing excess reagents with an initial wash with a solvent mixture that was similar to the electrolyte i.e. 1: 1 (v/v) acetonitrile/toluene without any metal salt. This avoided the precipitation of palladium due to sudden changes in the solvent composition. The second step used a metal salt to displace any residual palladium ions absorbed on the silica. Various metal salts were tried and a comparison showing the effect of each salt is shown in Figure 3.9A. From Figure 3.9A there was no difference in the percentage palladium with change in the metal salt used; however, there was a change in the percentage palladium with or without a metal salt.

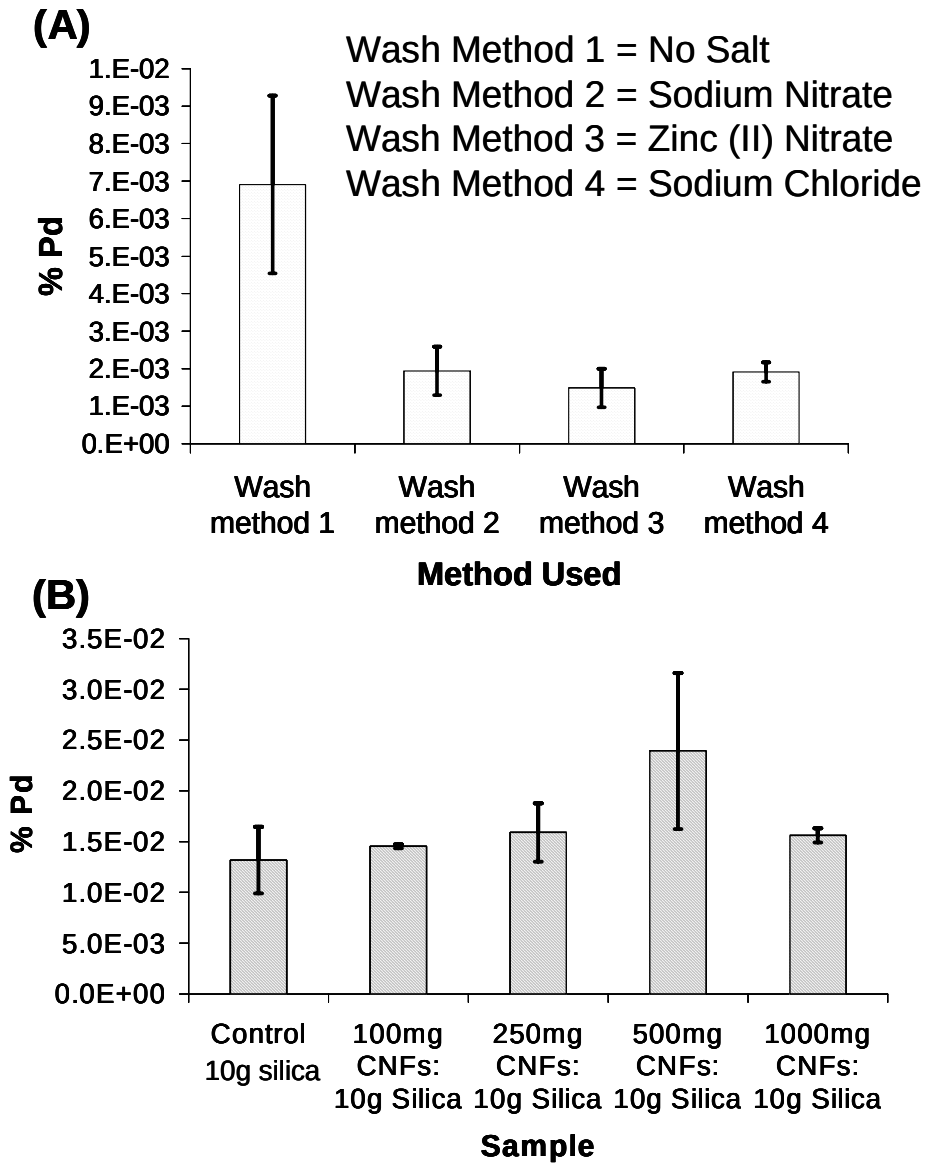

Figure 3.9. Part (A) shows the effect of the wash method used on the percentage of palladium. Part (B) shows the change in the percentage of palladium with the change in CNF loading.

Sodium nitrate was chosen over the other two salts simply because of its high solubility, and if any future catalytic studies were conducted it would not be expected to have an effect. Sodium chloride was rejected because it would interfere with any future energy dispersive X-ray (EDS) analysis. Any chlorine detected in the EDS spectrum could be easily identified with palladium chloride and not just the sodium chloride, thus introducing unnecessary ambiguities.

AAS results showed no difference, in terms of the %Pd, between blank silica samples (silica with no carbon nanofibers) and CNF/silica samples (Figure 3.9B) that had been exposed to an electrical field. Possible explanations for this result are that the application of the electrical field deposits palladium onto the silica particles as well as the CNF, or the CNF loading is too high or a good amount of palladium off the feeder electrode is being collected. The first reason is dismissed as highly unlikely because silica is non conductive and has no surface groups for any electrochemical processes in the current system. The high loading of CNF would lead to a short circuit in the system and thus no deposition would occur on any of the CNF. No high current reading to indicate such a condition was recorded and CNF with bipolar deposit were found (Figure 3.10). High loading would reduce the total surface area for deposition. A simple analysis of a system with two nanofibers shows that when the nanofibers are in contact there is only one surface for deposition. When the nanofibers are not in contact the number of surfaces available for deposition has doubled, illustrated in Figure 3.11. No special precautions were taken to shield the electrodes. Covering the electrodes with a membrane or with Kimwipes would presumably prevent the palladium deposit on the electrodes from entering the system.

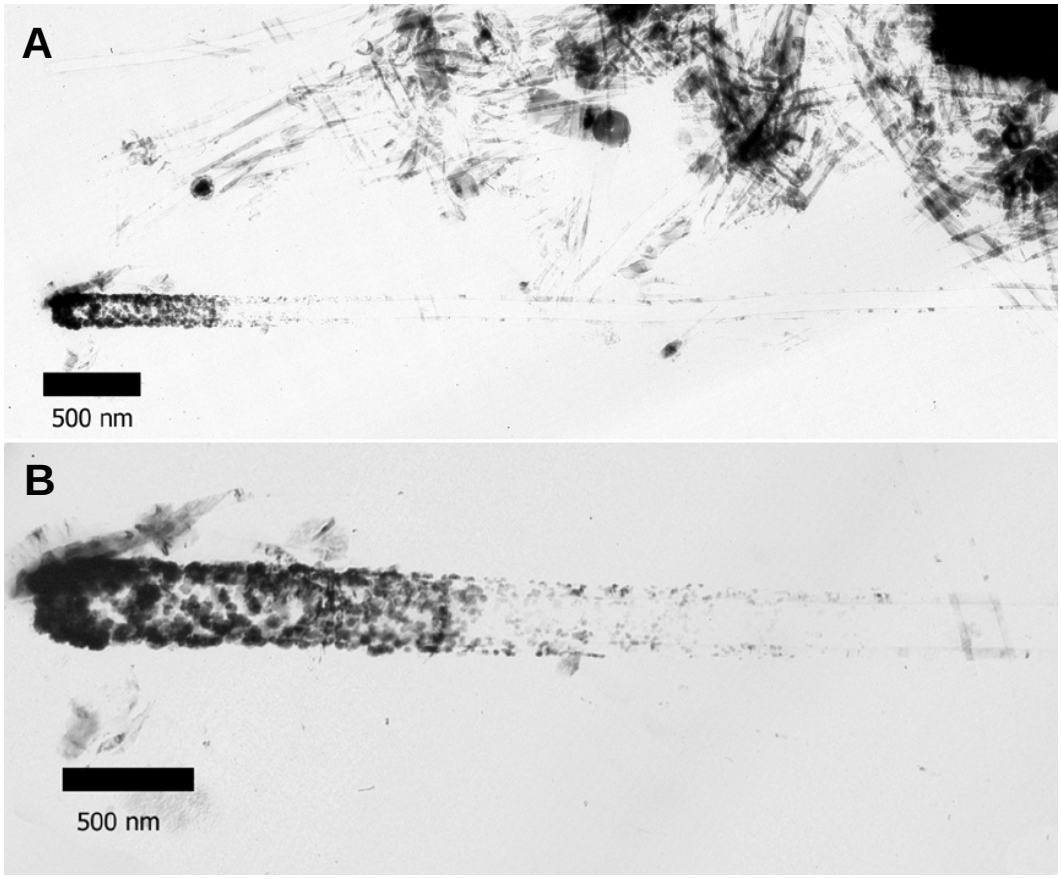

Figure 3.10. TEM images of CNF with bipolar electrodeposited palladium. The CNF had been exposed to a 20 second (total on-time) 6000V/cm pulsed dc electric field (on-time: 1.0millisecond, off-time: 8.0milliseconds) in a 1.0 mM palladium chloride solution (1: 1 toluene: acetonitrile both dried over calcium hydride).

When such experiments were done, the percentage of palladium was the same as in the samples without protected electrodes. Thus the major source of palladium was not from the electrodes. Although the amount of carbon nanofibers in the silica matrix had increased significantly from the model setup, that is CNF on glass, the orientation of the carbon nanofibers in the silica was totally random and the carbon nanofibers were immobilized. Thus deposition onto the carbon nanofibers was limited to the small fraction of carbon nanofibers that were orientated with the electric field. This accounts for the small percentage of palladium. The random distribution of the silica particles may have resulted in the hindrance of the deposition of palladium on parts of the carbon nanofibers. The small size of the silica particles results in good contact between some areas of the carbon nanofibers and the silica, resulting in little to no deposition at these contact points. As a result the palladium deposit on the carbon nanofibers would look like patches of deposit, as seen in Figure 3.10, unlike the deposits observed on the glass experiments. There was an order of magnitude difference, in the %Pd, between the samples with no applied electrical field and the samples subjected to an electrical field **(**Figure 3.9A and B).

The density of the carbon nanofibers (2.0 g/cm^{-3}) is very close to that of the silica (2.1 g/cm^{-3}) used. Thus separation by solvent extraction methods were carried out with limited success. The recovered CNF were always mixed with a small amount of silica, as seen in the TEM micrographs in Figure 3.10.

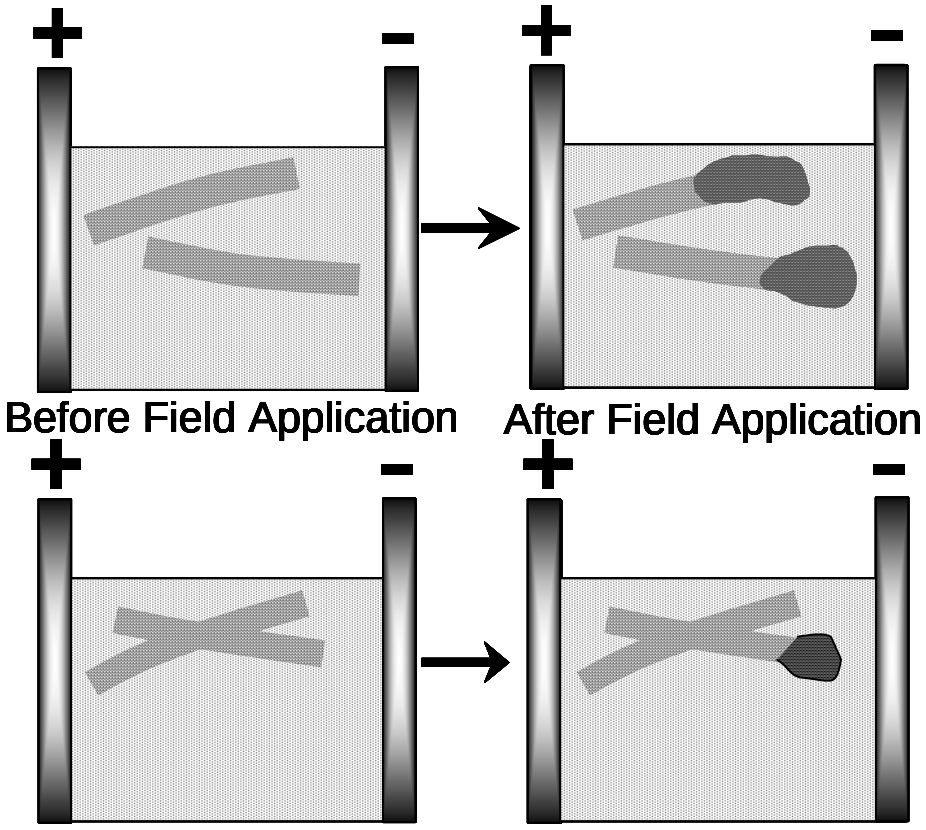

Figure 3.11. Change in the available area for electrodeposition between two nanofibers that are in contact and non contact.

TEM studies revealed carbon nanofibers with palladium on one tip, proving a bipolar mechanism. The AAS analysis proved that a very small fraction of the nanofibers were being modified. A significant amount of silica was seen in the TEM analysis. The silica could not be separated adequately from the carbon nanofibers.

3.6 Bipolar Electrodeposition of Pd on Carbon Nanofibers Suspended in Tetrahydrofuran

These experiments were done to take full advantage of bipolar electrochemistry. With no need for direct contact between the carbon nanofibers and the electrodes, the deposition can be done on a suspension of carbon nanofibers. The advantages include the ability to do bulk processing, an important step in providing enough sample for further study, and simpler processing.

3.6.a Background

In terms of palladium electrodeposition the conditions that induced palladium electrodeposition on the carbon nanofibers immobilized on the glass (or in the silica) will be the same for the carbon nanofibers suspended in a solution. The carbon nanofiber will have a set minimum length for electrodeposition, and will have to be aligned with the direction of the applied electrical field. With the carbon nanofibers suspended in a suitable solvent, the carbon nanofibers are free to rotate and move when the electric field is applied. The rotation of the carbon nanofibers can be controlled by the on-time of the applied electrical field.[30] The movement of the carbon nanofibers in an applied electrical field i.e. dielectrophoresis, can be restricted by selecting appropriate on-time of the

electric field. Previous studies have used dc electric fields to manipulate carbon nanotubes.[31, 32]

3.6.b Experimental

Carbon nanofibers were refluxed in a mixture of concentrated nitric acid and concentrated sulfuric acid (3: 2 v/v) for two hours. The nanofibers were then filtered using a sintered glass funnel connected to a laboratory line vacuum. The nanofibers were thoroughly washed with distilled water then acetone. 10.0 mg of the nanofibers were then sonicated in 100.0 mL of dry tetrahydrofuran (THF) for 42 hours. 0.1 mL of the resulting suspension was mixed with dry THF, and palladium chloride dissolved in acetonitrile in a glass vial. The final concentration of carbon nanofibers was 0.001 mg/mL, in a solution of 1.0 mM palladium chloride in 1: 4 (v/v) THF/acetonitrile. Carbon electrodes were added to the glass vial; and to maintain separation of the electrodes a teflon spacer was placed between the electrodes inside the vial, and a borosilicate glass tube (Pasteur pipette) was placed on top of the vial between the electrodes. A pulsed DC electrical field (approximately 7400 V/cm) was applied by sending the potential from a high voltage power supply through a high voltage switch (Behlke HTS 651-03-LC) controlled by a HP33120A function generator. The on-time of the applied pulse was 1.0 millisecond and the off-time of the pulse was 24.0 milliseconds or 48.0 milliseconds. A 100 millisecond pulse at approximately 250 V/cm was applied just before field application; the same set up was used. The total on-time for field application was 40.0 seconds. A variation on this experiment used carbon tetrachloride instead of THF. After field application the mixture was transferred to a 15.0 mL

centrifuge tube mixed with 4.5 mL of acetonitrile and centrifuged in a bench top centrifuge, the supernatant was discarded and 14.0 mL of HPLC grade acetonitrile was mixed with the remaining pellet, and the sample centrifuged. This was repeated one more time; the pellet was then mixed with approximately 3.0 mL of acetone, and 50 μL of the suspension was drop dried onto a Holey carbon membrane supported on a 400 mesh copper TEM grid. The samples were examined using TEM.

3.6.c Results and Discussions

Bipolar electrodeposited palladium was found on the carbon nanofibers (Figure 3.12C). An analysis of 85 different images from 4 different samples found that the percentage of nanofibers with bipolar electrodeposited palladium were 7%. An unexpected result was that 16% of the total number of nanofibers imaged had a complete coverage of palladium deposit, as seen in Figure 3.12B. These nanofibers with palladium (an example is shown in Figure 3.12B) had deposits that typically covered the whole nanofiber. Such deposits were either nanofibers that had come in contact with the feeder electrode and fallen off or had been in contact with the cathode tip of another nanofiber. The low percentage of functionalized nanofibers can not be simply accounted for by the field parameters used. If we consider that the parameters were such that the majority of nanofibers moved to the electrodes and deposited on the electrodes, this would not affect the deposition of palladium onto the remaining nanofibers in the solution. The deposition of palladium will occur on the nanofibers aligned with the electrical field and with the minimum length needed for deposition.

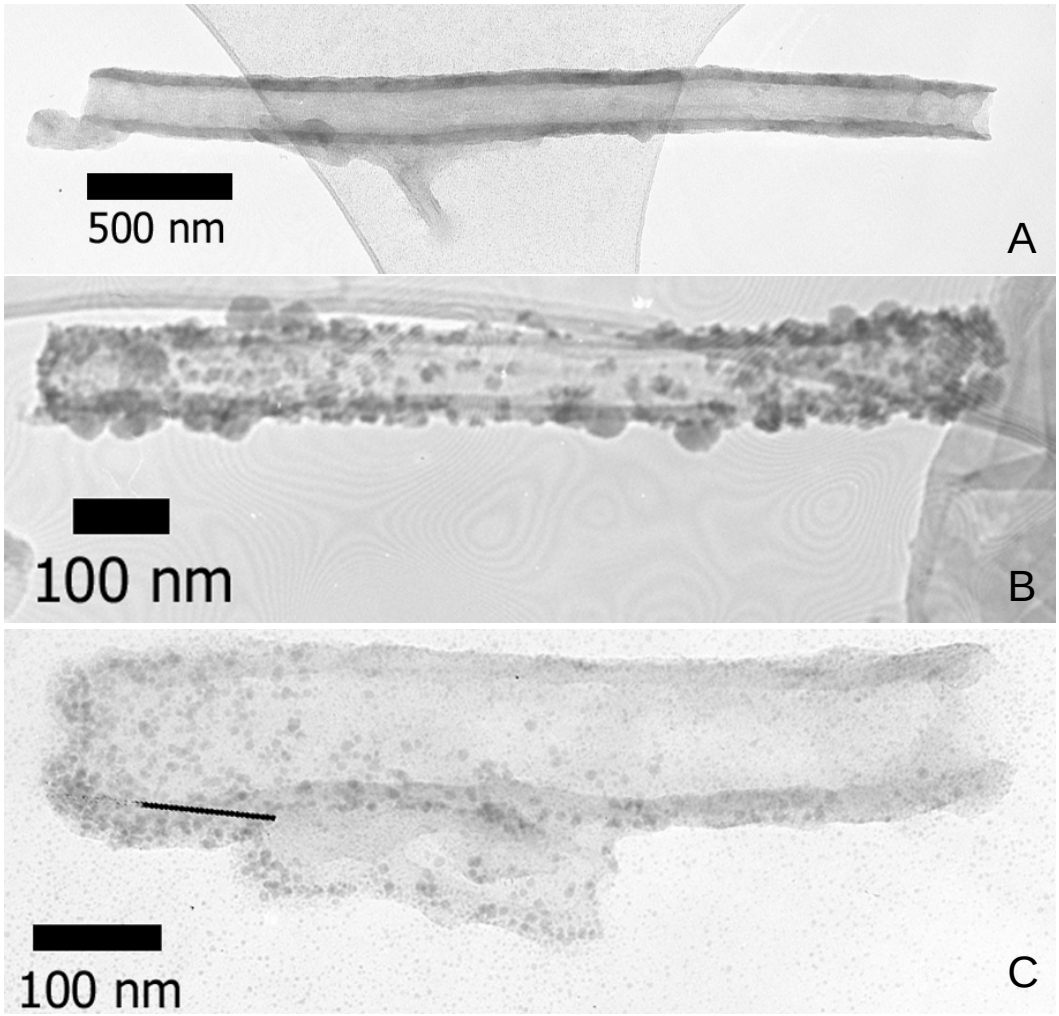

Figure 3.12. TEM images of carbon nanofibers recovered after field application on nanofibers suspended in THF.

From Figure 3.12, nanofibers with a 1 μm length do have palladium deposit on one tip, and nanofibers with greater lengths do not have any deposit. This discrepancy cannot be explained by bipolar electrodeposition. The nanofibers taken for TEM examination were only a small part of the whole sample, thus a thorough examination of the sample needed to be taken. Filtering the suspension after field application recovered all the nanofibers, and provided a larger sample for electron microscopy examination. The SEM examination found extremely large nanofibers that were 20-100 μm in length with diameters varying from 250-500 nm in diameter. These large nanofibers dominated the system. The applied electric field induces a dipole moment on the nanofibers, larger nanofibers will have a larger induced dipole, and the dipoles between nanofibers can interact and result in the nanofibers sticking together.[30] These nanofibers then contact the larger nanofibers on various parts of these larger nanofibers. If a nanofiber is in complete contact with the cathode area of the larger nanofibers then the nanofiber will be completely covered (Figure 3.12B). If the nanofiber is in contact with the anodic section of the larger nanofiber than it will have no palladium deposit on it at all (Figure 3.12A). Only a small sample of nanofibers in such a system will be modified by bipolar electrodeposition. There are two ways to overcome this problem. The first is by diluting the nanofiber suspension further. This would limit the interaction between adjacent nanofibers and ideally limit nanofiber interaction to nil. The second is to separate the larger nanofibers by filtration.

Experiments that separated the nanofibers by filtration were conducted; however, the following bipolar experiments did not reveal a significant change in the functionalization of the nanofibers. This result suggests that on the time scale of the experiment the

nanofibers were settling in the system or in retrospect the concentration of nanofibers in the solution was still too high. The concentration factor was actually elucidated in the experiments that used carbon nanotubes.

3.7 Conclusions

The original goal of the work presented in this chapter was too deposit palladium metal onto carbon nanofibers. Once this was accomplished, the second objective was to devise a procedure for the bulk synthesis of carbon nanofibers with bipolar electrodeposited palladium. Using bipolar electrochemistry palladium was deposited onto the tips of carbon nanofibers. The lengths of the functionalized nanofibers varied between 0.5–15 μm (nominal diameter 250 nm). In a solution of 1: 1 acetonitrile/toluene with 1.0 mM palladium chloride, the amount of palladium deposit can be controlled using the time the electrical field is applied. In silica, the nanofibers are immobilized and orientated in random directions. As a result, in the silica matrix, only a small fraction of the nanofibers can be functionalized by bipolar electrochemistry. Thus, nanofibers in a silica matrix are a non-ideal method to produce large quantities of metal modified nanofibers. The oxidized nanofibers are not easily modified as a suspension. The variation in length in the carbon nanofibers resulted in larger nanofibers dominating the system, and in the production of bipolar functionalized nanofibers, and nanofibers with complete coverage of palladium deposits. To overcome this problem the larger nanofibers should be filtered out of the suspension and a greater dilution of nanofibers should be used.

Possible future work on this project would be to develop methods that optimize procedures for the bipolar electrodeposition of palladium onto suspensions of carbon nanofibers. Such methods would need to address the issue of removing the larger nanofibers by filtration (or any other suitable method), and the ideal concentration of a suspension of carbon nanofibers for bipolar electrodeposition. Besides palladium, experiments to deposit other metals onto the tips of nanofibers should be conducted. Once suitable quantities of the bipolar functionalized nanofibers are produced, the activity of the structures can be tested in simple catalytic reactions. It should be noted the catalytic reactions are suggested as a means to test whether the deposited material is functional after deposition. The use of the bipolar electrodeposited nanofibers in catalytic applications may not offer any significant advantages over catalysts produced in the traditional way. However, one plausible scenario that may merit some investigation is if two metals on opposite ends, e.g. gold and palladium, could simplify some synthetic methods down to a one-pot synthesis.

References

1. Bradley, J.-C.; Ma, Z. Contactless Electrodeposition of Palladium Catalysts. *Angew. Chem. Int. Ed.* **1999,** *38,* 1663-1666.

2. Bradley, J.-C.; Babu, S.; Mittal, A.; Ndungu, P.; Carroll, B.; Samuel, B. Pulsed Bipolar Electrodeposition of Palladium onto Graphite Powder. *J. Electrochem. Soc*. **2001,** *148,* C647-C651.

3. Bradley, J.-C.; Babu, S.; Carroll, B.; Mittal, A. A Study of Spatially Coupled Bipolar Electrochemistry on the Sub-Micrometer Scale: Colloidal Particles on Surfaces and Cylinders in Nuclear-Track Etched Membranes. *J. Electroanal. Chem.* **2001,** *522,* 75-85.

4. Rodriguez, N. M.; Kim, M.-S.; Baker, R. T. K. Carbon Nanofibers: A Unique Catalyst Support Medium. *J. Phys. Chem.* **1994,** *98,* 13108-13111.

5. Rodriguez, N. M.; Chambers, A.; Baker, R. T. K. Catalytic Engineering of Carbon Nanostructures. *Langmuir* **1995,** *11,* 3862-3866.

6. Bessel, C. A.; Laubernds, K.; Rodriguez, N. M.; Baker, R. T. K. Graphite Nanofibers as an Electrode for Fuel Cell Applications. *J. Phys. Chem. B* **2001,** *105,* 1115-1118.

7. Serp, P.; Corrias, M.; Kalck, P. Carbon Nanotubes and Nanofibers in Catalysis. *Appl. Catal., A* **2003,** *253,* 337-358.

8. Merkulov, V. I.; Lowndes, D. H.; Wei, Y. Y.; Eres, G. Patterned Growth of Individual and Multiple Vertically Aligned Carbon Nanofibers. *Appl. Phys. Lett.* **2000,** *76,* 3555-3557.

9. Endo, M.; Kim, Y. A.; Hayashi, T.; Fukai, Y.; Oshida, K.; Terrones, M.; Yanagisawa, T.; Higaki, S.; Dresselhaus, M. S. Structural Characterization of Cup-Stacked-Type Nanofibers with an Entirely Hollow Core. *Appl. Phys. Lett.* **2002,** *80,* 1267-1269.

10. Ledoux, M. J.; Vieira, R.; Pham-Huu, C.; Keller, N. New Catalytic Phenomena on Nanostructured (fibers and tubes) Catalysts. *J. Catal.* **2003,** *216,* 333-342.

11. Lozano, K.; Barrera. E. V. Nanofiber-Reinforced Thermoplastic Composites. I. Thermoanalytical and Mechanical Analyses. *J Appl Polym Sci.* **2001,** *79,* 125-133.

12. Ma, X.; Wang, E.; Zhou, W.; Jefferson, D. A.; Chen, J.; Deng, S.; Xu, N.; Yuan, J. Polymerized Carbon Nanobells and Their Field-Emission Properties. *Appl. Phys. Lett.* **1999,** *75,* 3105-3107.

13. Guillorn M, A.; Melechko, A. V.; Merkulov, V. I.; Ellis, E. D.; Britton, C. L.; Simpson, M. L.; Lowndes, D. H.; Baylor, L. R. Operation of a Gated Field Emitter Using an Individual Carbon Nanofiber Cathode. *Appl. Phys. Lett.* **2001,** *79,* 3506-3508.

14. Teo, K. B. K.; Chhowalla, M.; Amaratunga, A. J.; Milne, W. I.; Pirio, G.; Legagneux, P.; Wyczisk, F.; Pribat, D.; Hasko, D. G. Field Emission From Dense, Sparse, and Patterned Arrays of Carbon Nanofibers. *Appl. Phys. Lett.* **2002,** *80,* 2011-2013.

15. Fan, Y.-Y.; Liao, B.; Liu, M.; Wei, Y.-L.; Lu, M.-Q.; Cheng, H.-M. Hydrogen Uptake in Vapor Grown Carbon Nanofibers. *Carbon* **1999,** *37,* 1649-1652.

16. Van Dijk, N.; Fletcher, S.; Madden, C. E.; Marken, F. Nanocomposite Electrodes Made of Carbon Nanofibers and Black Wax. Anodic Stripping Voltammetry of Zinc and Lead *Analyst* **2001,** *126,* 1878-1881.

17. Steigerwalt, E. S.; Deluga, G. A.; Cliffel, D. E.; Lukehart, C. M. A Pt-Ru/Graphitic Carbon Nanofiber Nanocomposite Exhibiting High Relative Performance as a Direct-Methanol Fuel Cell Anode Catalyst *J. Phys. Chem. B* **2001,** *105,* 8097-8101.

18. Tang, H.; Chen, J.; Nie, L.; Liu, D.; Deng, W.; Kuang,Y.; Yao, S. High Dispersion and Electrocatalytic Properties of Platinum Nanoparticles on Graphitic Carbon Nanofibers (GCNFs). *J. Colloid Interface Sci*. **2004,** *269*, 26-31.

19. Yan, X.; Gao, X.; Li, Y.; Liu, Z.; Wu, F.; Shen, Y.; Song, D. The Surface Decoration and Electrochemical Hydrogen Storage of Carbon Nanofibers. *Chem. Phys. Lett*. **2003,** *372,* 336-341.

20. Volfkovich, Y. U.; Rychagov, A. Y.; Efimov, O. N.; Tarasov, B. P.; Krinichnaya, E. P.; Sosenkin, V. E.; Nikolskaya, N. F.; Moravskii, A. P. Structural and Electrochemical Properties of Carbon Nanotubes and Nanofibers. *Russ. J. Electrochem.* (*Engl. Transl.*) **2002,** *38,* 663.

21. Murphy, M. A.; Marken, F.; Mocak, J. Sonoelectrochemistry of Molecular and Colloidal Redox Systems at Carbon Nanofiber Ceramic Composite Electrodes *Electrochim. Acta* **2003,** *48,* 3411-3417.

22. Marken, F.; Gerrard, M. L.; Mellor, I. M.; Mortimer, R. J.; Madden, C. E, Fletcher, S.; Holt, K.; Foord, J. S.; Dahm, R. H.; Page, F. Voltammetry at Carbon Nanofiber Electrodes. *Electrochem. Commun*. **2001,** *3,* 177-180.

23. Murphy, M. A.; Wilcox, G. D.; Dahm, R. H.; Marken, F. Adsorption and Redox Processes at Carbon Nanofiber Electrodes Grown onto Ceramic Fiber Backbone. *Electrochem. Commun*. **2003,** *5,* 51-55.

24. Guillom, M. A.; McKnight, T. E.; Melechko, A.; Merkulov, V. I.; Britt, P. F.; Austin, D. W.; Lowndes, D. H.; Simpson, M. L. Individually Addressable Vertically Aligned Carbon Nanofiber Based Electrochemical Probes. *J. Appl. Phys.* **2002,** *91,* 3824-3828.

25. McKnight, T. E.; Melechko, A. V.; Guillorn, M. A.; Merkulov, V. I.; Doktycz, M. J.; Culbertson, C. T.; Jacobson, S. C.; Lowndes, D. H.; Simpson, M. L. Effects of Microprocessing on the Electrochemistry of Carbon Nanofiber Electrodes. *J. Phys. Chem. B* **2003,** *107,* 10722-10728.

26. Winkler, K.; Bettencourt-Dias, A. D.; Balch, A. L. Electrochemical Studies of C60/Pd Films Formed by the Reduction of C60 in the Presence of Palladium(II) Acetate Trimer. Effects of Varying C60/Pd(II) Ratios in the Precursor Solutions. *Chem. Mater*. **2000,** *12,* 1386-1392.

27. Bradley, J.-C.; Chen, H.-M.; Crawford, J.; Eckert, J; Ernazarova, K.; Kurzeja, T.; Lin, M.; McGee, M.; Nadler, W.; Stephens, S.G. Creating Electrical Contacts Between Metal Particles using Directed Electrochemical Growth. *Nature* **1997,** *389,* 268-271.

28. Min, B.K.; Santra1, A.K.; Goodman. D.W. Understanding Silica-Supported Metal Catalysts: Pd/Silica as a Case Study. *Catal. Today* **2003,** *85,* 113-124.

29. Toebes, M. L.; van Dillen, J. A.; de Jong, K. P. Synthesis of Supported Palladium Catalysts. *J. Mol. Catal. A: Chem*. **2001,** *173,* 75-98.

30. Fishbine, B. H. Carbon Nanotube Alignment and Manipulation Using Electrostatic Fields. *Fullerene Sci. Technol.* **1996,** *4*, 87-100.

31. Yamamoto, K.; Nakayama, Y. Orientation of Carbon Nanotubes Using Electrophoresis. *Jpn. J. Appl. Phys.* **1996,** *35,* L917-L918.

32. Kumar, M. S.; Lee, S. H.; Kim, T. Y.; Kim, T. H.; Song, S. M.; Yang, J. W.; Nahm, K. S.; Suh, E.-K. DC Electric Field Assisted Alignment of Carbon Nanotubes on Metal Electrodes *Solid-State Electron.* **2003,** *47*, 2075-2080.

Chapter 4: A Non-Contact Method to Address and Modify Isolated Carbon Nanotubes

4.1 Summary Statement

The objective of the work in this chapter was to develop a method to reliably functionalize carbon nanotubes using bipolar electrochemistry.

Work in this chapter presents a non-contact method to modify the tips of isolated carbon nanotubes. A methodology was developed that allows us to place polymers or a wide variety of metals on the tips of isolated carbon nanotubes. The method is simple and does not require lengthy lithographical techniques or long processing times. Palladium, gold, cobalt, nickel, cadmium, tin, zinc, and polypyrrole were successfully deposited on the tips of commercial and home grown (by chemical vapor deposition) multi-walled carbon nanotubes. The experimental techniques discussed in this chapter are a completely new tool in the ever growing field of nanotechnology. Results showing the potential applications for nanotubes modified by bipolar electrodeposition are also discussed.

4.2 Carbon Nanotubes

Carbon nanotubes are a unique material with enormous potential as fundamental building blocks for devices composed of nano-sized architectures. The potential of carbon nanotubes stems from the structure and resulting electronic and physical properties of carbon nanotubes.

Carbon nanotubes consist of a sheet or sheets of graphene rolled around a central axis, and the center of the nanotube is hollow.[1,2,3] Ideally the walls of the nanotubes have no defects and as a result can be considered as a single crystal[4]. One or both of these criteria (single crystal or hollow center) are often used to distinguish carbon nanotubes from carbon nanofibers. If the nanotube consists of a single sheet it is termed a single walled carbon nanotube (SWCNT); if the nanotube has two or more sheets it is classified as a multi-walled nanotube (MWCNT).[1-5,6,7,8,9,10] The manner in which the graphene sheet is rolled around the central axis is described as the chirality. The way the graphene sheet can be rolled around the central axis determines the electronic properties of a SWCNT.[5] In MWCNT the same effect is thought to occur, however, if one of the walls of a MWCNT is rolled in such a way as to be semi-conducting in nature, it can be easily obscured by another wall that is metallic in nature.[1-10]

4.2.a Carbon Nanotube Synthesis

Carbon nanotubes can be synthesized using various methods or a variant of these three methods. The methods consist of arc discharge, laser vaporization, and chemical vapor deposition.[1-10]

The arc discharge method is important historically, because it is the method used by Iijima when he first synthesized and characterized multi-walled carbon nanotubes[11]. This method was then optimized by various groups to produce significant yields of nanotubes and eventually the first observations of single walled nanotubes.[11] In the arc discharge method, two high purity graphite rods in an inert atmosphere such as helium or argon are brought close together. A large current is passed between the two rods, and an intense

electrical arc is formed between the two rods. The extreme environment of the arc vaporizes the carbon from the anode, consuming the graphite rod making up the anode, and as the anode is consumed the distance between the two electrodes is adjusted to keep the distance constant and thus maintain the arc. The vaporized carbon produced by the arc reforms on the cathode as a mixture of carbon nanotubes, amorphous carbon, and metal particles. The process has been optimized by varying gas pressure, current, amount and type of catalyst in the graphite rod. This method can be used to produce single walled carbon nanotubes or multi-walled carbon nanotubes.[2,3,12,13,14]

In the laser ablation method, a graphite rod in an inert atmosphere is targeted by a laser; the resulting plume containing various carbon species is carried by a buffer gas towards a cooled metal rod (usually copper). A carbon soot deposits on the metal rod. Initial experiments used an Nd: YAG laser, a graphite rod in a 1200 ºC furnace, and argon as the buffer gas.[3,15] This setup produced multi-walled carbon nanotubes in the collected soot. When small amounts of various transition metals were incorporated into the graphite rod single walled carbon nanotubes were found in the resulting soot. Nickel was found to produce the largest percentage of single walled carbon nanotubes in the soot. Subsequent developments in the laser ablation technique started using a CO_2 laser. This setup does not require a furnace, and produces 2 – 3 times more material than the optimized Nd: YAG method. Irrespective of the method used, the soot is always a mixture of nanotubes, amorphous carbons, and metal catalyst particles.[3,15,16]

Sunlight concentrated onto a graphite target with metal catalyst has been used to produce carbon nanotubes. This method can result in temperatures of up to 3000 K in the reaction chamber, and can produce up to 100mg of material an hour, but this depends on

the weather. This method is unique in it does not use lasers or high current. It is similar to laser methods because the carbon material is vaporized using light.[15]

The growth of carbon nanotubes by arc discharge or laser vaporization always produces nanotubes with a significant amount of impurities. The impurities often require extensive harsh processing to purify the nanotubes. Another drawback to the arc discharge and laser vaporization method is they are not amenable to scale up. To overcome these drawbacks in the arc discharge and laser vaporization methods researchers began exploring chemical vapor deposition methods. Chemical vapor deposition is a method that produces high purity carbon nanotubes. Nanotubes produced by CVD are free of amorphous carbon deposits, carbon nanoparticles and, depending on the technique used, can be free of catalyst particles. There are a myriad of variations on the CVD method, however the basic process in CVD synthesis involves a precursor gas that is flowed through a CVD system and the gas decomposes on a substrate (with or without catalyst particles) to produce nanotubes. If the CVD system uses elevated temperatures (usually above 500 ºC) it is sometimes referred to as thermal CVD.[9] If the CVD system uses a plasma it is often referred to as plasma-assisted CVD.[9] The CVD method can produce multi-walled or single walled nanotubes.[2,3,5,7,9,10,17,18,19,20]

A CVD method of particular interest is the CVD growth of carbon nanotubes inside an alumina membrane. This method can grow nanotubes with or without the use of catalysts, can tailor the length and diameter of the nanotube, and can control the wall thickness of the nanotube.[17-20]

There are two methods used for the catalyst free growth of carbon nanotubes using an alumina membrane template, these are, chemical vapor deposition (CVD),[17-20] and

carbonization.[21,22] The advantages of anodized aluminum are: it is stable at the temperatures needed for decomposition of the precursor, it has straight well ordered channels,[17-20] it can be synthesized to meet specific criteria,[20] and it is easily removed without significant damage to the carbon nanotubes. [17-20] Anodized aluminum can be obtained commercially under the brand name Whatman Anodisc membrane filters, and comes in a variety of pore sizes from 20-250 nm.[23,18] The channels, however, have been found to be of similar diameter (250–300 nm).[24] In order to use temperatures above 600-700 ˚C, the commercial membranes are usually preheated before use. If this is not done, the membrane will curl during CVD synthesis.[18] The curling of the membrane is associated with different phase changes of the alumina.[18] It is not uncommon to find researchers' that grow their own templates; and this is because of several key advantages, which include; the size of the pore openings, the channel diameter, and the channel branching can be controlled. With this precise control of the template, carbon nanotubes with specific diameters, specific lengths,[17,19,20] and, if so desired, multiple branches can be grown.[20] The templates are usually grown from a high purity aluminum sheet, which is preprocessed using various combinations of either annealing, polishing (mechanically and/or electrochemically), and washing. The sheet is then anodized using either a one or two-step method in one of various acidic solutions (phosphoric, oxalic or sulfuric acids). After growing the carbon nanotubes, the template can be easily removed using either sodium hydroxide or hydrofluoric acid.[17-22]

In the catalyst-free CVD synthesis of carbon nanotubes in an alumina membrane the precursor is usually a gaseous unsaturated hydrocarbon such as ethylene, acetylene, or propylene[17-20]; however, there are examples of a solid unsaturated hydrocarbon being

used (pyrene[18]). The CVD system is usually flushed with an inert gas, such as nitrogen or a noble gas, and then the precursor is introduced either pre-mixed in an inert gas or mixed in house before entering the CVD system. Pyrolysis of the precursor (usually above 600 ˚C) results in the deposition of carbon nanotubes along the inside of the channels and a thin (~30 nm) carbon film on the surface of the anodized alumina template. For the carbonization method, a polymer is introduced into the pores of the alumina membrane. The polymer is dried, and then in an inert atmosphere the alumina membrane is heated to a high temperature (above 750 ˚C). At the high temperature the polymer carbonizes to form carbon nanotubes in the pores of the alumina template. Using a polymer precursor can result in carbon nanotubes with a bamboo like structure. Although described as nanotubes in the literature, these structures are more accurately identified as nanofibers. The use of a polymer precursor requires long carbonization times and higher temperatures than the CVD method. The main advantage of the carbonization method is that there is no handling of any gas and thus no need for setting up any gas handling apparatus. The CVD method requires relatively short synthesis times (can be as short as 4 minutes[19]), and at a specific temperature the thickness of the carbon nanotube walls can be controlled by the flow rate of the precursor gas and the deposition time. In both methods, the nanotubes produced are amorphous; however, annealing under vacuum at high temperature will result in highly ordered nanotubes. No matter the method chosen, a carbon film forms on the surface of the template. In the case of carbonization, removing the polymer on the surface of the template before carbonization can prevent the formation of the carbon film. For the CVD method the film can only be removed after deposition.[17-22]

4.2.b Exploiting the Unique Properties of Carbon Nanotubes

One area that carbon nanotubes are expected to have a great impact is in the area of nanoscale electronic devices. As the limits of current silicon based devices are approached, researchers are exploring new materials, as well as new methods for the fabrication of future electronic devices. The properties that make carbon nanotubes such attractive materials for nanoscale devices include the high current-carrying capacity, good thermal conductivity, ballistic conductivity, and they are chemically inert at standard temperature and pressure. The high current-carrying capacity of carbon nanotubes has been measured to be about 1000 times greater than copper. One fundamental issue with metal nanowires with similar dimensions is that at the small diameters comparable to nanotubes, the metal nanowires fail due to electromigration, and the smaller the diameter the lower the resistance to electromigration. Current induced mass transport i.e. a series of oxidative processes will remove material from one area causing a break (open circuit), and the corresponding series of reductive processes will deposit material in another area leading to short circuits. The covalent bondings of the carbon atoms in a nanotube help prevent similar breakdowns in nanotubes. The observed ballistic transport of current along nanotubes means that electrons can be transported along relatively long distances without scattering the electrons i.e. little to no resistance. The thermal conductivity of nanotubes has been measured to be greater than 3000W/mK. These thermal and electrical properties, coupled with the chemical and physical stability of carbon nanotubes, makes them attractive candidates for the building of nanoscale electronic devices.[6,7,10,25]

4.2.b.I Carbon Nanotube Electronic Nanoscale Devices

Using carbon nanotubes, various nanoscale electronic devices have been built and characterized. Simple interconnects, field effect transistors, nanoscale spintronic devices, carbon nanotube actuators, and low voltage field emission devices are examples of nanotube devices that have been built and characterized by various groups.[6,7,10,25]

One way in which carbon nanotube interconnects have been fabricated is by first sonicating nanotubes in a suitable solvent, and then drop drying a few drops of the suspension onto an oxidized silicon substrate. The nanotubes are located by AFM or SEM and electrodes are fabricated onto the opposite ends of the nanotubes using focused ion beams. A slight variation of this method is to drop dry or spin coat the nanotubes onto the electrodes that have been pre-fabricated using lithography. Prefabricating the electrodes is the least favorable method, because this often leads to high contact resistance between the nanotube and the metal electrodes, which negates the advantages of the nanotubes. One way to overcome the high contact resistance is to anneal the structures.[26,27] Using similar methods to produce a nanotube interconnect i.e. fabricating electrodes onto immobilized MWCNTs, a spintronic device was investigated by depositing cobalt as the electrodes and measuring the magnetization behavior of the device. The high contact resistance at the metal nanotube junction resulted in large spin scattering at the nanotube metal junction.[26]

By using the CVD method, nanotubes can be grown onto prefabricated electrodes. In a recent study, molybdenum catalysts on pre-fabricated electrodes were used to grow SWCNTs across the electrode gap and bridge the separate electrodes. The SWCNTs were shown to be semi-conducting by measuring the current-voltage characteristics.[28] The method of CVD growth onto pre-fabricated structure for subsequent device

demonstration has been successfully applied to the demonstration of a nanotube memory device.[29]

When arrays of MWCNTs or SWCNTs are contacted to a power source as a cathode, and an anode is placed opposite the nanotube array, electrons will tunnel from the tips of the nanotubes when a potential is applied between the nanotubes and the anode. When the electrons are directed by an electric field onto a phosphor coated screen the device is a display (usually flat panel). If the electrons are directed towards a metal screen, X-rays are produced (with a narrower range than thermionic sources), thus the device is an X-ray generator. A lamp can be made by placing the nanotube array cathode and opposing anode in a low pressure gas system (eg mercury lamps). Other devices that have been demonstrated include microwave generators and gas discharge tubes for power surge protection. The emission properties of nanotubes can be improved by opening the tips of the nanotubes. The advantages nanotubes offer compared to thermionic sources such as tungsten or molybdenum tips is that they can operate in higher vacuum (10^{-6} Pa vs 10^{-8} Pa), they provide stable emission, have longer lifetimes, and operate at lower currents.[6,30]

One aspect of the electronic nanoscale devices is the metal used to contact the nanotubes is patterned using conventional lithographic techniques. As a result, the metal connects significantly increase the size of the device to the extent that the overall dimensions approaches that of conventional silicon based devices. With bipolar electrochemistry, we eliminate the need for lithographic methods to attach metal onto the nanotubes, and we provide metal deposits similar in size and dimension to the nanotube, thus offering the possibility to produce nanotube devices on dimensions much smaller than the conventional silicon based architectures.

4.2.b.II Use of Carbon Nanotubes in Composites

In the early 1990's Hyperion Catalysis International Inc. started producing MWCNTs by the ton, and selling the MWCNTs as a component of plastics. This was the first successful commercial application of MWCNTs[6]. The addition of MWCNTs to plastics improves the conductivity of the plastic.[5,3,6,8] A loading of 5% can produce conductivities between 0.01 – 0.1 S. The low loading used maintains or does not significantly alter the plastics mechanical and physical properties, specifically the low melt flow viscosity. This is important for molding the plastic. Low loadings of MWCNTs are usually used to help prevent the accumulation of electrostatic charge. Such plastics are currently used in automotive gas lines, gas filters, plastic computer chip carriers, conductive plastic auto parts, and electromagnetic shielding in cell phones and computers. By using single walled carbon nanotubes in composites the loading level can be significantly reduced to one tenth the current level used with MWCNTs.[6,8, 31] Compared to the more conventional additive, carbon black, nanotubes are a significant improvement. Carbon black loading can vary between 30 – 50%; at such high levels the performance of the plastic is severely compromised. The plastic either becomes unusable or can no longer be molded, and particles embedded in the plastic stick out of the surface and easily break off i.e. sloughing. Nanotubes can be used at much lower loading levels because of their high aspect ratios. The aspect ratio is the length to diameter ratio. Nanotubes have a high aspect ratio (~ 1000: 1), whilst carbon blacks are comparatively low (essentially 1: 1). The long lengths of nanotubes results in extended connected networks inside a polymer matrix.[31] Another area where nanotubes have been used to

alter the electrical properties of a host polymer is in the incorporation of nanotubes into organic light emitting diodes and photovoltaic cells. The incorporation of nanotubes has improved the electrical properties and the thermal stability of these devices, and has actually improved the quantum efficiency of the photovoltaic cells.[1]

Besides changing the electrical properties of the plastics, nanotubes have been shown to change their mechanical and thermal properties. This has been realized by simply dispersing the nanotubes in the polymer. Methods used include functionalizing the nanotubes with functional groups that aid in uniformly dispersing the nanotubes in the monomer, dispersing the nanotubes in the monomer with minimal processing of the nanotubes, or adding surfactants or polymers that coat individual nanotubes and prevent the nanotubes from coagulation. This area of research is still very active because a few fundamental issues need to be overcome; these include a reliable method to disperse high purity nanotubes, efficient transfer of mechanical load to the nanotubes and the reduction in cost of high purity nanotubes.[1,3,6,8]

4.3 Modification of Carbon Nanotubes

In order to utilize carbon nanotubes in devices, methods need to be developed that can reliably modify and manipulate nanotubes as needed. The modification of carbon nanotubes can be accomplished by covalent methods, non-covalent methods, and electrochemistry.

Covalent methods are usually accomplished by oxidizing the tips and sidewalls of the nanotube. The oxidation methods produce carbonyl containing functionalities on the tips and sidewalls. The oxidation is usually achieved by using a combination of acids such as

concentrated nitric and sulfuric acids, or piranha (sulfuric acid mixed with hydrogen peroxide) solutions, or just one acid such as hydrochloric acid. In addition to the aforementioned methods, ozone treatment of single walled nanotubes has been shown to introduce various carbonyl functionalities onto the tips and sidewalls. The oxidation produces a variety of carbonyl functionalities on the sidewalls and the tips of the nanotubes, but the majority of the groups are carboxylic acids. Once the carboxylic acid groups have been introduced onto the tips and sidewalls of the nanotubes, the nanotubes can then be subjected to various well known organic chemical methods. Examples of the modification of nanotubes through oxidation and then subsequent organic chemical methods include esterification and the introduction of amide linkages. [1-3,5-8,10,16] Through the use of amide linkages or ester bonds various alkyl amines, anilines, lipophilic and hydrophilic dendron species, DNA nucleotides, and polymers have been attached to SWCNTs.[5,32, 33]

In addition to various molecules, colloids and quantum dots have been linked to SWCNTs and MWCNTs. The colloid or quantum dot is bound to a molecule that contains both a suitable capping agent that attaches to the colloid or quantum dot and a functionality that can form either an amide bond or ester link with the carboxylic acid groups on the nanotube.[32, 34]

The covalent chemistry of carbon nanotubes extends beyond amide and esterification reactions. Using elemental fluorine and high temperatures the sidewalls and tips can be bonded with fluorine atoms. The fluorine functionalized nanotubes can then undergo a variety of reactions which include; organolithium reactions, alkylation by Grignard reagents, alkoxylations, oxidation by peroxides, and addition of undecyl radicals via

lauroyl peroxide. The fluorination of nanotubes completely alters the electric properties, optical properties and solubility properties of the nanotubes.[35]

Metal co-ordination complexes such as Vaska's complex (trans-[$IrCl(CO)(PPh_3)_2$]) and Wilkinsons adduct [$RhCl(PPh_3)_3$] have been linked to the sidewalls of SWCNTs. The resulting adducts increased the solubility of SWCNTs in such solvents as DMF and DMSO, and the adducts helped to separate SWCNTs from larger bundles. Solution ozonoylsis reactions on SWCNTs were shown to purify the tubes, and oxidize the tubes without significant damage to the tubes.[36] The sidewalls and tips of SWCNTs have been modified covalently with different moieties using carbenes, nitrenes, 1,3 dipolar cycloaddition, and arylation..[5,33,36, 37]

Covalent chemistry on carbon nanotubes is often a very harsh and destructive process that can completely alter the properties of the carbon nanotubes. One highly desirable goal is the ability to disperse carbon nanotubes in various solvents without altering the sidewalls through covalent chemistry. This has been achieved by using various surfactants such as sodium dodecylsulfate and benzylalkonium chloride. Surfactants can be avoided by using molecules with large aromatic groups such as pyrenes. The aromatic groups on the pyrenes lie alongside the aromatic rings in the nanotube walls; this adsorption on the nanotube walls is often described as $\pi-\pi$ stacking. By attaching a chain of molecules to the pyrene group the nanotube solubility in various solvents can be increased without disrupting the properties of the nanotube.[37]

By wrapping a suitable polymer chain around a nanotube, the solubility of the nanotube in various solvents can be increased. Depending on the polymer used the

interaction between polymer and nanotube is either π–π stacking or some form of van der Waals forces.[37]

4.3.a Electrochemical Deposition onto Carbon Nanotubes

Electrochemical deposition onto carbon nanotubes offers a way to control the way in which the nanotubes are modified by controlling the amount of deposit, and the type of material deposited onto the nanotube. The following paragraphs will briefly review work on electrodeposition onto carbon nanotubes.

MWCNTs bundles in the form of whiskers obtained from an arc discharge system were used as electrodes in the electropolymerization of polyaniline. The electropolymerization did not address individual nanotubes, but did result in fully covered nanotubes.[38]

Burghard et al. dispersed SWCNTs onto prefabricated electrodes on an oxidized silicon surface. Under an applied potential substituted phenyl groups formed radicals that directly attacked and attached to the carbons on the SWCNTs, and after applying the potential for sufficient time the phenyls polymerized to form nanometer coatings on the SWCNTs. This method did functionalize individual nanotubes as well as bundles of nanotubes.[39]

Using CVD methods, aligned dense arrays of MWCNTs were synthesized and used as an electrode for the electropolymerization of polypyrrole and polyaniline. The resulting nanotubes were covered with uniform thin polymer coatings. The covered arrays of MWCNTs were shown to have superior redox properties when compared to bare MWCNTs arrays or polymer films on metal electrodes, and the polymer covered

MWCNTs exhibited superior charge storage applications. These nanotube composites may find use in optoelectronic devices (eg OLED), super capacitors, or secondary batteries.[40, 41, 42]

MWCNTs were grown by the CVD method (acetylene at 700 ºC and cobalt vanadium particles dispersed on a zeolite), purified, ultrasonically dispersed in ethanol and then sprayed onto hot platinum or highly orientated pyrolytic graphite (HOPG) surfaces. Cycling the potential in sulfuric acid solutions detected and removed surface impurities on the MWCNTs immobilized on platinum and HOPG surfaces. Using cyclic voltammetry, metal electrodeposition onto the MWCNTs was studied by monitoring the electrodeposition of copper from aqueous solutions. MWCNTs on platinum exhibited two oxidation peaks, that were assigned to copper (0) and copper (I), and one reduction peak which corresponded to the copper (II) reduction. Copper deposition occurred preferentially along MWCNTs on a HOPG surface. The copper deposits were randomly distributed along the length of the nanotubes and differed in size. This observation was attributed to defects in the nanotubes' walls providing high energy areas for metal nucleation.[43]

SWCNTs were grown by pulsed laser vaporization, ultrasonically dispersed in 1, 2-dichloroethane, and then spin coated onto a silicon substrate with a 200 nm oxide layer and prefabricated palladium electrodes. The current-voltage properties of the resulting carbon nanotube field effect transistor (CNFET) were measured. From these initial measurements the nanotube was determined to be semi-conducting and the device was of the p-channel type. The palladium electrodes were then contacted and used as the cathode for electrodeposition of gold from a commercial electroplating solution. The

current-voltage properties of the CNFET were then measured after the electrodeposition. AFM characterization showed gold covering the palladium electrodes and no gold on the nanotube sidewalls. Previous studies by the authors found gold deposition on the sidewalls of the nanotube when the nanotube was metallic in nature. The authors suggested that the low energy of the electrons in this region could not reduce gold ions from the solution, and thus no gold was found on the sidewalls of the semi-conducting nanotube. This was not the case for electrons located where the SWCNT contacts the palladium electrodes. The current-voltage measurements after the deposition revealed a decrease in the contact resistance between nanotube and the electrodes, and a change in the current voltage characteristics.[44]

CVD synthesized carbon nanotubes were ball milled, ultrasonically dispersed in an electrolyte, and under ultrasonic agitation electrochemically co-deposited with nickel onto carbon steel substrates. The resulting metal nanotube composite showed improved wear resistance and enhanced mechanical properties.[45]

SWCNTs synthesized by the CVD method were purified and shortened using ultrasonic agitation and mixed acids (sulfuric, nitric acid mixes, and sulfuric acid, hydrogen peroxide mixes). The resulting SWCNTs were 10 – 40nm in length and the tips were terminated with carboxylic acid groups. The SWCNTs were then chemically assembled onto gold substrates terminated with amine functionalities. To chemically assemble the SWCNTs, 11-amino-n-undecylmercaptan monolayers were attached to the gold substrates. The sulfur end of the 11-amino-n-undecylmercaptan attached to the gold substrate, and the amine end provided a link for the SWCNTs by forming an amide bond with the carboxylic acid groups on the SWCNT. Using AFM, the majority of the

SWCNTs were shown to be vertically aligned with respect to the surface of the gold substrate. In a ruthenium hexaamino trichloride solution the cyclic voltammograms of the SWCNT array electrode were similar to that of a bare gold electrode, and from an aqueous solution copper could be electrodeposited onto the SWCNT array electrode. Through-bond tunneling was the proposed mechanism for electron transfer from the gold substrates through the covalent bonds connecting the SWCNT and the gold substrate.[46]

The advantages bipolar electrochemistry offers include; the ability to modify either a single tip or both tips of a carbon nanotube without the need to contact the nanotube, the ability to control the amount of deposit, and the ability to modify carbon nanotubes with very little preliminary processing. Current methods of contacting nanotubes for nano-electronic devices uses microlithography techniques that often result in nanotubes contacted to large metal pads. The resulting device is usually not that much larger than the conventional silicon cousins. Bipolar electrodeposition offers the possibility of contacting nanotubes with metal connects on a similar size scale to the nanotube.

The work in this chapter was done to develop methods that would produce unique functionalized carbon nanotube structures through the use of bipolar electrochemistry.

4.4 Bipolar Electrodeposition onto Isolated Carbon Nanotubes

The successful electrodeposition of various metals, a semiconductor, and a polymer onto one tip of isolated carbon nanotubes has been demonstrated. The basic strategy involved dispersing the carbon nanotubes in a suitable solvent such as toluene, diluting the nanotubes to a very low concentration, immobilizing the nanotubes on a non-conductive support, applying the electrical field with the nanotubes in a suitable

electrolyte, and finally examining the nanotubes under scanning electron microscopy. This method has the advantage of addressing individual nanotubes with out the need for lengthy processing procedures.

4.4.a Experimental Methods

Two sources of multi-walled carbon nanotubes were used. The first source was a commercial source of nanotubes obtained from Nanolab, Inc. The commercial MWCNTs had a nominal diameter between 30-50 nm, and lengths between 1-5 μm. The second source of MWCNTs was synthesized in house by the CVD method adapted from methods developed by Martin, et al.[18]

4.4.a.I CVD Synthesis of MWCNT

The CVD synthesis method was adapted from methods developed by Martin, et al[18]. An alumina membrane (Whatman Anodisc 13 mm diameter, and a 100 nm pore size) was set up in a quartz reaction vessel (Figure 4.1). The quartz reaction vessel was placed in a tube furnace, and argon gas was flowed at a rate of 20 mL/min. Under an argon atmosphere the temperature was ramped to 670 ºC. Once the temperature had stabilized at 670 ºC the gas flow was switched to a premixed mixture of 30% ethylene and 70% helium at a flow rate of 20 mL/min. After approximately 6 hours the flow was switched back to argon (flow rate = 20 mL/min) and the furnace was left to cool to room temperature overnight. Using this set up a maximum of 12 alumina membranes could be set up for CVD synthesis of MWCNT, but the system can be used with larger batches (Figure 4.1).

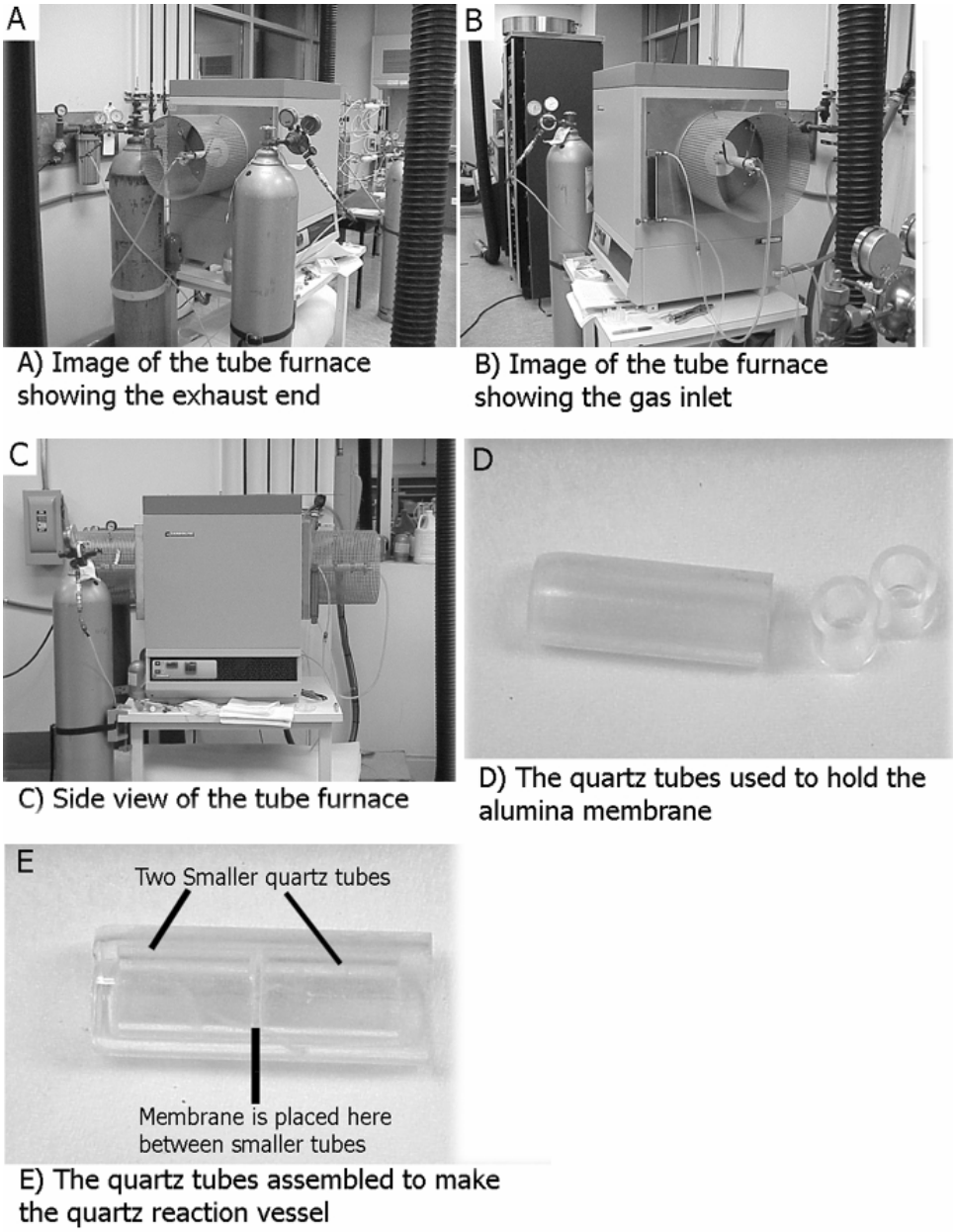

Figure 4.1. The experimental set up used for CVD synthesis of MWCNTs in an alumina membrane template. The two smaller quartz tubes were cut in half, and as a result three alumina membranes could be placed in one quartz reaction vessel. Four quartz reaction vessels could be placed in the furnace at once; this would produce a total of twelve alumina membranes with MWCNTs.

In Initial experiments, the alumina membrane was shattered and mounted on a scanning electron microscopy (SEM) stub for direct examination by SEM. In subsequent experiments and for use in bipolar experiments; the membrane was processed and the MWCNTs recovered for use. The alumina membrane was processed by shattering the membrane in a glass vial, and then agitating the fragments in a 4.0 M sodium hydroxide solution. After overnight agitation, the sample was sonicated for 10 to 20 seconds in a bath sonicator. This step was necessary to disperse the MWCNT. The resulting suspension of MWCNT was filtered through a polyester nuclear track etched membrane with 100 nm pores (Osmonics Laboratory Products, 13 mm diameter). The polyester membrane was supported by a Büchner funnel with a glass frit (porosity = coarse); and the Büchner funnel was connected to a standard lab vacuum line via a filtering flask. The MWCNTs were washed with copious amounts of water and acetone. Once dry, the MWCNTs were dispersed in toluene to make an original suspension. The suspension of MWCNTs for the bipolar experiments was made by diluting 1.0 mL of the original suspension in 99.0 mL of toluene to make a second suspension. The second suspension had a concentration of approximately 0.1μg/mL.

4.4.a.II Electrical Field Application

1.0 mL of a 0.1 μg/mL suspension of carbon nanotubes (solvent was toluene) was filtered through a 100 nm polyester nuclear track etched membrane (13.0 mm diameter, Osmonic Laboratory products). A strip measuring approximately 5 mm wide by 13 mm long was cut out of the center of the polyester membrane using a razor blade.

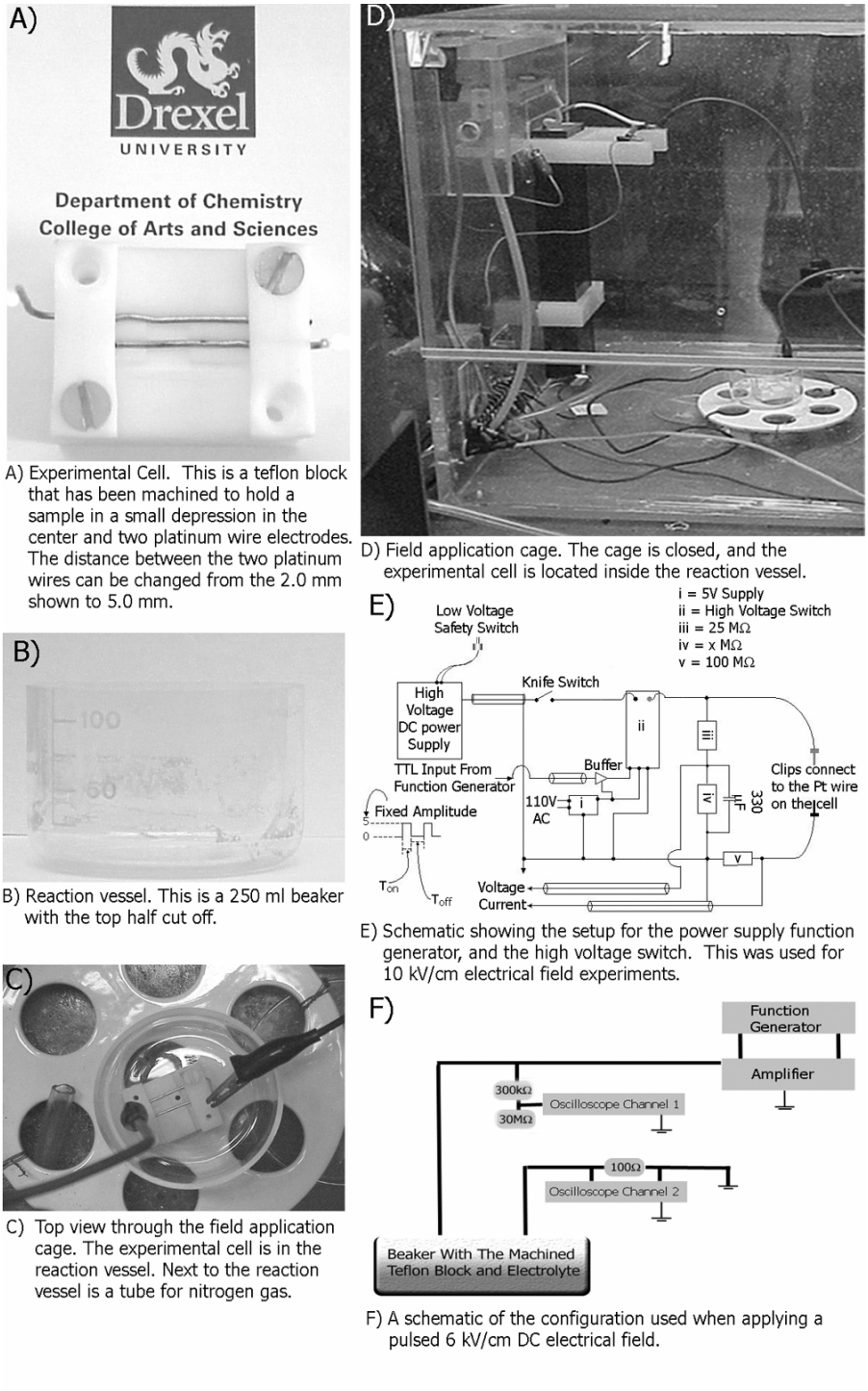

A) Experimental Cell. This is a teflon block that has been machined to hold a sample in a small depression in the center and two platinum wire electrodes. The distance between the two platinum wires can be changed from the 2.0 mm shown to 5.0 mm.

B) Reaction vessel. This is a 250 ml beaker with the top half cut off.

C) Top view through the field application cage. The experimental cell is in the reaction vessel. Next to the reaction vessel is a tube for nitrogen gas.

D) Field application cage. The cage is closed, and the experimental cell is located inside the reaction vessel.

E) Schematic showing the setup for the power supply function generator, and the high voltage switch. This was used for 10 kV/cm electrical field experiments.

F) A schematic of the configuration used when applying a pulsed 6 kV/cm DC electrical field.

Figure 4.2. Experimental materials and the schematics for the electrical field application experiments.

The polyester strip was placed in an experimental cell and extraneous bits of the membrane strip were cut off. The cell was connected to the electrical field application apparatus and 50.0 mL of electrolyte (see table 1) was added. In case an errant spark occurred, all experiments were done under nitrogen. A pulsed dc electrical field was applied using one of two possible methods. In the first method, the output from a dc power supply was sent through a high voltage switch (Behlke HTS 651-03-LC) and then across two platinum electrodes (Figure 4.2). The second method used a pre-programmed pulse from an HP33120A function generator amplified through a Trek P0674 high voltage amplifier, which was then applied across the platinum electrodes (Figure 4.2F). The dc electrical field varied between 5000 V/cm – 10000 V/cm and the on-time used was always 1.0 millisecond, and the off-time was always 24.0 milliseconds.

To remove excess reagents after field application, the experimental cell was immersed in the solvent used to dissolve the metal salt or monomer (and dopant) used for electrodeposition. For example, in the electrodeposition of cadmium the solvent used to dissolve cadmium chloride was dimethylsulfoxide (DMSO). After cadmium electrodeposition, the experimental cell was immersed in HPLC grade DMSO for five minutes, and then followed by five minutes in distilled acetone to remove the DMSO. Typically the solvent used to dissolve metal salts was acetonitrile, and after immersing the cell for five minutes in HPLC grade acetonitrile the cell was left to air dry. Once dry, the membrane strip was mounted on a scanning electron microscopy (SEM) stub, gold coated, and examined under a SEM. The SEM used was either an AMRAY 1830, or a Philips XL30 environmental SEM (ESEM).

Table 4.1. A table showing the composition of the electrolytes used, type of MWCNT used, and the time used to try to electrodeposit onto one tip of an isolated carbon nanotube.

Material Deposited	Nanotubes Used	Electrolyte	Ratio Solvent: Toluene (v/v)	Total on-time (seconds)
Palladium	commercial MWCNT	1.0 mM palladium (II) chloride, acetonitrile + toluene	3: 7	60
Gold	commercial MWCNT	0.2 mM gold (III) bromide, acetonitrile + toluene	1:4	60
Nickel	commercial MWCNT	1.0 mM nickel (II) chloride, N, N-dimethylformamide+ toluene	1:4	60
Cobalt	commercial MWCNT	1.0 mM cobalt (II) chloride, acetonitrile + toluene	1:4	60
Samarium	commercial MWCNT	1.0 mM samarium (II) iodide, acetonitrile + toluene	1:4	60
Samarium/Cobalt	commercial MWCNT	0.5 mM cobalt (II) chloride, 0.5 mM samarium (II) iodide, acetonitrile + toluene	3: 7	60
Lead	commercial MWCNT	0.5 mM lead nitrate, DMSO + toluene	1:4	10
Cadmium	commercial MWCNT	1.0 mM cadmium chloride, DMSO + toluene	1:4	60
Tin	CVD MWCNT	1.0 mM tin (II) chloride, acetonitrile + toluene	1:4	10
Silver	CVD MWCNT	1.0 mM silver chloride, acetonitrile + toluene	1:4	20
Zinc	CVD MWCNT	1.0 mM zinc (II) nitrate hexahydrate, acetonitrile + toluene	1:4	40
Polypyrrole	CVD MWCNT	0.2 mM toluene sulfonic acid sodium salt, 1.0 M Pyrrole acetonitrile + toluene	2:3	10
Cadmium Sulfide	CVD MWCNT	0.2 mM cadmium chloride, 0.5 mM elemental sulfur, Acetonitrile + toluene	1:4	20

4.4.b Results

Figure 4.3 shows a commercial MWCNT with palladium deposit on one tip of the nanotube. The combined length of the nanotube and deposit is approximately 5 μm. The deposit is ramified, extends off the nanotube, and is approximately 1.5 μm in length. A micrometer long nanotube with no deposit on either end is located near the center of the image. Energy dispersive X-ray spectroscopy (EDS) on the deposit showed a distinctive palladium peak.

In Figure 4.4 three SEM micrographs on three different commercial MWCNTs are presented. In Figure 4.4A the nanotube and deposit has an overall length of about 3.5 μm, and the deposit has an overall length of 2.0 μm. The deposit is ramified and the EDS on the deposit revealed a significant gold peak. In Figure 4.4B the nanotube and deposit structure has an overall length of approximately 6 μm, and the deposit is a mixture of ramified and large 'needle shaped' deposits. The deposit in Figure 4.4B has an average length of 3 μm. In Figure 4.4C the total length of the nanotube deposit structure is approximately 9 μm, and the deposit is around 3 μm in length. The deposit consists only of 'needle shaped' structures.

The nanotubes in Figure 4.5 vary in length. In Figure 4.5A the nanotube is about 12 μm in length with the deposit having an approximate length of 4 μm. In Figure 4.5B the total length of nanotube cobalt structure is about 8 μm and the deposit measures 1.5 μm. In Figure 4.5C the length from the bare tip of the nanotube to the end of the cobalt deposit is 4.5 μm.

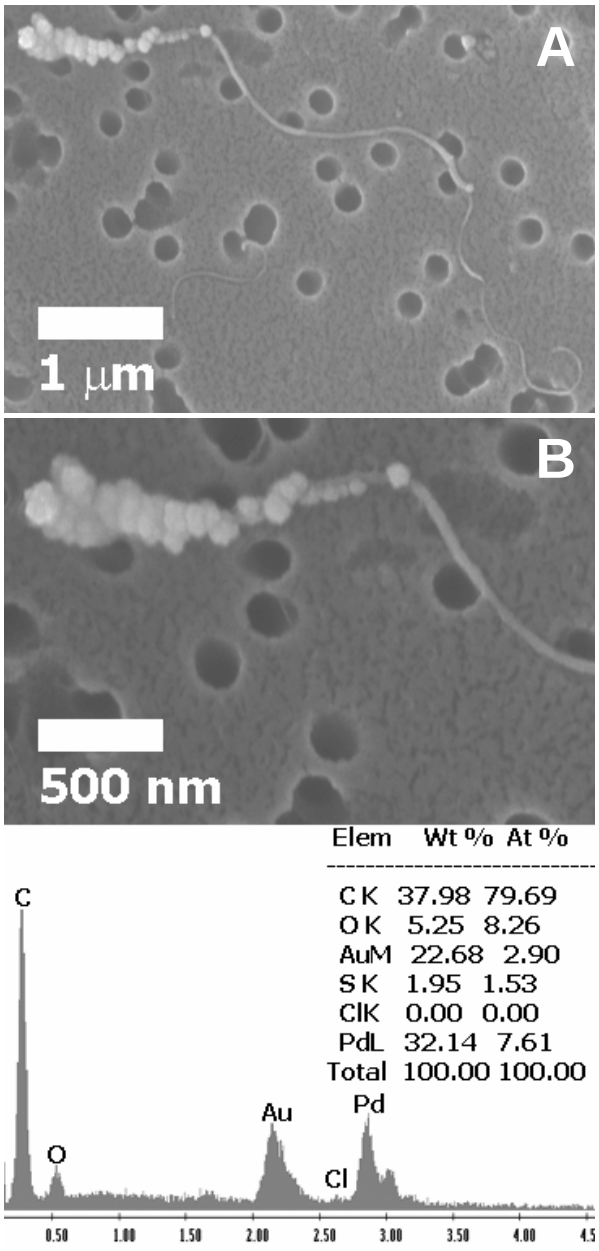

Figure 4.3. A commercial MWCNT with palladium metal deposited on one tip of the nanotube. The pulsed DC electrical field was 10kV/cm, with an on-time of 1.0 millisecond, an off-time of 24.0 milliseconds, the electrolyte used was 1.0 mM palladium chloride in 3: 7 acetonitrile/toluene, and the total on-time was 60 seconds. The acetonitrile and toluene had been distilled over calcium hydride. The EDS spectrum shows a significant palladium peak with no chlorine. Sample was examined on a Philips XL30 ESEM**.**

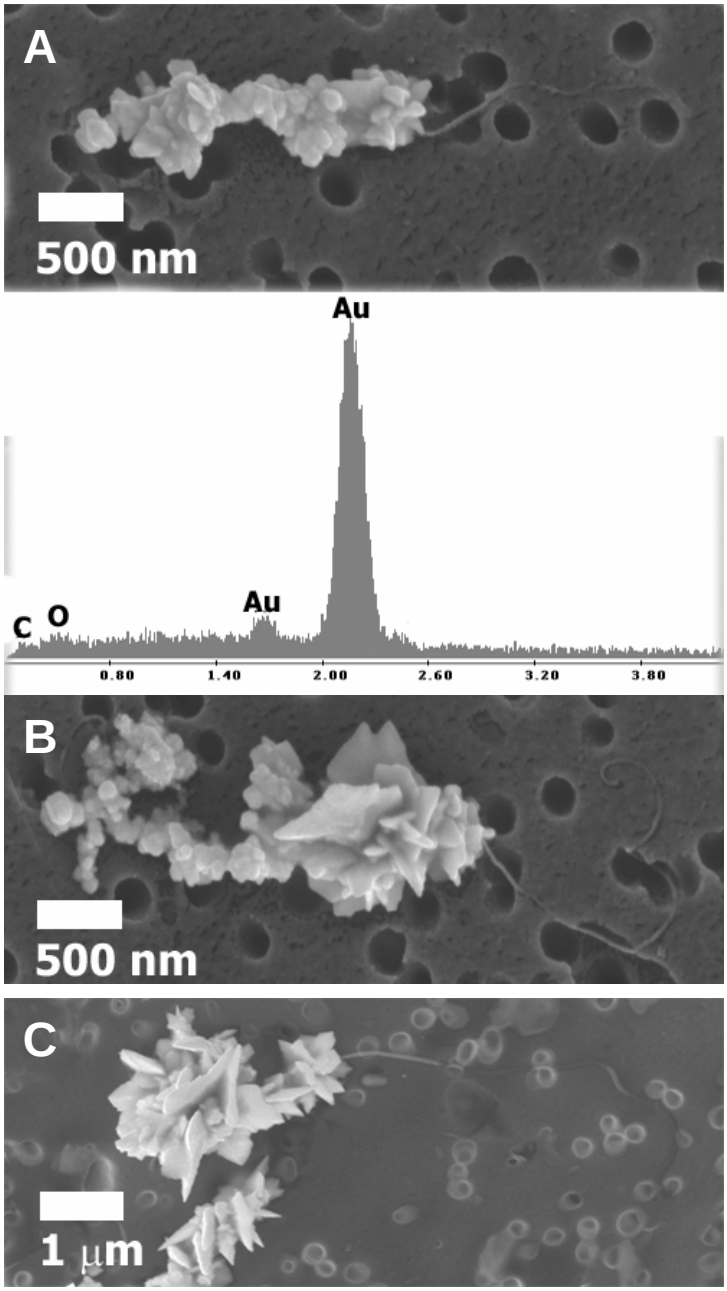

Figure 4.4. Three different commercial nanotubes with gold deposited onto one tip. The electrolyte consisted of 0.2 mM gold (II) bromide in a solvent mixture of 1: 4 (v/v) acetonitrile/toluene (both dried over calcium hydride). The pulsed DC electrical field was applied at 10kV/cm, with an on-time of 1.0 millisecond, an off-time of 24.0 milliseconds and for a total on-time of 60 seconds. SEM micrograph obtained on a Philips XL30 ESEM.

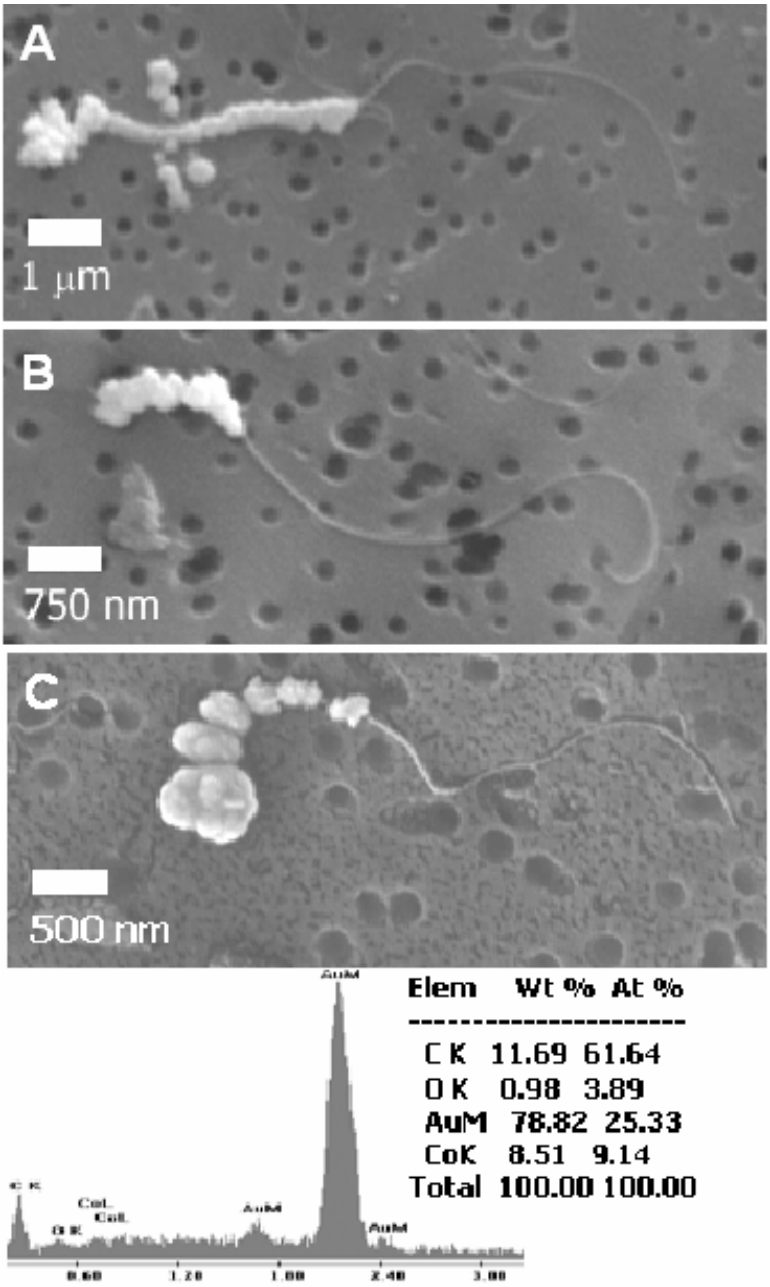

Figure 4.5. Commercial MWCNT with cobalt on one tip. Electrolyte was 1.0 mM cobalt (II) chloride in 1: 4 (v/v) acetonitrile/toluene (both dried over calcium hydride). A 10kV/cm DC pulsed electrical field (on-time: 1millisecond, off-time: 24milliseconds) was applied for a total on-time of 60.0seconds.

The deposit extends for approximately 1.5 μm, and unlike the previous examples the deposit has distinct separate bulbous regions. In all samples the cobalt deposits appear ramified.

Figure 4.6 presents SEM micrographs obtained on an AMRAY 1830 (Figure 4.6A and 4.6B), and a micrograph obtained on a Philips XL30 ESEM. In Figure 4.6 all nanotubes have a deposit on the tip. In Figure 4.6A the nanotube has a length of 3.0 μm and the deposit faintly resembles ramified metal deposits seen in previous experiments with palladium, gold, and cobalt. Figures 4.6B and 4.6C have small metal deposits on the tips of the nanotubes which could not be resolved with either SEM. The small metal deposit in 4.6C was characterized by EDS and nickel was identified in the EDS spectrum.

The first attempts at depositing a bimetallic species i.e. samarium cobalt are presented in Figure 4.7. Deposits with the characteristic ramified metal deposits were found on the tips of nanotubes. EDS characterization of the deposit revealed significant peaks of samarium, cobalt and chlorine.

Figure 4.8 is a combination of two SEM micrographs and an EDS spectrum of the deposit in Figure 4.8B. When measured from the uncoated tip to the end of the deposit, the nanotube in Figure 4.8A has a total length of approximately 9 μm. The total length of the deposit is approximately 5 μm, and it covers over half the length of the nanotube. Figure 4.8B shows a nanotube and deposit with an overall length of approximately 10 μm. The deposit in Figure 4.8B has an overall length measuring 4.0 μm. From the EDS spectrum shown in Figure 4.8B cadmium and chlorine are identified in the deposit.

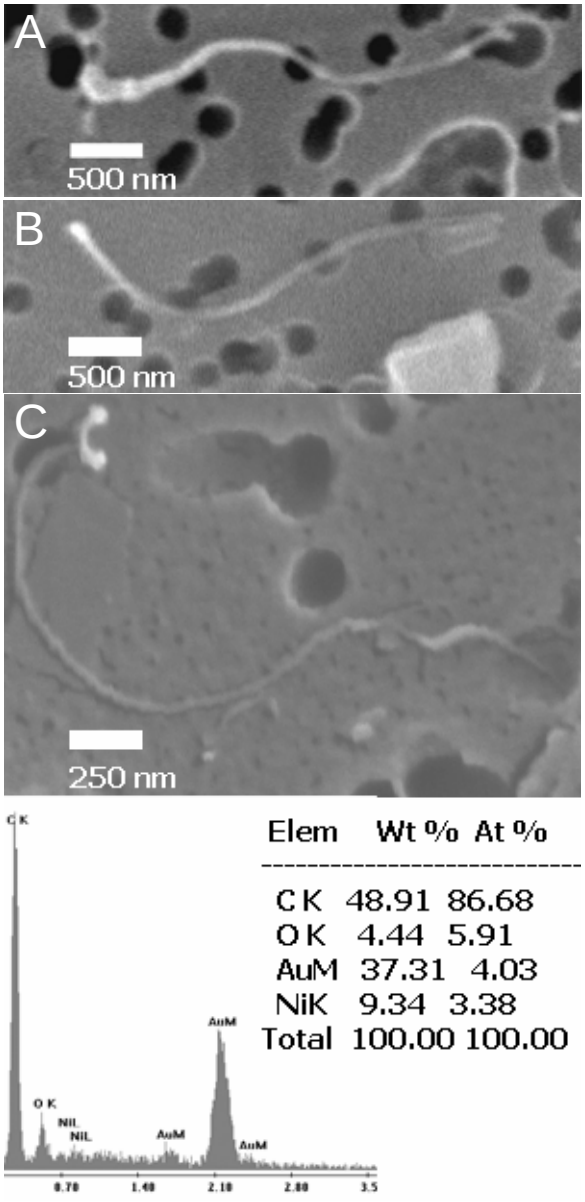

Figure 4.6. Nickel deposit on the tips of MWCNTs. Pulsed DC electrical field; 10kV/cm, 1.0 millisecond on-time, 24.0 millisecond off-time, and applied for a total on time of 60 seconds. The electrolyte consisted of 0.5 mM nickel (II) chloride in 1: 4 dry N, N-Dimethylformamide (obtained from Sigma Aldrich, used straight from the bottle): toluene (dried over calcium hydride). SEM images obtained on an Amray 1830 (images A and B), and a Philips XL 30 ESEM (image C).

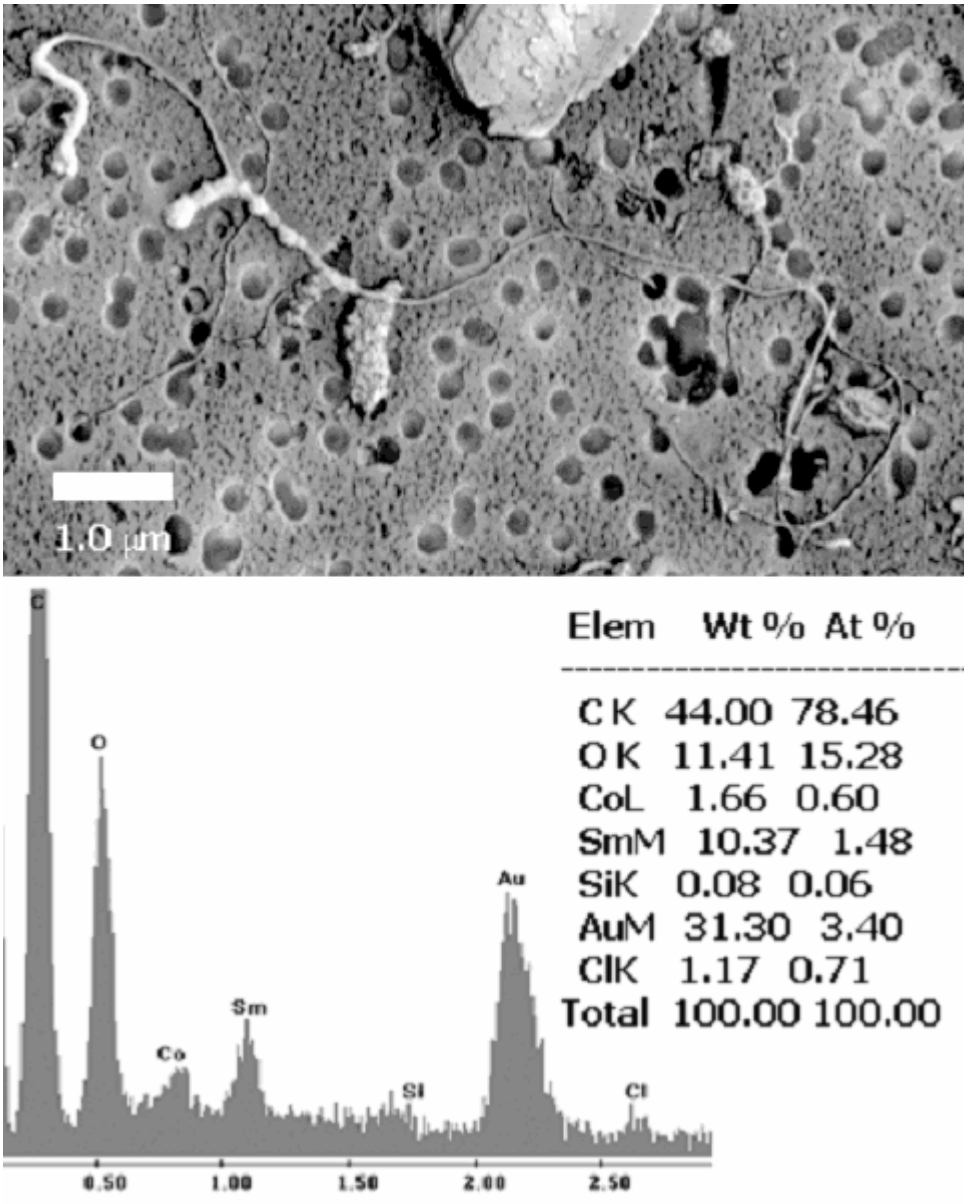

Figure 4.7. Ramified deposit on the tips of commercial carbon nanotube. Electrical field: 10kV/cm, on-time: 1.0millisecond, off-time: 24.0milliseconds, electrolyte: 3: 7 (v/v) acetonitrile/toluene (both dried over calcium hydride); 0.5 mM cobalt chloride; 0.5 mM samarium (II) iodide, the total on-time was 60 seconds. SEM micrographs obtained on a Philips XL 30 ESEM.

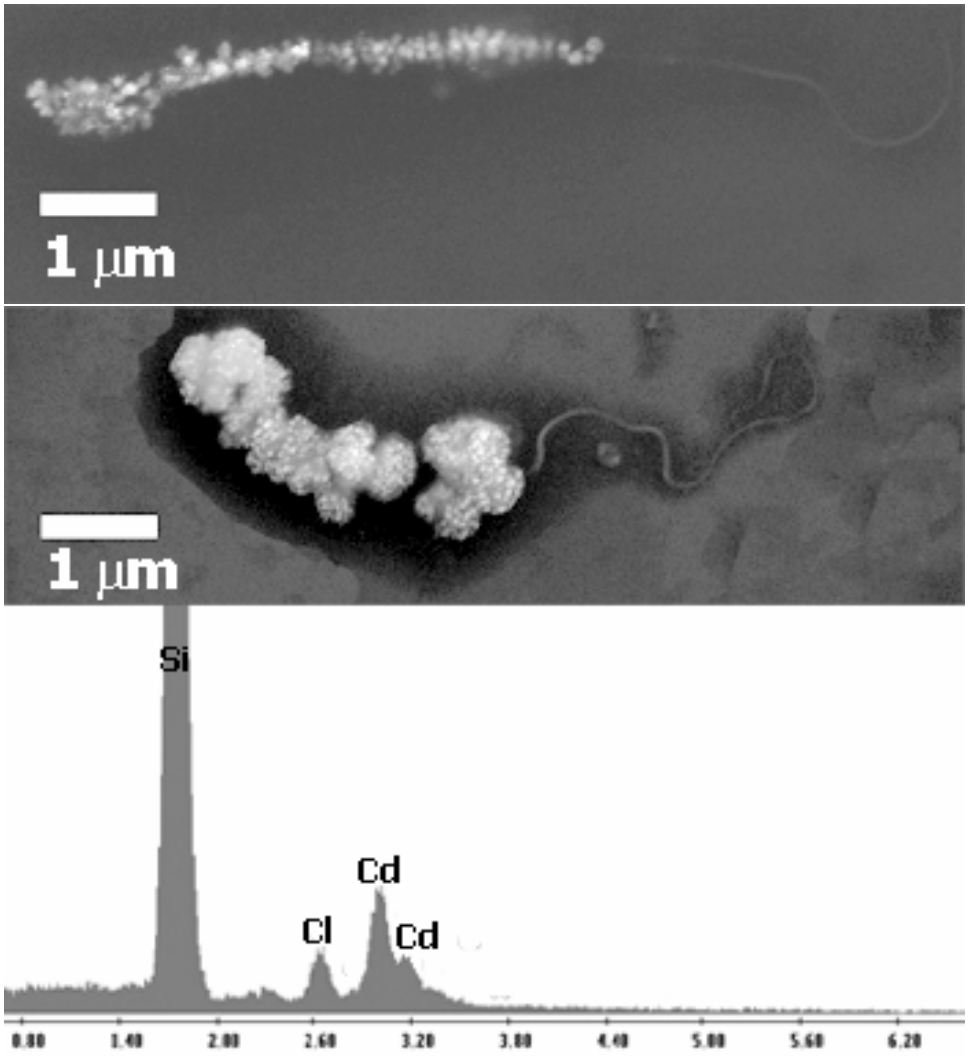

Figure 4.8. Cadmium deposits on one tip of commercial MWCNT. Deposition conditions were a 10kV/cm pulsed DC electrical field with an on-time of 1.0 millisecond, an off-time of 24.0 milliseconds, and a total on-time of 60.0 seconds. The electrolyte used was 1.0 mM cadmium (II) chloride in a solvent mixture of 1: 4 dimethylsulfoxide (dried over calcium hydride under reduced pressure): toluene (dried over calcium hydride). SEM characterization was done on a Philips XL30 ESEM.

Figure 4.9 shows unique whisker like deposits on one tip of isolated CVD grown MWCNTs. The morphology of the deposits differed from previous experiments on MWCNTs. The isolated MWCNT in Figure 4.9A has a length of 3 μm and the deposit has a large number of whiskers. In Figure 4.9B the nanotube has a length of 2.5 μm and the length of the whisker like deposits vary between 200-400 nm. In Figure 4.9B EDS characterization of the deposit identified tin and chlorine.

The ESEM micrographs in Figure 4.10 show deposition on the single tips of aligned MWCNT. The lengths of the nanotubes vary between 6-12.0 μm. The deposits were highly ramified and the EDS spectrum showed a large silver peak, and a small chlorine peak. A Philips XL30 ESEM was used to examine the sample.

Figure 4.11 is a combination of ESEM images, EDS spectra, and EDS quantitative data tables. Figure 4.11A is an electron micrograph of a 27 μm CVD grown MWCNT with a 5 μm dendritic zinc growth on one tip. A 24 μm CVD grown MWCNT with a dendritic growth of zinc on one end of the nanotube is presented in Figure 4.11B. The corresponding EDS spectrum and quantitative data table identifies zinc in the deposit. The zinc growth extends approximately 4 μm from the tip of the nanotube and is non continuous with large gaps located in various parts of the zinc deposit. The image in Figure 4.11C shows an 11 μm CVD grown MWCNT with a zinc growth that extends 4.0 μm from one tip of the nanotube. The growth is not as branched as the growth in Figures 4.11A and 4.11B, and zinc is identified in the EDS spectrum.

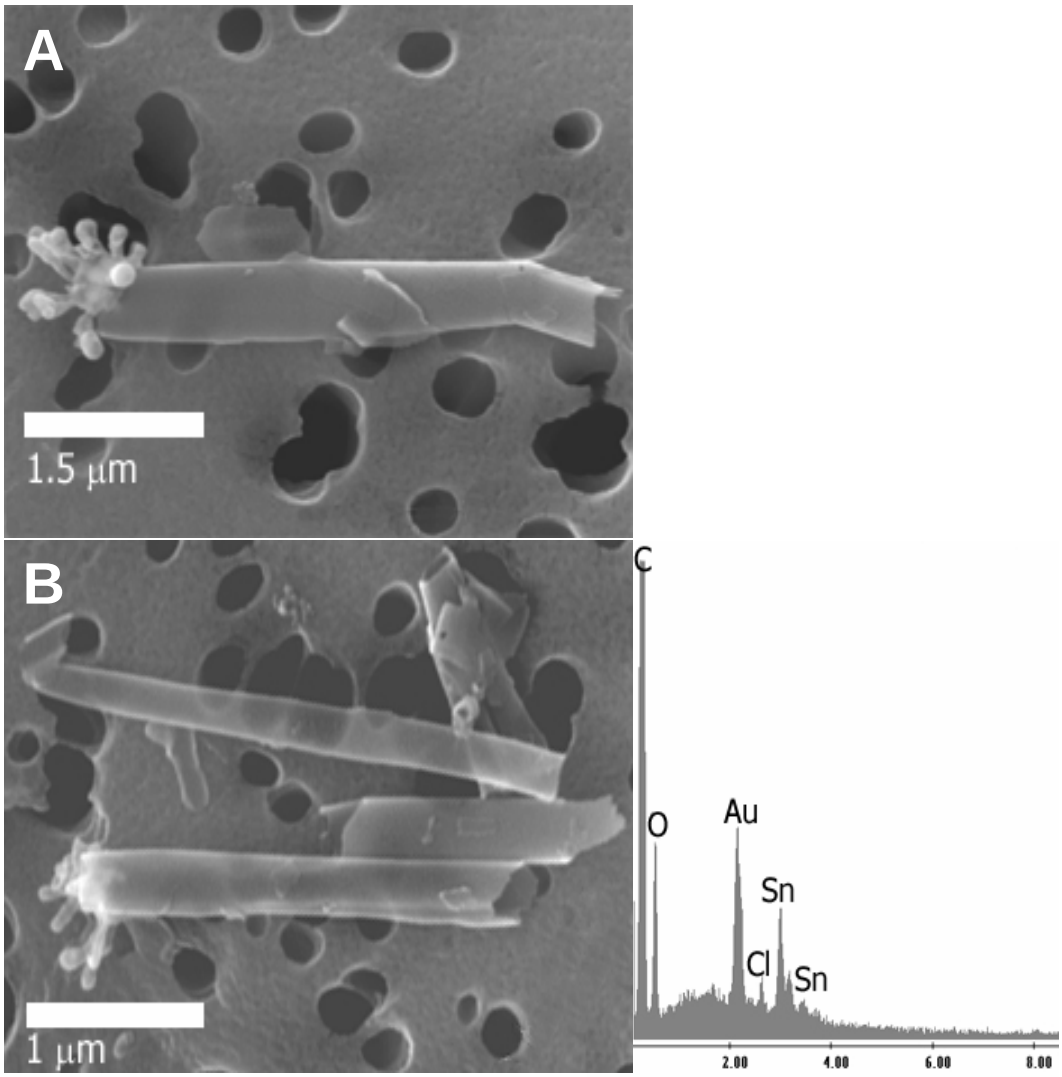

Figure 4.9. CVD grown MWCNT with tin on one tip. The electrolyte used consisted of 1.0 mM tin (II) chloride in 1: 4 (v/v) acetonitrile/toluene (both dried over calcium hydride). A pulsed DC electrical field with an on-time of 1.0millisecond, an off-time of 24.0milliseconds, a total on-time of 10 seconds, and a field intensity of 10kV/cm was applied. Sample was examined on a Philips XL30-ESEM.

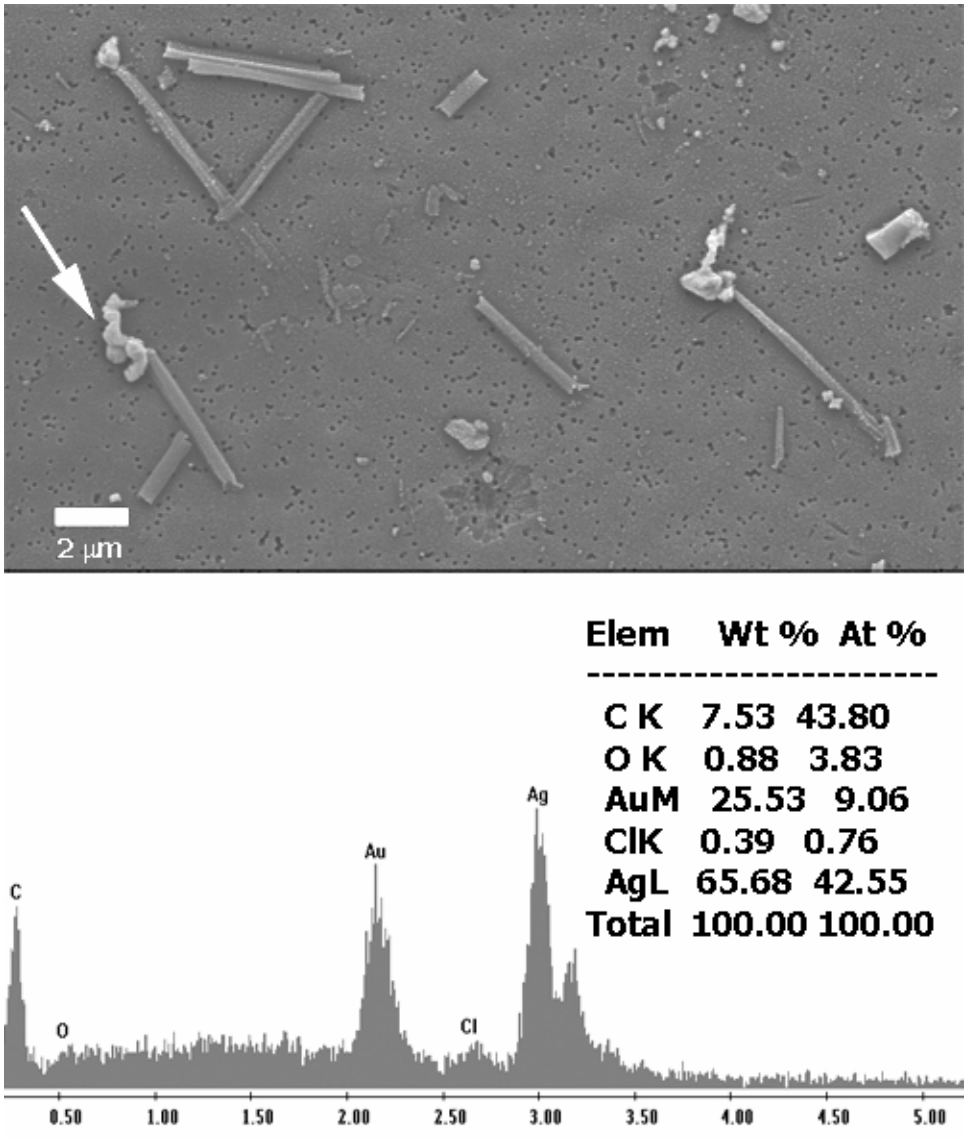

Figure 4.10. Bipolar electrodeposition of silver onto isolated CVD grown MWCNT. Solution used consisted of 1.0 mM silver nitrate in 1: 4 acetonitrile: toluene (both dried over calcium hydride). The electric field used had a field intensity of 10kV/cm, an on-time of 1.0milliseconds, an off-time of 24.0milliseconds, and was applied for a total on-time of 20seconds. The white arrow indicates the sample used for EDS characterization. SEM analysis was done on a Philips XL 30 ESEM.

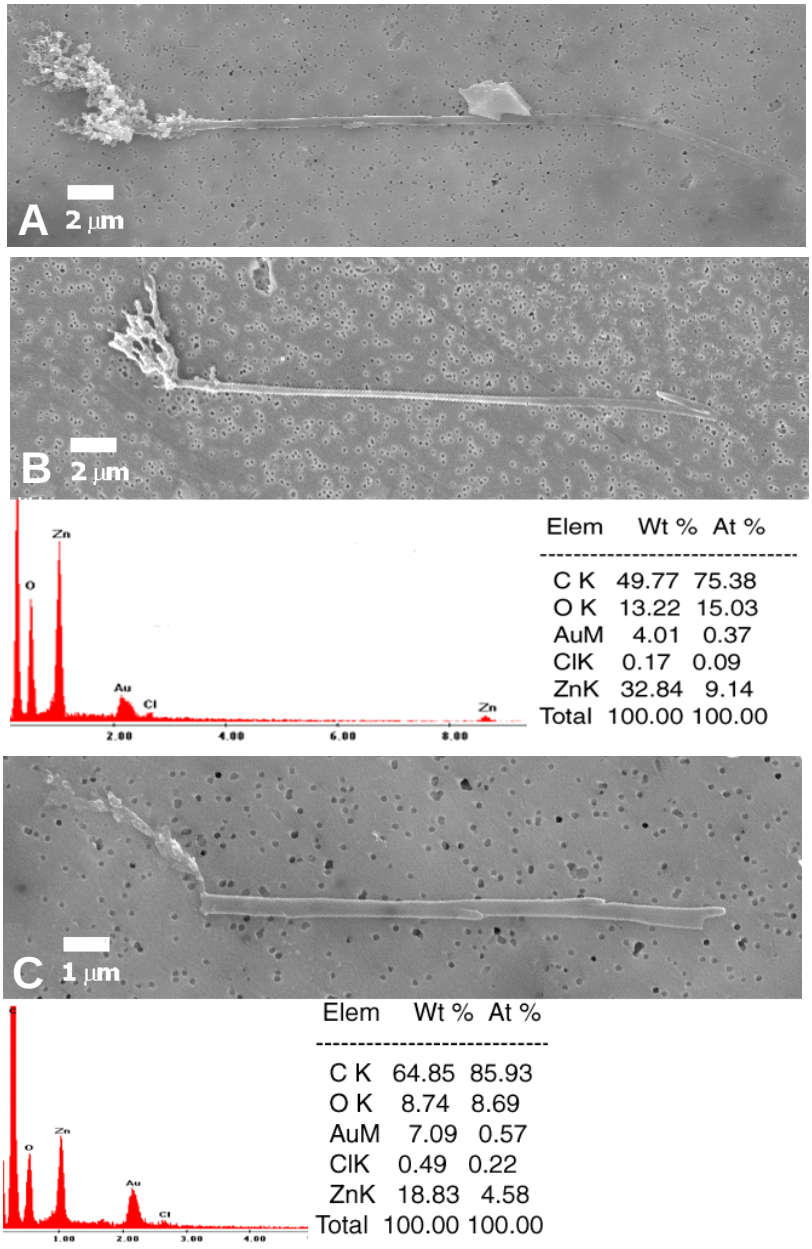

Figure 4.11. CVD grown MWCNT with zinc metal deposit on one tip**.** 10kV/cm pulsed dc electrical field, on-time: 1.0 millisecond, off-time: 24.0 milliseconds, total on-time: 40 seconds, and the electrolyte was 1.0 mM zinc (II) nitrate hexahydrate; 1: 4 (v/v) acetonitrile/toluene (both dried over calcium hydride). Images were obtained on a Philips XL30 ESEM.

Figures 4.12 and Figure 4.13 show examples of the bipolar electrodeposition of gold and then palladium on opposite tips of isolated CVD grown MWCNTs. In Figure 4.12 the MWCNT has over 95% of the surface covered by deposit. The nanotube deposit structure is approximately 5 μm in length and the center of the nanotube seems to have collapsed. The EDS spectra and quantitative data tables of the deposits on opposite tips, show one tip with gold and very little palladium, and the opposite tip to have significant amounts of palladium and gold. In Figure 4.13 the CVD grown MWCNT is 1.5 μm in length, the deposit is limited to the tips and the quantitative data tables from the EDS spectrum show gold and palladium on both tips.

The SEM micrographs in Figure 4.14 show a dendritic growth off one tip of an isolated 12 μm nanotube (Figure 4.14A), and a branched growth off one tip of an isolated 5 μm nanotube (Figure 4.14B). The dendritic growth in Figure 4.14A is about 4 μm, and in Figure 4.14B it is about 2 μm. A few interesting features in Figure 4.14 are the transparent nature of the nanotube in Figure 4.14A, in Figure 4.14B the deposit seals one end of the nanotube, and the differences in the morphology of the deposits obtained on the 12 μm nanotube and the 5 μm nanotube.

A 15 μm isolated CVD grown MWCNT with deposits on both tips is presented in the electron micrographs in Figure 4.15. From the higher magnification image in Figure 4.15B the deposit has a length of approximately 4 μm, has two branches, and seals the end of the nanotube. In Figure 4.15C the deposit is highly branched, seals the end of the nanotube, and from Figure 4.15A the deposit extends about 7 μm from the tip of the nanotube.

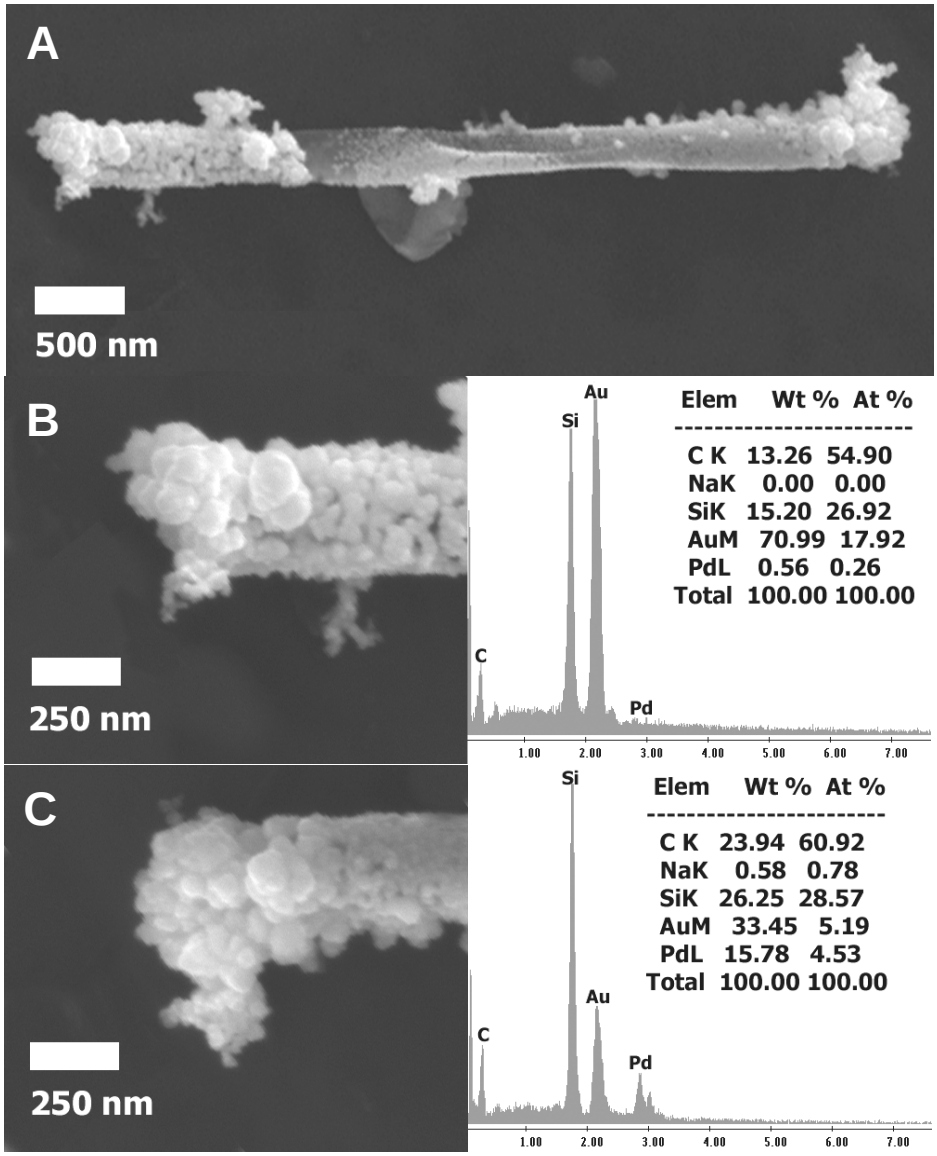

Figure 4.12. SEM (Philips XL30 ESEM) micrographs showing the bipolar electrodeposition of palladium and gold onto opposite tips of an isolated CVD grown MWCNT. Two field application experiments were conducted on one sample. The first experiment deposited gold on one tip and the second deposited palladium on the opposite tip. For both experiments a pulsed DC electrical field with a field intensity of 10kV/cm, an on-time of 1.0millisecond, and an off-time of 24.0milliseconds. The first electrolyte used had 0.2 mM gold (III) bromide in a mixture of 1: 4 acetonitrile: toluene. The second electrolyte used consisted of 1.0 mM palladium (II) chloride in 1: 4 acetonitrile: toluene. The solvents used had been dried over calcium hydride before use.

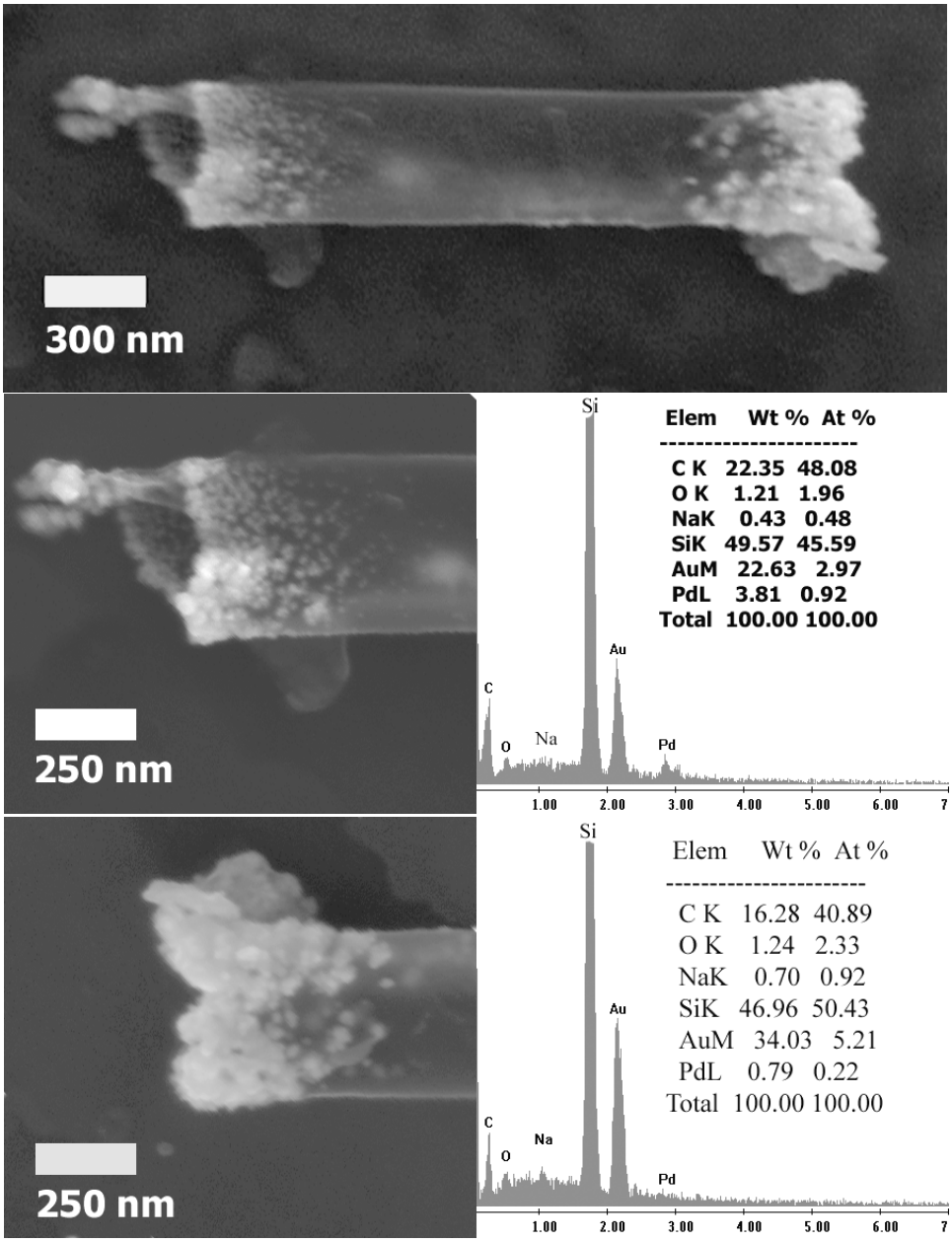

Figure 4.13. A Second example of the bipolar electrodeposition of gold and palladium onto opposite tips of an isolated CVD grown MWCNT. For both experiments a pulsed DC electrical field was used (on-time: 1.0millisecond, off-time: 24.0milliseconds), solvent mixture was 1: 4 acetonitrile: toluene (both dried over calcium hydride), and the concentrations of metal salt were 0.2 mM gold (III) bromide for the first deposition, and 1.0 mM palladium (II) chloride for the second deposition. SEM micrographs obtained on a Philips XL30 ESEM

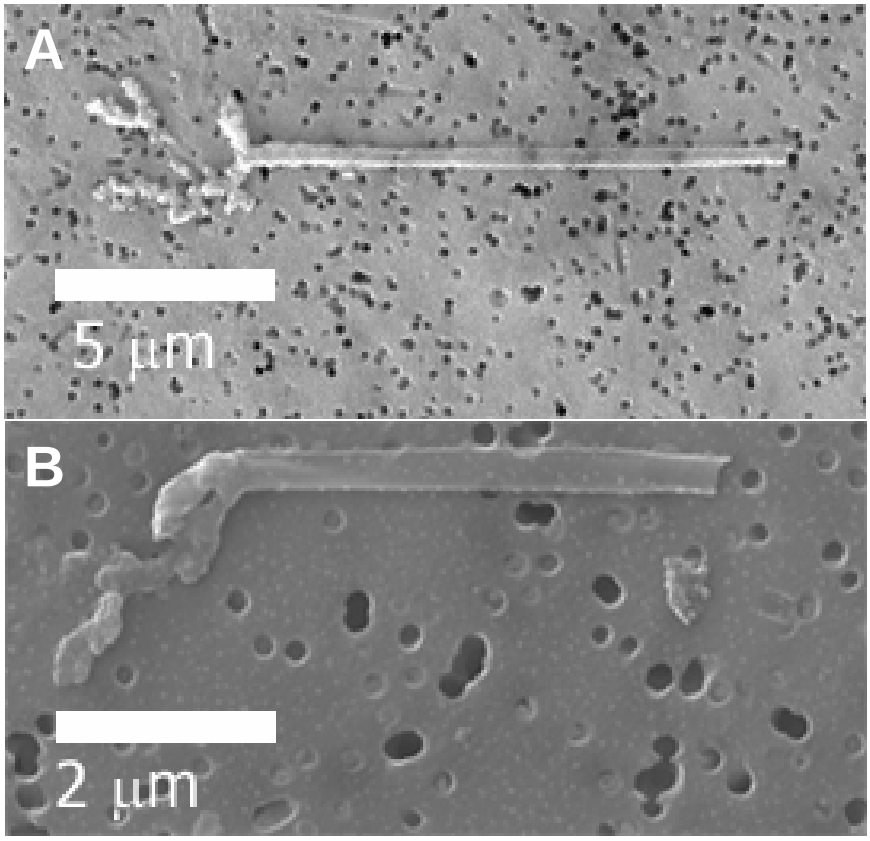

Figure 4.14. ESEM micrographs of polypyrrole deposits on one tip of a CVD grown MWCNTs. The electrolyte consisted of 0.35 mM sodium salt of p-toluene sulfonic acid and 0.70 M pyrrole in a mixture of 40% acetonitrile and 60% toluene (both dried over calcium hydride). The field used was a pulsed DC electrical field with an intensity of 10kV/cm, an on-time of 1.0millisecond, and an off-time of 24.0milliseconds. The total on-time used was 10 seconds.

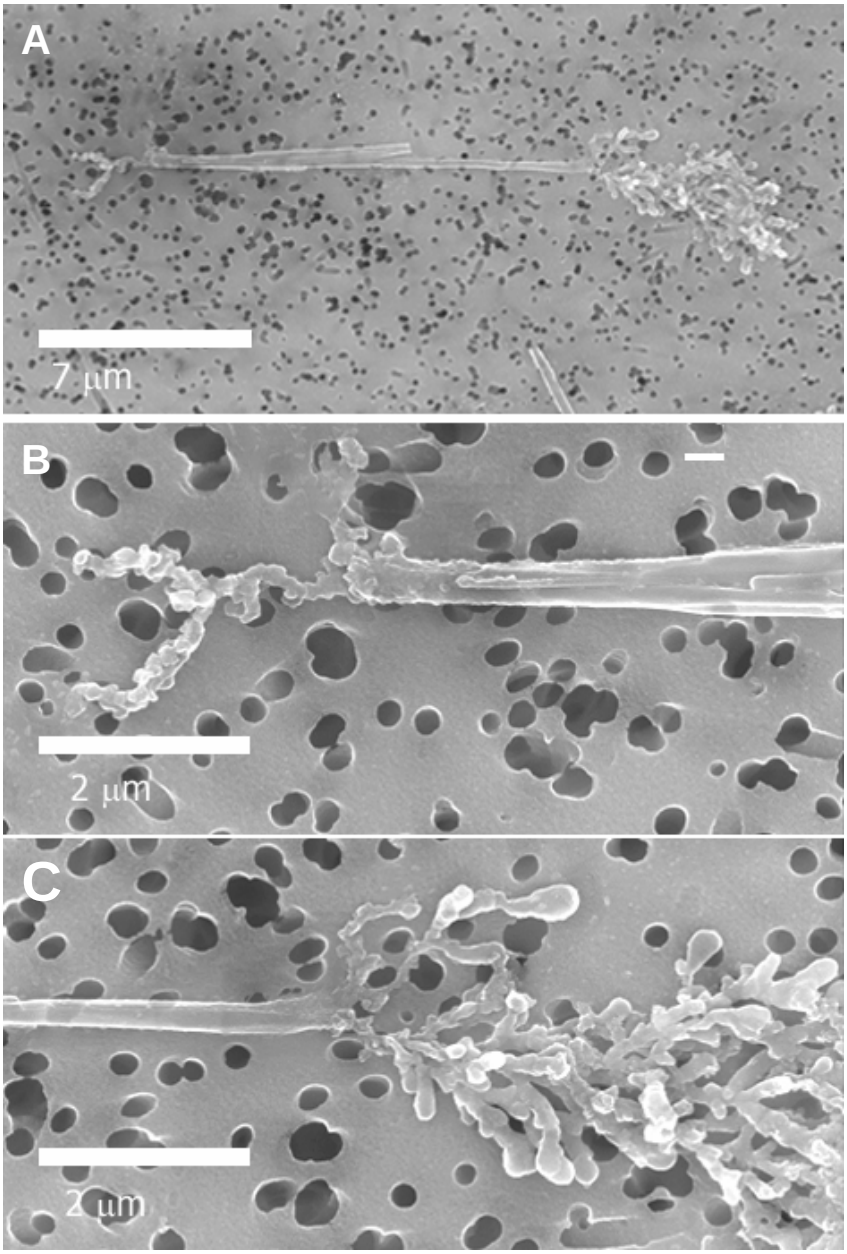

Figure 4.15. An example of the successful bipolar electrodeposition of polypyrrole onto opposite tips of an isolated CVD grown MWCNT. The electrolyte consisted of 0.40 mM sodium salt of p-toluene sulfonic acid and 0.80 M pyrrole in 40% acetonitrile and 60% toluene (both dried over calcium hydride). For both field applications a 10kV/cm pulsed electrical field (on-time: 1.0millisecons, off-time: 24.0milliseconds) was applied for a total on-time of 5seconds**.**

The nanotube in Figure 4.15 is a Y-branched nanotube, and is transparent under SEM (Philips XL 30 ESEM).

4.4.c Discussion

When an isolated carbon nanotube is immersed in a suitable electrolyte and an electrical field is applied across the nanotube, a potential difference is induced across the nanotube. The potential difference polarizes the solution nanotube interface. If the applied electrical field is increased it will reach a magnitude great enough to induce electrochemistry on the tips of the nanotubes. The tip of the nanotube facing the cathodic feeder electrode will act as the anode, and the tip of the nanotube facing the anodic feeder electrode will act as the cathode. Located on each nanotube there will be a cathode/anode pair. A direct consequence of this is that metal deposition will occur on one tip i.e. the cathode, and in the case of electropolymerization of polypyrrole the deposition occurs on the anode tip.

The potential difference across the tips of the isolated nanotubes used in the various experiments can be estimated. If the nanotube is aligned with the direction of the applied electrical field, the potential difference (V_d) is calculated by taking the product of the electrical field (E) and the length (L) of the nanotube.

(1) $\circ V_d = E \times L$

In a 10kV/cm electric field a 10μm long nanotube will have a potential difference of 10.0V (10, 000V/cm x 0.001cm).

If the nanotube is at an angle (θ) to the direction of the applied electrical field the potential drop across the nanotube is calculated from equation (2):

$$(2) \circ V_d = E \times L \times \cos\theta$$

These equations can be easily applied to the CVD MWCNT, but when looking at the commercial MWCNT the curvaceous nature of the nanotubes has to be accounted for. When the commercial MWCNT are aligned with the field the actual length that produces the potential difference is not the true length of the nanotube. The actual length that produces the potential drop is the distance from the modified tip to the furthest part of the nanotube that curves back towards the functionalized tip (Figure 4.16). A clear example is presented in Figure 4.3. The unmodified tip of the nanotube, seen in the lower right corner of Figure 4.3A, curls back on the nanotube and there are several curls and bends in the nanotube. The nanotube (plus deposit) has a true length of 6.8 μm, while the actual length that results in the potential difference for bipolar electrodeposition is 3.3 μm. From these values the potential drop across the nanotube was 3.3 V. This value is above the potential required for palladium metal deposition in our system, and it is well above the empirical value seen in earlier studies on the carbon nanofibers and on graphite platelets. Figure 4.16 helps to illustrate two important factors in bipolar electrodeposition. Nanotubes aligned with the applied electrical field must have a minimum length in order for the potential drop to reach the minimum value for electrodeposition of the metal of interest i.e. if the nanotube is too short no metal will deposit on the tip. Figure 4.10 presents a clear example.

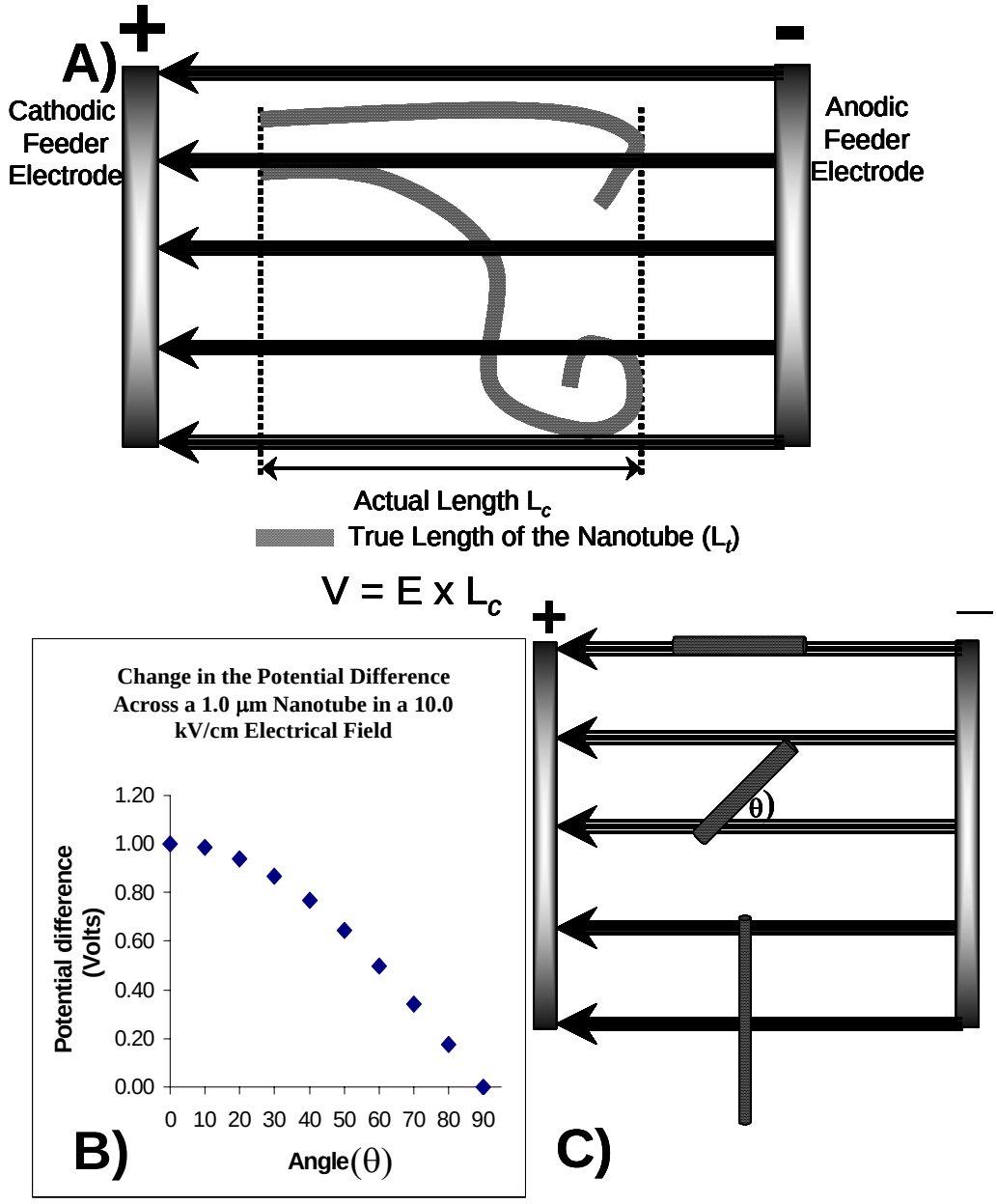

Figure 4.16. The illustration demonstrates how the potential drop (V) across a commercial MWCNT is calculated, and the dependence of the nanotubes angle in the applied electric field.

The nanotube in the center of the image has a length of 3.0 μm, and the shortest nanotube with deposit has a length of 6.0 μm.

In all examples for the bipolar electrodeposition of a metal onto the tip of an isolated commercial MWCNT, the length of the nanotube is estimated. A true length can not be given because the tip is completely covered with metal deposit. The nature of this coverage can occur in one of two ways. In both types of growth, nucleation will occur on the tip of the nanotube and along the nanotube at points where the potential has a value equal to or greater than the potential required for metal deposition. Continued growth will occur preferentially on the nucleation sites; however, the growth can follow an isotropic growth pattern, or an anisotropic growth pattern.

In the isotropic growth pattern the metal deposition occurs on all nucleation sites equally resulting in the ramified deposits seen in Figures 4.3 through 4.8. In this case the length of the nanotube can be estimated with an error of a few tens of nanometers. In the anisotropic growth pattern the metal deposition occurs preferentially on nucleation sites with a higher potential i.e. the tip of the nanotube. As the metal deposits on the tip of the nanotube the overall length of the nanotube increases and the potential drop across the nanotube increases. Thus, the most preferential site for continual deposition will be the growing tip. In this growth pattern, the deposit may extend for several micrometers, thus the length of the nanotube cannot be determined with any accuracy. The pattern of growth is most likely anisotropic because this is what was seen on the carbon nanofibers (chapter 2) and in the growth of copper wires from isolated copper beads.[47]

Palladium, gold, nickel, cobalt, samarium/cobalt, and cadmium deposition on the commercial MWCNT produced ramified deposits. The ramified deposits were similar in

morphology to the deposits seen on the graphite platelets and carbon nanofibers. The deposits were identified through the use of EDS. For all samples on the polyester membrane there are three common peaks; these are, carbon, oxygen, and gold. The gold peak is from the gold coating put on all of these samples before SEM characterization. The carbon and oxygen peak is from the polyester membrane. It is possible the oxygen peak is from the deposit if the oxide formed instead of the native metal. The likelihood of the oxide forming is very low. A source of oxygen is needed to form the oxide in the non-aqueous solvents used. Possible sources of oxygen include atmospheric oxygen, water of crystallization, or the metal counter ion. The experiments are conducted under nitrogen for safety reasons (a spark in a mostly toluene solvent will produce large fires), and as a result the amount of atmospheric oxygen is minimized. Dissolved oxygen in the solvents used will be low especially after distillation. Water of crystallization is not a factor, since for all experiments (except zinc deposition) anhydrous salts were used.

Another concern in the deposition experiments was the deposit was simply the metal salt re-crystallizing on the tip of the nanotube. EDS analysis helped to disprove this notion. Figure 4.3 has the quantitative data table for the palladium deposit, and no chlorine was present in the sample. When the chlorine was detected the amount did not correspond to stoichiometric quantities (Figure 4.7), thus the residual chlorine was attributed to insufficient washing of the sample after field application.

Figure 4.4 shows a transition in the morphology of the gold deposits from ramified to large needle like structures off one tip of the nanotubes. This transition is strange simply because bipolar electrodeposition favors a directional growth that, in the case of the nanotube, will produce a wire like growth off the tip.

Unusual metal deposits were observed with tin (Figure 4.9) and with zinc (Figure 4.11). With tin these deposits are similar to what was seen with tin electrodeposition from aqueous solutions.[48]

Cadmium electrodeposition onto commercial MWCNT produced large ramified deposits on one tip of the nanotube. This is very similar to what has been observed before on previous samples with palladium, gold, nickel and cobalt. What has not been observed before is the deposit accounting for more than 50% of the nanotube deposit structure. This is not possible in bipolar electrochemistry. The potential drop across a nanotube is going to vary from a cathodic potential at the tip where metal deposition occurs, to an anodic potential at the opposite tip. This variation between the two tips means at some point along the nanotube the cathodic potential will reach a minimum and then the anodic potential will begin to increase. This transition will occur at the midpoint of the nanotube and metal deposition will not occur at or past this point, therefore the deposit cannot account for over 50% of the length of the nanotube structure. Figure 4.17 illustrates two possible scenarios that will result in such large deposits. The majority of MWCNT 1 experiences a cathodic potential due to the numerous curves and bends. After deposition MWCNT 1 will produce a nanotube deposit structure that has over 50% of its length made up of metal deposit. MWCNT 2 is in the exact opposite scenario. The majority of MWCNT 2 experiences an anodic potential; however, the resulting nanotube deposit structure has metal deposit for over 50% of its length. In the case of MWCNT 2 the deposit grew off the tip of the nanotube to produce a long ramified metal deposit, which is consistent with what has been observed with previous results on carbon nanofibers.

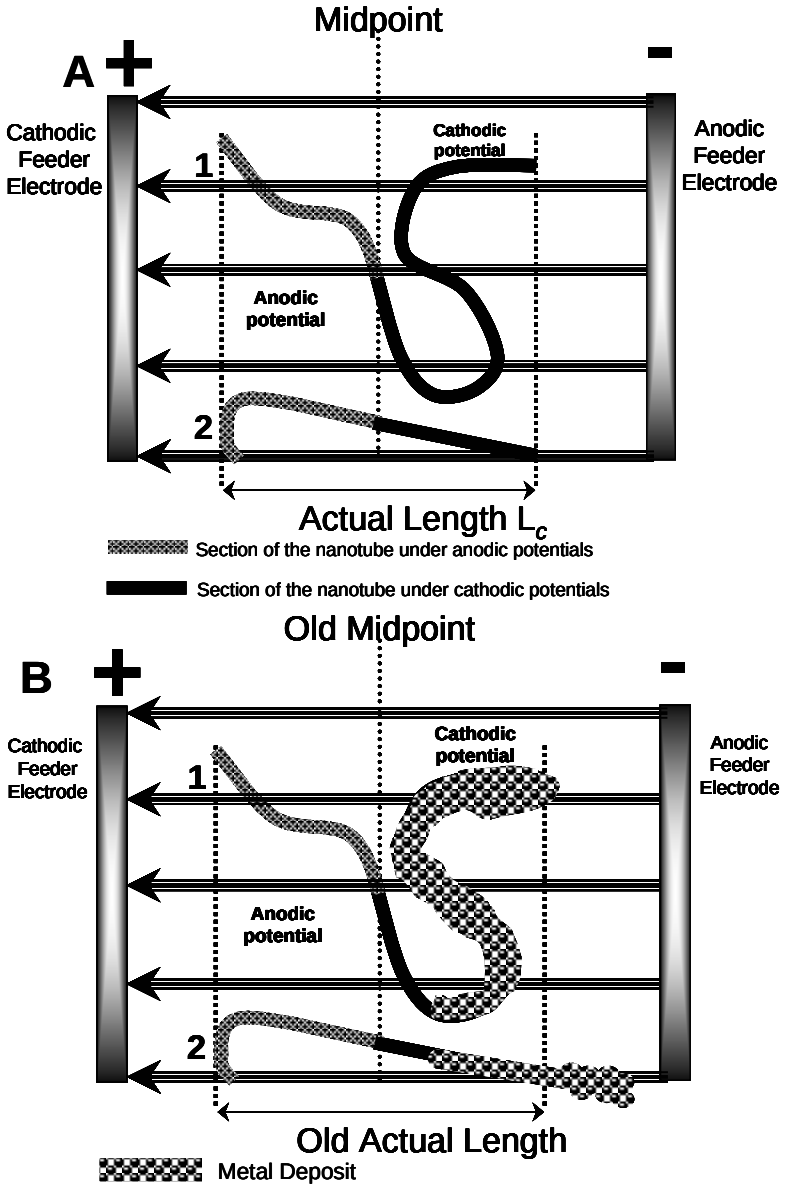

Figure 4.17. Illustration of how the metal deposit can make up more than 50% of the nanotube deposit structure. In MWCNT 1, the majority of the nanotube experiences a cathodic potential as a result more than 50% of the nanotube is covered with deposit. On MWCNT 2 the deposit simply grows off the tip resulting in a long deposit that is more than 50% of the total structure.

Gold and palladium were deposited on opposite tips of a CVD grown MWCNT (Figure 4.12 and Figure 4.13). The double deposition experiment followed the same general method i.e. nanotubes on a polyester membrane were exposed to a pulsed dc electrical field (10 kV/cm, on-time: 1.0 millisecond, off-time: 24.0 milliseconds). The difference is two successive deposition cycles were done on the sample. The first cycle used 0.2 mM gold (III) bromide in 1: 4 (v/v) acetonitrile/toluene (both dried over calcium hydride). After the first deposition the experimental cell was placed in 100 mL HPLC grade acetonitrile for five minutes, removed, and left to air dry. Once dry the experimental cell was set up for the second field application. The second cycle was applied by switching the leads to the platinum electrodes. The solution used was 1.0 mM palladium chloride in 3: 7 (v/v) acetonitrile/toluene (both dried over calcium hydride). For both cycles the total time (on-time) the field was applied was 10 seconds. After a second immersion in 100 mL of HPLC grade acetonitrile the dry membrane was transferred to a test tube. After the addition of 0.5 mL of 200 proof ethanol (Pharmco) the test tube was sonicated (Branson bath sonicator) for 30 seconds. 50 microliters of the resulting suspension of modified nanotubes were then drop dried onto an n-doped silicon wafer (approximately 2.0 mm by 3.0 mm), and a separate 50.0 microliters was drop dried onto a 200 mesh copper TEM grid (Holey carbon membrane, SPI Inc) . The SEM analysis was done on a Philips XL 30 ESEM. The logic behind removing the nanotubes from the membrane was to obtain a suspension that could be mounted for TEM studies. Unfortunately, TEM examination of the sample proved fruitless. The fact nanotubes with deposits on opposite ends were found attests to the robust nature of the metal nanotube interaction. The EDS analysis on the deposit on the left side of the nanotube in Figure 4.12A shows the deposit

is gold. The gold deposit has a small percentage of palladium, which are possibly palladium ions that were not washed off the deposit. This deposit was the first to be deposited. The second deposit, on the right of the nanotube in Figure 4.12A, is a mixture of gold and palladium. The mixture of gold and palladium on the second deposit is likely due to the electrodissolution of gold. When the direction of the field is reversed the tip with the first deposit of gold becomes the anode. This is also true of the feeder electrodes. Thus there are two sources of gold the tip of the nanotube and the anodic feeder electrode. This system consists of multiple nanotubes and it is quite possible that any number of nanotubes in the vicinity would also provide a source of gold. Gold is a very stable metal and will not typically electrodissolve in most electrochemical applications, hence its use as an electrode. Gold; however, can electrodissolve in acetonitrile solutions with NaSCN present.[49] In aqueous solutions, the electrodissolution of gold has been shown to be aided by the presence of chloride ions.[50] Gold oxidation occurs at -1.498V.[51] The potentials across the nanotubes in Figure 4.12 and 4.13 were 5.0V and 1.5V, thus it is possible the potential at the ends of the nanotubes could induce the oxidation of gold. The dissolution of the gold from the feeder electrode is the likely source for the gold on the deposit on the opposite tip. The unusual coverage of the nanotube in Figure 4.12A is attributed to a similar mechanism that produced the long structures of cadmium off of commercial MWCNT (Figure 4.8).

Cadmium sulfide is a group II-VI semiconductor and it is used in a variety of applications such as photocatalysis, solar cells, and other opto-electronic devices. The interest in depositing cadmium sulfide onto carbon nanotubes is to provide a direct connection between nanotubes and semiconductor nanocrystals. Such nanostructures

may find use in various nanoscale optoelectronic devices. Semi-conductor nanocrystals have been attached to carbon nanotubes via ester or amide linkages using wet chemical processing. These methods usually result in complete coverage of the nanotubes with the nanocrystals.[52,53,54] In bipolar electrochemistry the tip of the nanotube is covered with the nanocrystals. It is important to note that an uncapped nanotube tip has exposed graphene layers that may provide an electron rich area for nanocrystal nanotube interaction. The bipolar electrochemical deposition of cadmium sulfide onto one tip of an isolated nanotube was successfully demonstrated. The solution composition used was adapted from Xu et, al[55]. A primary concern with this method of deposition is the separate deposition of cadmium and sulfur as opposed to cadmium sulfide. The EDS analysis gave percentages of cadmium and sulfur that correspond to the stoichiometric amount for cadmium sulfide.

Deposition of polypyrrole expanded the ability to modify carbon nanotubes through bipolar electrodeposition. By depositing polymers on one tip of a nanotube, the tip can be further modified by attaching different functionalities to the polymer modified tip. Figure 4.14 shows two types of deposits. The first type is dendritic in nature (Figure 4.14A) and the second has only two branches (Figure 4.14B). This difference can be explained by considering the potential across the two nanotubes. High applied potentials result in polypyrrole growths with a large amount of dendrites.[56] In Figure 4.14A the potential across the nanotube is 12.0 V (10.0 kV/cm x 12.0 μm), and in Figure 4.14B the potential is 5.0 V (10.0 kV/cm x 5.0 μm). Thus, in Figure 4.14A the nanotube with the higher potential has the larger number of dendrites.

The double deposition of polypyrrole resulted in sealed nanotubes. The first deposit seen is the shorter deposit on the left of the nanotube in Figure 4.15A. When the first polypyrrole structure deposits on the tip of the nanotube, it increases the total length of the nanotube polypyrrole structure. In this example the total length increases from 15.0 μm (no deposit) to 19.0 μm (4.0 μm deposit). The potential across the nanotube changes from 15.0 V, during the first deposition, to 19.0 V for the second deposition. This increase in the potential results in the larger highly branched second deposit.

4.5 Potential Applications with Carbon Nanotubes Modified by Bipolar Electrochemistry

With the development of a system to reliably modify carbon nanotubes with polymers, semi-conductors, and metals, the next steps will involve the characterization of the physical, optical or electrical properties of the resulting nanostructures. In order to apply the resulting nanostructures, it is not absolutely necessary to fully characterize the structures. Two examples that illustrate this point are presented.

4.5.a Nanofluidics

The movement of fluid in to a nanotube i.e. nanofluidics[57] is an area in which bipolar electrochemistry can be applied. A logical assumption in this regard would be experiments conducted that traps various liquids in nanotubes by sealing the ends, with a suitable material, using bipolar electrochemistry. Such experiments are in the preliminary stages with little success so far.

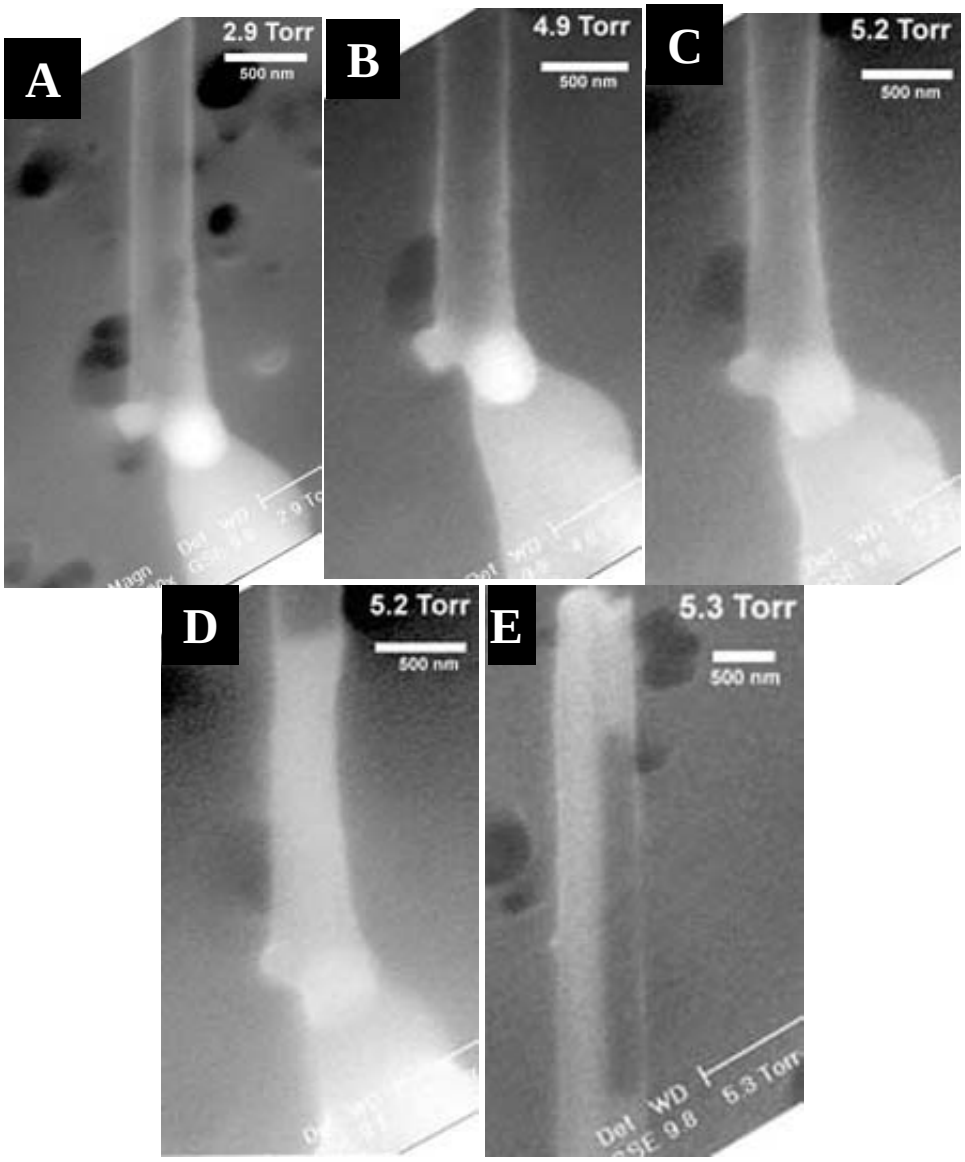

Figure 4.18. Water condensation inside CVD grown carbon nanotubes functionalized with polypyrrole. The nanotubes were exposed to a 10kV/cm pulsed (on-time: 1.0millisecond, off-time: 24.0milliseconds, 1.0M pyrrole, 0.3 mM p=toluene Sulfonic acid sodium salt, 30%: 70% acetonitrile/toluene) for a total on-time of 5.0 seconds. The CNTs were imaged in a Philips XL-30 ESEM in environmental mode. The sample was mounted on an SEM stub. The SEM stub was placed on peltier stage and the temperature was maintained at 5 degrees Celsius. Water was condensed by slowly increasing the water vapor pressure from 2.5 Torr to 5.3 Torr.

However, imaging the condensation of water on isolated carbon nanotubes with polypyrrole on one tip did reveal some interesting results (Figure 4.18). The carbon nanotubes had been modified with polypyrrole on one tip, and when water was forced to condense onto the substrate, water condensed on the tips with polypyrrole and filled the nanotube from the functionalized tip and into the nanotube. The mechanism for this is unknown, but it may be due to the highly hydrophilic polypyrrole deposit. The experiment does demonstrate an alternative method for the directed and controlled filling of carbon nanotubes.

4.5.b Carbon Nanotube Arrays

One of the first attempts made to apply this non-contact method to end use applications was the synthesis of an array of nanotubes modified by bipolar electrodeposition. Similar arrays have been synthesized with or without modifying the tips of the nanotubes. The arrays are simply the CVD grown nanotubes in the alumina template, as shown in the ESEM micrograph in figure 4.19.

The array was made by first removing the carbon layer on top of the alumina membrane. The removal was attempted by sonicating the membrane in toluene for about 5 minutes. To expose the tips of the nanotubes, 4.0M sodium hydroxide was placed on top of the membrane for 5 minutes. After rinsing and drying the membrane fragment, the fragment was exposed to a pulsed (t-on: 1millisecond; t-off: 24milliseconds) DC electrical field at 10kV/cm for 20 seconds.

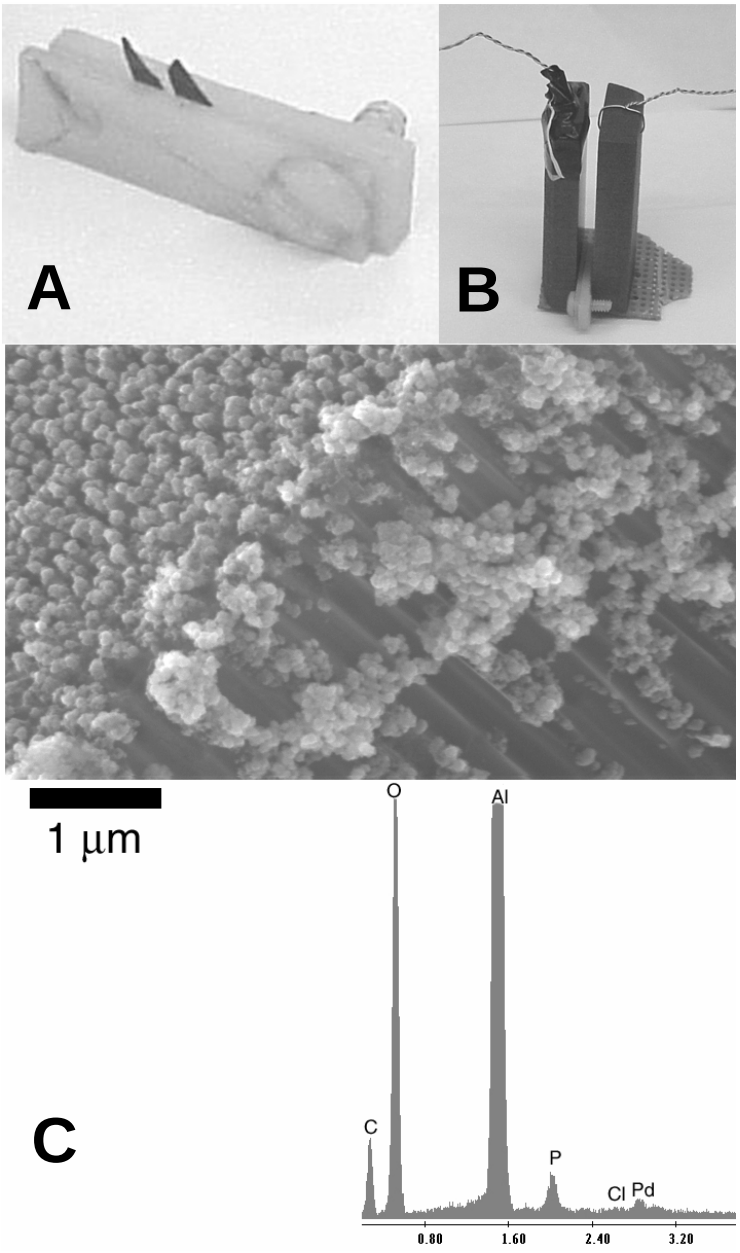

Figure 4.19. Image (A) shows two Teflon blocks used to hold the membrane fragment. The Teflon block was placed between two graphite electrodes (image B) and set up for field application using same field application seen in Figure 4.2. The sample was exposed to a pulsed dc electrical field (10kV/cm, t-on: 1.0millisecond, t-off: 24.0millisecond) in a 1.0 mM solution of palladium chloride in 20% acetonitrile: 80% toluene (both dried over calcium hydride). Image (C) is an ESEM micrograph with the corresponding EDS of the deposit seen on the top of the membrane**.**

The electrolyte used consisted of 1.0 mM palladium chloride in 3: 7 (v/v) acetonitrile/toluene. On ESEM examination palladium deposits were found on the tips of the nanotubes. This simple array could be used in catalysis. One possible method would be to construct a setup that would allow for the use of the nanotubes as pipes that flow the reaction mixture to the palladium particles, thus constraining the reaction to the dimensions of the nanotubes. Another possible method would be to simply place the array in a container with the reaction mixture.

4.6 Conclusions

The goal of the work presented in this chapter was to develop a method that could produce carbon nanotubes that had been modified by bipolar electrochemistry.

Using bipolar electrochemistry (a non-contact method) various metals, a semi-conductor and a polymer were deposited onto the tips of isolated carbon nanotubes. Double deposition experiments, using gold and palladium or pyrrole, successfully modified both tips of isolated carbon nanotubes. Bipolar electrodeposition was demonstrated on carbon nanotubes from either a commercial source or from CVD nanotubes, which were successfully grown in house using the CVD method. The system developed can be used to demonstrate the deposition of electropolymers, metals and semiconductors onto the tips of carbon nanotubes.

An area that will need to be pursued is the functionalization of single-walled nanotubes by bipolar electrodeposition. Single-walled carbon nanotubes exhibit a wide range of unique electrical and physical properties, the direct coupling of nanocrystals on the tips of single-walled nanotubes is sure to produce a variety of unique nanostructures.

One aspect to note about bipolar electrochemistry is it can be applied to any conductive structure, thus any metal, polymer or possibly semi-conductors in a variety of forms besides nanotubes can be functionalized via bipolar electrodeposition. Thus another possible path for future work would be to synthesize and fully characterize bipolar functionalized nanostructures other than carbon.

The non-contact method offers a new level of control in functionalizing carbon nanotubes, and other conductive nanostructures. The direct and controlled deposition of material onto the tips of carbon nanotubes produces unique nanotube-metal, nanotube-semiconductor, or nanotube-polymer nanostructures. Elucidating the properties of these unique nanostructures will help determine potential applications and can form the basis for future work. Other future work could include the deposition of ferromagnetic materials on the tips of the nanotubes, and the separation of the functionalized nanotubes from non-functionalized nanotubes using a powerful magnet. The bulk synthesis of functionalized nanotubes is an area that merits future study.

A good source of bipolar functionalized nanotubes would allow for the construction of potential nanoscale devices such as opto-electronic devices, biosensors, or biocompatible autonomous agents. Examples of such devices include; CdS capped nanotubes that are incorporated into polymer based photovoltaic devices to help increase quantum efficiency, arrays of nanotubes with tin oxide for use as gas sensors with exceptional sensitivity, or polymer capped nanotubes with the relevant bio-markers for drug delivery. In general a nanotube with two different functionalities, on opposite ends, is a device within itself. The challenge will be how to incorporate or functionalize such a device so that it can interact with the macro-scaled world.

References

1. Dai, L.; Mau, A. W. H. Controlled Synthesis and Modification of Carbon Nanotubes and C60: Carbon Nanostructures for Advanced Polymeric Composite Materials. *Adv. Mater.* **2001,** *13,* 899-915.

2. Rao, C. N. R.; Satishkumar, B. C.; Govindaraj, A.; Nath, M. Nanotubes. *ChemPhysChem* **2001,** *2,* 78-105.

3. Thostenson, E. T.; Renb, Z.; Choua, T.-W. Advances in the science and technology of carbon nanotubes and their composites: a review. *Composites Science and Technology*, **2001,** *61,* 1899-1912.

4. Merkulov, V. I.; Lowndes, D. H.; Wei, Y. Y.; Eres, G. Patterned Growth of Individual and Multiple Vertically Aligned Carbon Nanofibers. *Appl. Phys. Lett.* **2000,** *76,* 3555-3557.

5. Hirsch, A. Functionalization of Single-Walled Carbon Nanotubes. *Angew. Chem. Int. Ed*. **2002,** *41,* 1853-1859.

6. Baughman, R. H.; Zakhidov, A. A.; De Heer, W. A. Carbon Nanotubes—the Route Toward Applications. *Science* **2002,** *297,* 787-792.

7. Dai, H. Carbon Nanotubes: Synthesis, Integration, and Properties. *Acc. Chem. Res.* **2002,** *35,* 1035-1044.

8. Lau, K.-T.; Hui, D. The Revolutionary Creation of New Advanced Materials-Carbon Nanotube Composites. *Composites: Part B* **2002,** *33,* 263-277.

9. Meyyappan, M.; Delzeit, L.; Cassell, A.; Hash, D. Carbon Nanotube Growth by PECVD: A Review. *Plasma Sources Sci. Technol.* **2003,** *12,* 205-216.

10. Dai, L.; Patil, A.; Gong, X.; Guo, Z.; Liu,L.; Yong, L.; Zhu, D. Aligned Nanotubes. *ChemPhysChem* **2003,** *4,* 1150-1169.

11. Iijima, S. Carbon Nanotubes: Past, Present, and Future. *Physica B.* **2002,** *323,* 1-5.

12. Journet, C.; Maser, W. K.; Bernier, P.; Loiseau, A.; Chapelle, M. L.; Lefrant, S.; Deniard, P.; Lee, R.; Fischer, J. E. Large Scale Production of Single Wall Carbon Nanotubes by the Electric Arc Technique . *Nature* **1997,** *388,* 756-758.

13. Ajayan, P. M.; Ebbesen, T. W. Nanometre-size Tubes of Carbon. *Rep. Prog. Phys.* **1997,** *60,* 1025-1062.

14. Yua, J.; Lucasa, J.; Strezovb, V.; Wall, T. Coal and Carbon Nanotube Production. *Fuel* **2003,** *82,* 2025-2032.

15. Maser, W, K.; Benito, A, M.; Martınez, M, T. Production of Carbon Nanotubes: The Light Approach. *Carbon* **2002,** *40,* 1685-1695.

16. Zhou, O.; Shimoda, H.; Gao, B.; Oh, S.; Fleming, L.; Yue, Y. Materials Science of Carbon Nanotubes: Fabrication, Integration, and Properties of Macroscopic Structures of Carbon Nanotubes. *Acc. Chem. Res.* **2002,** *35,* 1045-1053.

17. Kyotani, T.; Tsai, L-f.; Tomita, A. Preparation of Ultrafine Carbon Tubes in Nanochannels of an Anodic Aluminum Oxide Film. *Chem. Mater.* **1996,** *8,* 2109-2113.

18. Che, G.; Miller, S. A.; Fisher, E. R.; Martin, C. R. An Electrochemically Driven Actuator Based on a Nanostructured Carbon Material. *Anal. Chem.* **1999;** *71,* 3187-3191.

19. Tsai, S.H.; Chiang, F.K.; Tsai, T.G.; Shieu, F.S.; Shih, H.C. Synthesis and Characterization of the Aligned Hydrogenated Amorphous Carbon Nanotubes by Electron Cyclotron Resonance Excitation. *Thin Solid Films* **2000,** *366,* 11-15.

20. Sui, Y. C.; Acosta, D. R.; Saniger, J. M.; González-León, J. A.; Bermudez, A.; Feuchtwanger, J.; Cui, B. Z.; Flores, J. O.; Saniger, J. M. Structure, Thermal Stability, and Deformation of Multibranched Carbon Nanotubes Synthesized by CVD in the AAO Template, *J. Phys. Chem. B* **2001,** *105,* 1523-1527.

21. Pradhan, B. K.; Toba, T.; Kyotani, T.; Tomita, A. Inclusion of Crystalline Iron Oxide Nanoparticles in Uniform Carbon Nanotubes Prepared by a Template Carbonization Method. *Chem. Mater.* **1998,** *10,* 2510-2515.

22. Rajesh, B.; Thampi, K.; Bonard, J.-M.; Viswanathan, B. Preparation of a Pt-Ru Bimetallic System Supported on Carbon Nanotubes. *J. Mater. Chem.* **2000,** *10,* 1757-1759.

23. Whatman Company Website. http://www.whatman.com (accessed Jan 2004).

24. Xiao, Z. L.; Han, C. Y.; Welp, U.; Wang, H. H.; Kwok, W. K.; Willing, G. A.; Hiller, J. M.; Cook, R. E.; Miller, D. J.; Crabtree, G. W. Fabrication of Alumina Nanotubes and Nanowires by Etching Porous Alumina Membranes. *Nano Lett*. **2002;** *2;* 1293-1297.

25. Vajtai, R.; QWei, B.; Zhang, Z. J.; Jung, Y.; Ramanath, G.; Ajayan, P. M. Building Carbon Nanotubes and their Smart Architectures. *Smart Mater. Struct.* **2002,** *11,* 691-698.

26. Tsukagoshia, K.; Yoneyaa, N.; Uryua, S.; Aoyagia, Y.; Kandad, A.; Ootukad, Y.; Alphenaarf, B.W. Carbon Nanotube Devices for Nanoelectronics. *Physica B* **2002,** *323,* 107-114.

27. Avouris, P. Carbon Nanotube Electronics. *Chem. Phys.* **2002,** *281,* 429-445.

28. Franklin, N. R.; Wang, Q.; Tombler, T. W.; Javey, A.; Moonsub, S.; Dai, H. Integration of Suspended Carbon Nanotube Arrays into Electronic Devices and Electromechanical Systems. *Appl. Phys. Lett.* **2002,** *81,* 913-915.

29. Radosavljevic, M.; Freitag, M.; Thadani, K. V.; Johnson, A. T. Nonvolatile Molecular Memory Elements Based on Ambipolar Nanotube Field Effect Transistors. *Nano Lett.* **2002,** *2,* 761-764.

30. Dai, L. Light-Emmiting Polymers and carbon Nanotube Electron Emitters for Optoelectronic Displays. *Smart Mater. Struct.* **2002,** *11,* 645-651.

31. Colbert, D. T. Single-Wall nanotubes: A New Option for Conductive Plastics and Engineering Polymers. *Plastics Additives and Compounding* **2003,** *5,* 18-25.

32. Banerjee, S.; Kahn, M. G. C.; Wong, S. S. Rational Chemical Strategies for Carbon Nanotube Functionalization. *Chem. Eur. J.* **2003,** *9,* 1898-1908.

33. Niyogi, S.; Hamon, M. A.; Hu, H.; Zhao, B.; Bhowmik, P.; Sen, R.; Itkis, M. E.; Haddon, R. C. Chemistry of Single-Walled Carbon Nanotubes. *Acc. Chem. Res.* **2002,** *35,* 1105-1113.

34. Ravindran, S.; Chaudhary, S.; Colburn, B.; Ozkan, M.; Ozkan, C. S. Covalent Coupling of Quantum Dots to Multiwalled Carbon Nanotubes for Electronic Device Applications. *Nano Lett.* **2003,** *3,* 447-453.

35. Khabashesku, V. N.; Billups, W. E.; Margrave, J. L. Fluorination of Single-Wall Carbon Nanotubes and Subsequent Derivatization Reactions. *Acc. Chem. Res.* **2002,** *35,* 1087-1095.

36. Banerjee, S.; Kahn, M. G. C.; Wong, S. S. Rational Chemical Strategies for Carbon Nanotube Functionalization. *Chem. Eur. J.* **2003,** *9,* 1898-1908.

37. Tasis, D.; Tagmatarchis, N.; Georgakilas, V.; Prato, M. Soluble Carbon Nanotubes. *Chem. Eur. J.* **2003,** 9, 4000-4008.

38. Downs, C.; Nugent, J.; Ajayan, P. M.; Duquette, D. J.; Santhanam, K. S. V. Efficient Polymerization of Aniline at Carbon Nanotube Electrodes. *Adv. Mater.* **1999,** *11,* 1028-1031.

39. Kooi, S. E.; Schlecht, U.; Burghard, M.; Kern, K. Electrochemical Modification of Single Carbon nanotubes. *Angew. Chem. Int. Ed.* **2002,** *41,* 1353-1355.

40. Gao, M.; Huang, S.; Dai, L.; Wallace, G.; Gao, R.; Wang, Z. Aligned Coaxial Nanowires of Carbon Nanotubes Sheathed with Conducting Polymers. *Angew. Chem. Int. Ed.* **2000,** *39,* 3664-3667.

41. Chen, J. H.; Huang, H. P.; Wang, D. Z.; Wang, S. X.; Li, W. Z.; Wen, J. G.; Ren, Z. F. Electrochemical Synthesis of Polypyrrole Films Over Each of Well-Aligned Carbon Nanotubes. *Synth. Met.* **2002,** *125,* 289-294.

42. Hughes, M.; Shaffer, M.S.P.; Renouf, A.C.; Singh, C.; Chen, G.Z.; Fray, D.J.; Windle, A.H. Electrochemical Capacitance of Nanocomposite Films Formed by Coating Aligned Arrays of Carbon Nanotubes with Polypyrrole. *Adv. Mater.* **2002,** *14,* 382-385.

43. Dunsch, L.; Janda, P.; Mukhopadhyay, K; Shinohara, H. Electrochemical Metal Deposition on Carbon Nanotubes. *New Diamond Front. Carbon Technol.* **2001,** *11,* 427-434.

44. Austin, D. W.; Puretzky, A. A.; Geohegan, D. B.; Britt, P. F.; Guillorn, M. A.; Simpson, M. L. The Electrodeposition of Metal at Metal/Carbon Nanotube Junctions. *Chem. Phys. Lett.* **2002,** *361,* 525-529.

45. Chen, X. H.; Peng, J. C.; Li, X. Q.; Deng, F. M.; Wang, J. X.; Li, W. Z. Tribological Behavior of Carbon Nanotubes—Reinforced Nickel Matrix Composite Coatings, *J. Mater. Sci. Lett.* **2001,** *20,* 2057–2060.

46. Diao, P.; Liu, Z.; Wu, B.; Nan, X.; Zhang, J.; Wei, Z. Chemically Assembled Single-Wall Carbon Nanotubes and their Electrochemistry, *ChemPhysChem* **2002,** *3,* 898-901.

47. Bradley, J.-C.; Chen, H.-M.; Crawford, J.; Eckert, J; Ernazarova, K.; Kurzeja, T.; Lin, M.; McGee, M.; Nadler, W.; Stephens, S.G. Creating Electrical Contacts between Metal Particles using Directed Electrochemical Growth. *Nature* **1997,** *389,* 268-271.

48. Devers, T.; Kante, I.; Allam, L.; Fleury, V. Preparation of Dendritic Tin Nanoaggregates by Electrodeposition, *J. Non-Cryst. Solids* **2003,** *321,* 73-80.

49. Martins, M. E.; Castellano, C.; Calandra, A. J.; Arvia, A. J. The Electrochemistry of Gold in Acetonitrile Solutions Containing Thiocyanate Ions. *J. Electroanal. Chem. Interfacial Electrochem.* **1977,** *81,* 291-300.

50. Ammann, E.; Mandler, D. Local Deposition of Gold on Silicon by the Scanning Electrochemical Microscope. *J. Electrochem. Soc.* **2001,** *148,* C533-C539.

51. CRC Handbook of Chemistry and Physics 84th Edition 2003 – 2004. http://www.hbcpnetbase.com/ (Accessed Dec 2003).

52. Haremza, J, M.; Hahn, M, A.; Krauss, T, D.; Chen, S.; Calcines, J. Attachment of Single CdSe Nanocrystals to Individual Single-Walled Carbon Nanotubes. *Nano Lett.* **2002,** *2,* 1253-1258.

53. Kim, H.; Sigmund, W. Zinc Sulfide Nanocrystals on Carbon Nanotubes. *J. Cryst. Growth* **2003,** *255,* 114-118.

54. Banerjee, S.; Wong, S, S. In Situ Quantum Dot Growth on Multiwalled Carbon Nanotubes. *J. Am. Chem. Soc.* **2003,** *125,* 10342-10350.

55. Xu, D.; Xu, Y.; Chen, D.; Guo, G.; Gui, L.; Tang, Y. Preparation and Characterization of CdS Nanowire Arrays by DC Electrodeposit in Porous Aluminum Oxide Templates, *Chem Phys Lett.* **2000,** *.325,* 340-344.

56. Fujii, M.; Saeki, Y.; Arii, K.; Yoshino, K. Fractal Structure of Electrochemically Polymerized Polypyrrole and Growth Process as Function of Monomer Concentration, Electrolyte Concentration and Applied Voltage. *Jpn. J. Appl. Phys., Part 1* **1990,** *29,* 2501-2505.

57. Gogotsi, Y.; Libera, J.A.; Guvenc-Yazicioglu, A.; Megaridis, C.M. In Situ Multiphase Fluid Experiments in Hydrothermal Carbon Nanotubes. *Appl. Phys. Lett.* **2001,** *79,* 1021-1023.

Appendix 1: SMIRP

A1.1 Summary Statement

A basic description on what SMIRP is and how SMIRP works will be described. The actual programming of SMIRP was done by various other people. Thus this chapter will present SMIRP from the perspective of a user.

A1.2 Introduction to SMIRP:

Standard Modular Integrated Research Protocols (SMIRP)[1] is a web based system that incorporates the order and structure found in a computer database system, and incorporates the flexibility of a traditional paper based filing system. Unlike conventional database systems, SMIRP is a highly flexible, extremely adaptable, and a continually evolving system. SMIRP has been used as a laboratory management tool, and a research aid in the Bradley research group[2]. SMIRP has also been used as an interactive teaching aid and tool in various courses at Drexel University[3].

Within SMIRP there exists a primary structure called a SMIRP-space. The SMIRP-space consists of several secondary structures called Modules. Within each Module there is a tertiary structure called a record.

There are several primary structures i.e. there are a number of SMIRP-spaces (Figure A1.1). Each SMIRP-space can run independently, or one or more spaces can interact. When a user logs into SMIRP they are greeted with a screen displaying the SMIRP-spaces they have access to. A user cannot see and thus cannot access spaces they are not assigned too. If an outside group is interested in using SMIRP they can be assigned thier

own SMIRP-space and can organize it in whatever manner suits their group without fear of having other SMIRP users corrupting their space. The closest real world analogue of a SMIRP-space would be filling cabinet.

Once inside a SMIRP-space, navigation between modules is accomplished via a drop down menu (Figure A1.1). The modules are the part of SMIRP that gives it order and flexibility at the same time. For example, two modules of recent interest are the modules that describe experiments to synthesize carbon nanotube by the CVD method, and the second is how to modify the tips of carbon nanotubes by bipolar electrochemistry. These two modules contain descriptive experimental procedures that would allow a member of the group to repeat the experiments. Thus, the information is stored in these particular modules and can be accessed at any time. A modules closest real world analogue is the folders contained within a filling cabinet. Each module can be organized according to the module designer's preference.

Within a module, different events are stored as a record (Figure A1.1). Navigation through different records can be done using a drop down menu or a pop-up menu if there are more than 100 records. An event in this case would be an experiment carried out using the procedures outlined in the module. For example the modification of carbon nanotubes using bipolar electrochemistry utilized various metals. Each experiment that used a metal such as zinc or cadmium would be stored as a separate record. The information stored and presented in a record is organized in parameters. A parameter can store information and present information as text, as various office files, image files, or video files. Parameters in a record correspond to parameters in an experiment.

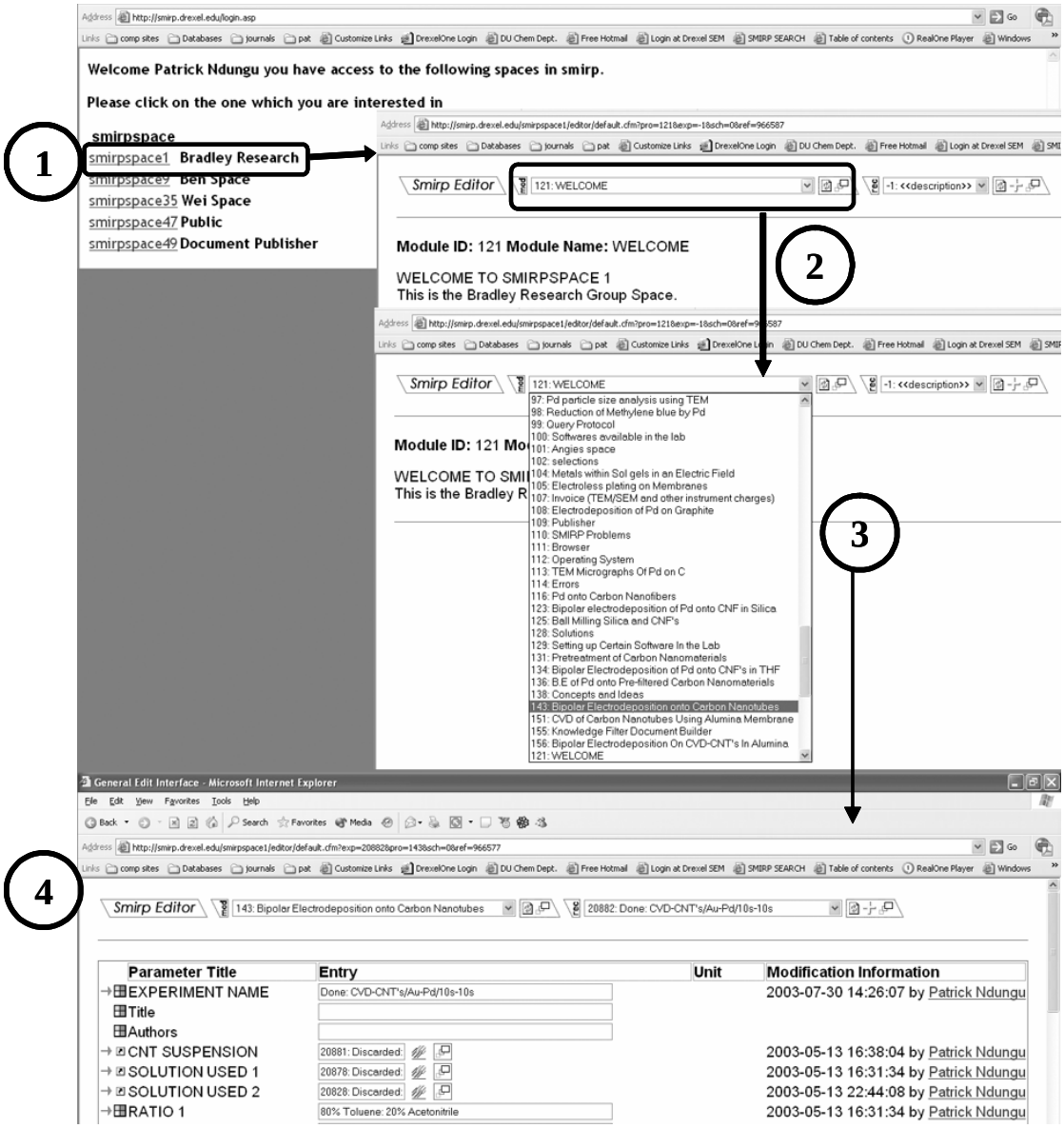

Figure A1.1. Navigation within SMIRP. (1) Is a partial image of the screen that displays the SMIRP spaces a user has access too. (2) By clicking on "smirpspace 1" on (1) the user is directed to a module, in this example the module has been set as "121: WELCOME". The module that greets a user can be set to be any module and does not necessarily have to be a welcome module. (3) Shows the drop down menu used to navigate between different modules. (4) Is a partial screen shot of a record within a module.

Any part of the experiment that the module designer deems necessary can be incorporated into the module and stored in any form in a parameter.

A1.3 SMIRP is More Than a Filing System

The simple description of a SMIRP-space representing a filling cabinet, the module the folders, and the records the actual papers is crude at best and does not begin to highlight the capabilities of SMIRP. This simplified description does offer a familiar reference point for a first time user but does not highlight SMIRP's many advantages. The first major advantage about SMIRP is that it is a web-based application. A web-based application means it can be accessed from anywhere in the world with an internet connection, and it requires minimal training to use. The next advantage is that linking between modules can be established. For example, there is a module called solutions. The solutions module contains records of the various solutions that have been prepared for use in various experiments. Whenever a new module is designed, and the protocol requires a solution, a parameter that links to any record created in the solutions module can be added to the new module. Thus, in the module that describes bipolar electrodeposition onto carbon nanotubes there is a parameter that is an actual link to the solutions module, and if the link is activated it will navigate to the solutions module (Figure A1.2). This eliminates the need to keep adding common parameters to every new module that is created. The linking can go beyond modules. In various modules there exist links to web sites. A good example can be found in the orders module. The orders module is used to keep track of what has been ordered for the lab.

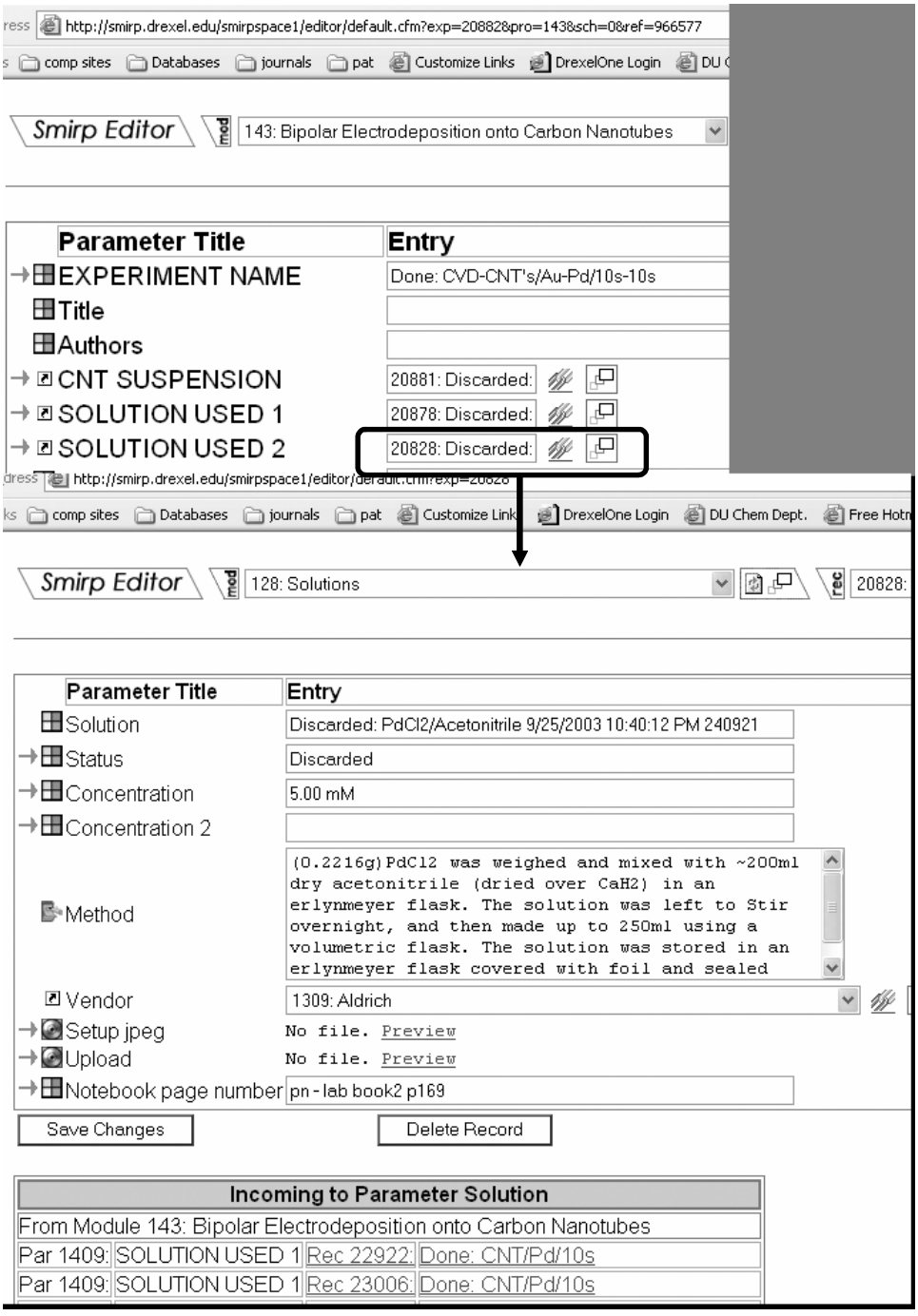

Figure A1.2. The activation of a link navigates the user to the relevant module. In this example the parameter labeled "SOLUTION USED 2" is a link that will navigate the user to a specific record in the module titled "128: Solutions". The record has a table labeled "Incoming to Parameter Solution" were all links from other records that are linked to this record are presented. This provides a way to determine what the solution was used for.

It has been useful to have a link to the manufacturer's website. This outside linking has made it possible to link different SMIRP space records.

Modules can be added anytime to a SMIRP-space, and parameters within the modules can be ordered in any manner the designer finds useful. Parameters can be added at anytime by a module designer, thus if a parameter in the protocol seemed to be unimportant at one point, it can be added later on and tracked. This does highlight one advantage of the SMIRP system, which is, the data is always live and accessible. As soon as a new record is created one can begin a cursory examination of the data

To go beyond looking at one record at a time in SMIRP, there is another feature known as the table view functionality. Table view displays all the records in a module as one page. The table view can be configured to include all parameters or exclude certain parameters. In table view all data is displayed, including pictures and text data. The only data not viewed in table view are any zip files that have been uploaded and the module description.

A1.4 SMIRP Can Do More than Data Storage

Besides the storage of data, SMIRP has various features that go beyond simple data storage. The first of interest is the alert system which provides a way to obtain information without actually looking for the information. The alerts keep track of new records or new activity in SMIRP. An alert can be set up that will send an e-mail with a summary of a record from a module of interest and a link to the record. The alert system in SMIRP is highly versatile and can be customized to the needs of the individual. An alert can be set up to e-mail an individual when a specific user works in SMIRP, or it can

e-mail an individual when any module is modified. The alerts can be set to check for the activity of interest every hour, day or week. An example where this has been useful is in obtaining literature. When an article cannot be obtained on-line, a request for the article can be made in a module called article requests. An alert can then be set up to send an e-mail when the link to the pdf version of the article is added to SMIRP.

Searching within SMIRP can be done using keyword searches. Searching can also be done by looking at the SMIRP logs. Logs are simply SMIRP recording all activity within SMIRP, this includes a user logging in, updating records, or adding new records. Logs can be downloaded as an excel file, or using the SMIRP excel tool. The SMIRP excel tool can be used to download modules as well as logs.

SMIRP bots are autonomous agents that carry out various functions in SMIRP. The alert system is an example of a SMIRP bot. The bots run automatically or manually depending on the function. An example of the work done by a bot is key word searching. The key word searching bot would take a string of text entered in SMIRP and use it to do a google search. This does return hits with links to websites of research groups using similar methods for totally different research.

A)

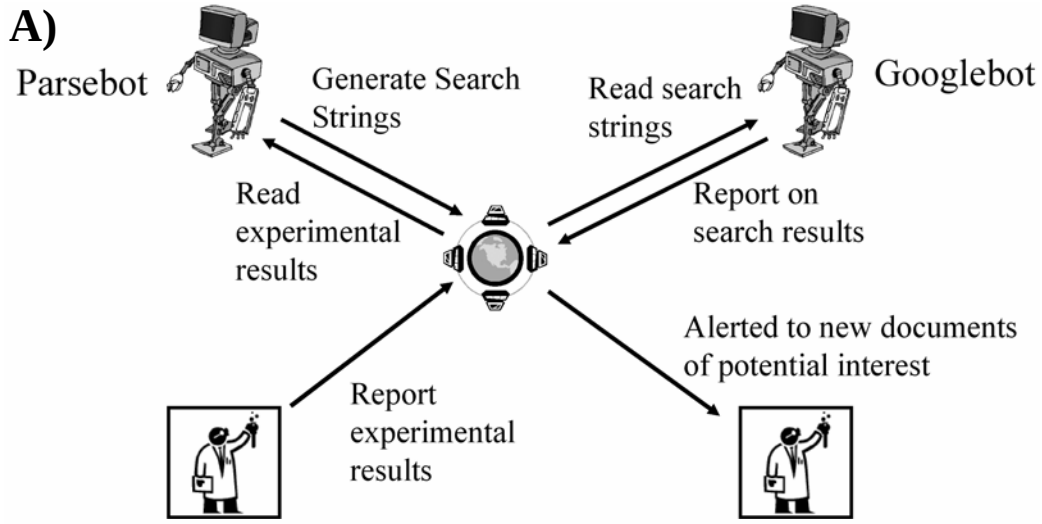

B)

Alert Name	new pdfs	**smirpspace**	smirpspace1	**Module ID**	15		
First name	Patrick	**Last name**	Ndungu	**Username**	patrick		
Include	None	**Exclude**	None				
Filter by users	None						

Date and time	First Name	Last name	Module ID	Module Name	Record ID	Record Name	Parameter Name	Parameter Value
1/22/2004 5:29:38 PM	Eric	Moore	15	Article Archive	33338	Carbon nanofiber-copper composite powder prepared by electrodeposition	article pdf format	smirpspace1_376042.pdf

C)

Module ID	Module Name	Record ID	Record Name	Parameter Name	Parameter Type	Parameter Value
15	find reference	1738	Application of Carbon Nanotubes as Supports in Heterogenous Catalysis	article title	name	Application of Carbon Nanotubes as Supports in Heterogenous Catalysis
15	find reference	2807	Direct fabrication of carbon nanotube circuits by selective area chemical vapour deposition on pre-patterned structures	article title	name	Direct fabrication of carbon nanotube circuits by selective area chemical vapour deposition on pre-patterned structures
27	Knowledge Filter	3795	Nanotubes/preparation/purification	knowledge filter	name	Nanotubes/preparation/purification
64	Orders	3683	Carbon NanoTubes (BUCKYUSA)	Order	name	Carbon NanoTubes (BUCKYUSA)
64	Orders	3685	Carbon NanoTubes (Hyperion)	Order	name	Carbon NanoTubes (Hyperion)
67	Protocol Prototyping	3792	Deposition of Ag onto Carbon Nanotubes	Protocol Prototype Title	name	Deposition of Ag onto Carbon Nanotubes
67	Protocol Prototyping	3840	Nanotubes(RU) -SEM analysis	Protocol Prototype Title	name	Nanotubes(RU) -SEM analysis
86	Project manager	2726	Paper14 Bipolar Electrodeposition on nanotubes	Project name	name	Paper14 Bipolar Electrodeposition on nanotubes

Figure A1.3. Summary of how SMIRP bots function, and examples of an e-mail alert and a key word search. In (A) the parse bot creates a search string from the experimental write up generated by a user. The google bot uses the search string in google and returns a link to the number of hits found with the search string used. (B) Shows an example of an e-mail alert sent when a new entry with a link to the pdf was uploaded in SMIRP. (C) Demonstrates how using the key word 'nanotubes' returns all records in the different modules with the word nanotubes.

A1.5 SMIRP as a Research Management tool

Within SMIRP various modules have been developed to store numerous experiments. Before implementing a set protocol to conduct experiments and finalizing the protocol as a module, the protocol undergoes various adjustments. A Module, called protocol prototyping, was designed to handle such experimentation. This module is the most flexible and dynamic module in SMIRP. Its development has taken years and there is little doubt it will continue to develop as time goes by. The Module began with simple parameters that could store text information, Microsoft office files and media files. The text parameters can be stored in two forms a short text data box, and a long data box. The short data box is designed to hold no more than a sentence. The long data box is unlimited. This simple arrangement allowed a user to type in a unique name to identify the record, an experimental description, a results description, upload any results, and a short conclusion.

Links to various modules were added as the need arose, and a link to records in the same module was later added. This module is used when various ideas are tested out and, if successful, refined to form an independent module. It is possible to trace the development of a module from protocol prototyping to a fully developed module.

As a research management tool the simplest example is the creation of a unique record id number that can be used as a number to store various samples. Samples can be stored in numerical order. With no need to question or refer to other lab personnel lab notebook, samples can be taken and used for the next phase of experiments.

One aspect of research work in the Bradley research lab has been how to manage undergraduate students interested in doing laboratory work. Generally the first step involves instructing a student to read the module description. Next the student is given one on one instruction on the experimental procedure. After these initial meetings the student is asked to complete at least one experiment in a week. Once this initial shake down period is over, the student is asked to complete a higher number of experiments per week. A module that has been extremely useful in maintaining a consistent work output is productivity tracking. Every week, after a meeting, the student enters a new record in this module with a description of what they believe they need to do for the next week. The new record can then be checked to see if the student's goals are in line with what was discussed in the meeting. The new record is e-mailed by an alert, thus avoiding the need to search for the information. If any changes need to be made to what the student has entered they can be notified before any unnecessary work is done. Ideally the student would have an alert telling them if such changes have been made, however experience has shown e-mailing the student directly is more effective. This module has and does ensure a consistent amount of work is done each week as well as helps to manage the work done.

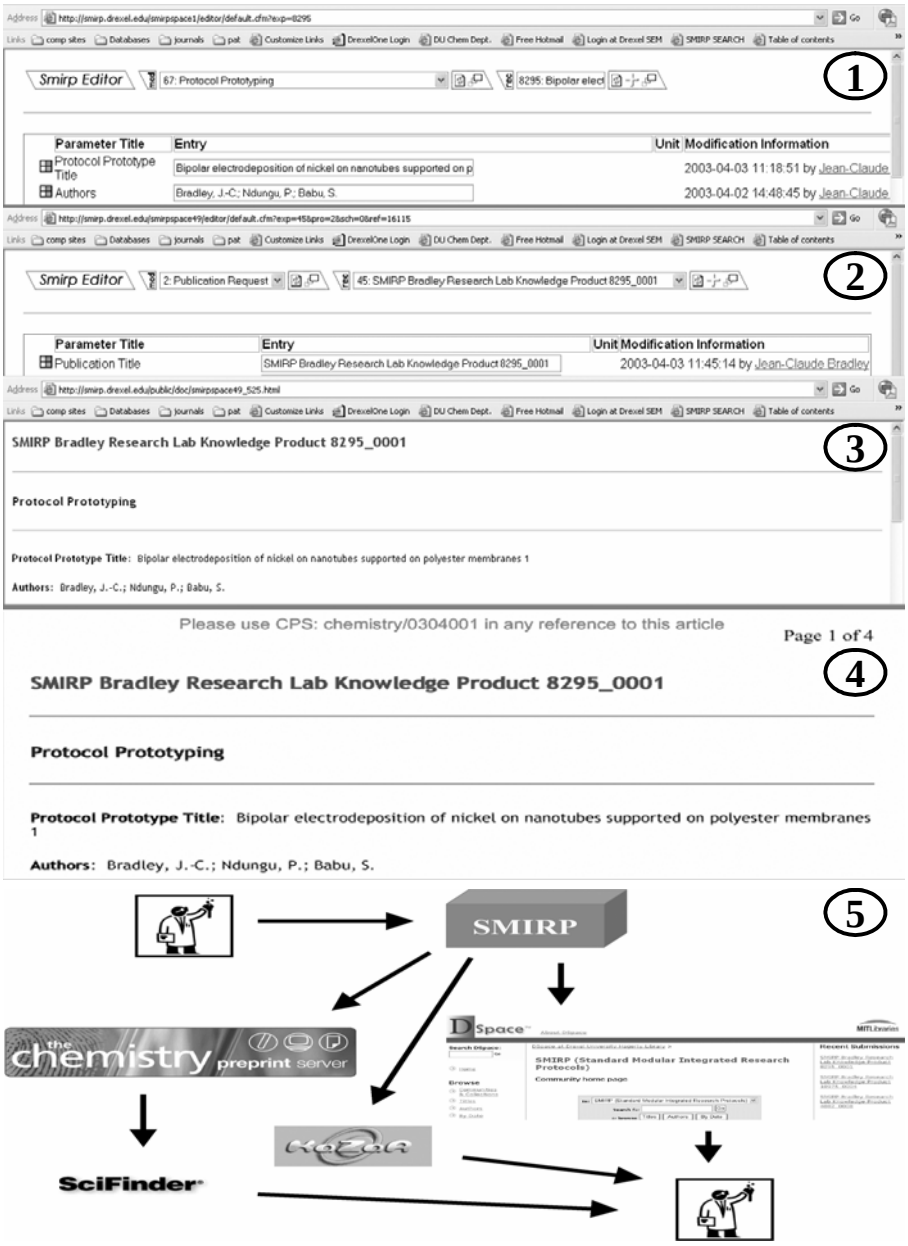

Figure A1.4. Quick document production and dissemination using SMIRP. (1) A suitable record is identified and the relevant information is updated and formatted if needed. (2) Pertinent parts of the record are transferred to a new record in a different SMIRP space. (3) The collected information is converted into an HTML document, which is then presented on a web page maintained on the SMIRP server. (4) The HTML document is converted to a pdf document, which is then submitted to the Chemweb pre-print server. (5) The finished document is abstracted by CAS; it is searchable on the World Wide Web, and on other mediums such as D-space and kazaa.

A1.6 Document Production in SMIRP

There are two ways used to produce documents for publication in SMIRP. The first method used developed a specific module, called document production, which collected text, figures and references. The main advantage with the module is that it allows direct linking to the references; however, links from the figures to the original records in which the figures were constructed from were not added. The second way to produce documents, illustrated in Figure A1.4, is by using specific records to make a pre-print. The module that contains the record of interest is modified by adding the relevant parameters necessary for a pre-print. These parameters are text boxes for an author list, an abstract, introduction, experimental description, results, discussion and conclusion as well as links to references and funding sources. This second method uses a separate SMIRP space and SMIRP bots (run manually) to create an HTML file of the record of interest. The HTML file is converted to an Adobe Acrobat file and once it has been scrutinized by the various authors, it is submitted to the Chemweb pre-print server. The Chemweb pre-print server is a free online service run by Elsevier for chemistry related articles. Articles are editorially reviewed before being published on-line and the principal author retains copyright. The advantages with this service are that it allows for large exposure in the shortest time possible, and a rough estimate of the amount of interest an article generates can be gauged.

A1.7 Personal Work Patterns in SMIRP

SMIRP keeps a record of all activity, such as when a person logs in to SMIRP, when a person modifies a record in SMIRP or if a person adds a new record in SMIRP. This abundance of information can be downloaded and graphed.

Using the SMIRP excel tool (which is Microsoft's' Excel program with a series of macros written specifically to interact with SMIRP) all new records entered by Patrick Ndungu for the years 1999 – 2003 were downloaded. Typically, a record has more than one parameter and when it is created or updated each parameter is counted as a new entry. For example if a record has 20 parameters, then when it is created SMIRP counts this as 20 new entries. If the same record is updated the next day and only 5 of the 20 parameters are updated, SMIRP counts these as 5 new entries. In order to graph the information, if such a new record was created it was counted as one new entry. If the record was updated the next day it was counted as one new entry. Updating a module a day later or days later is mainly due to limited access to specialized equipment such as a scanning electron microscope. Such specialized instrumentation can only be used days after the experiment is done, and the results from using such equipment are inevitably updated days later. The end result is the new entries are based on what was entered per day.

The obvious trends seen in a graph that shows all of Patrick's five years (Figure A1.5) are the blanks corresponding to breaks in the Drexel schedule, most notably in December. The large amounts of breaks in 1999 and 2000 (fewer than 1999) are due to the usual problems a graduate student encounters when trying to juggle teaching duties, classes and research.

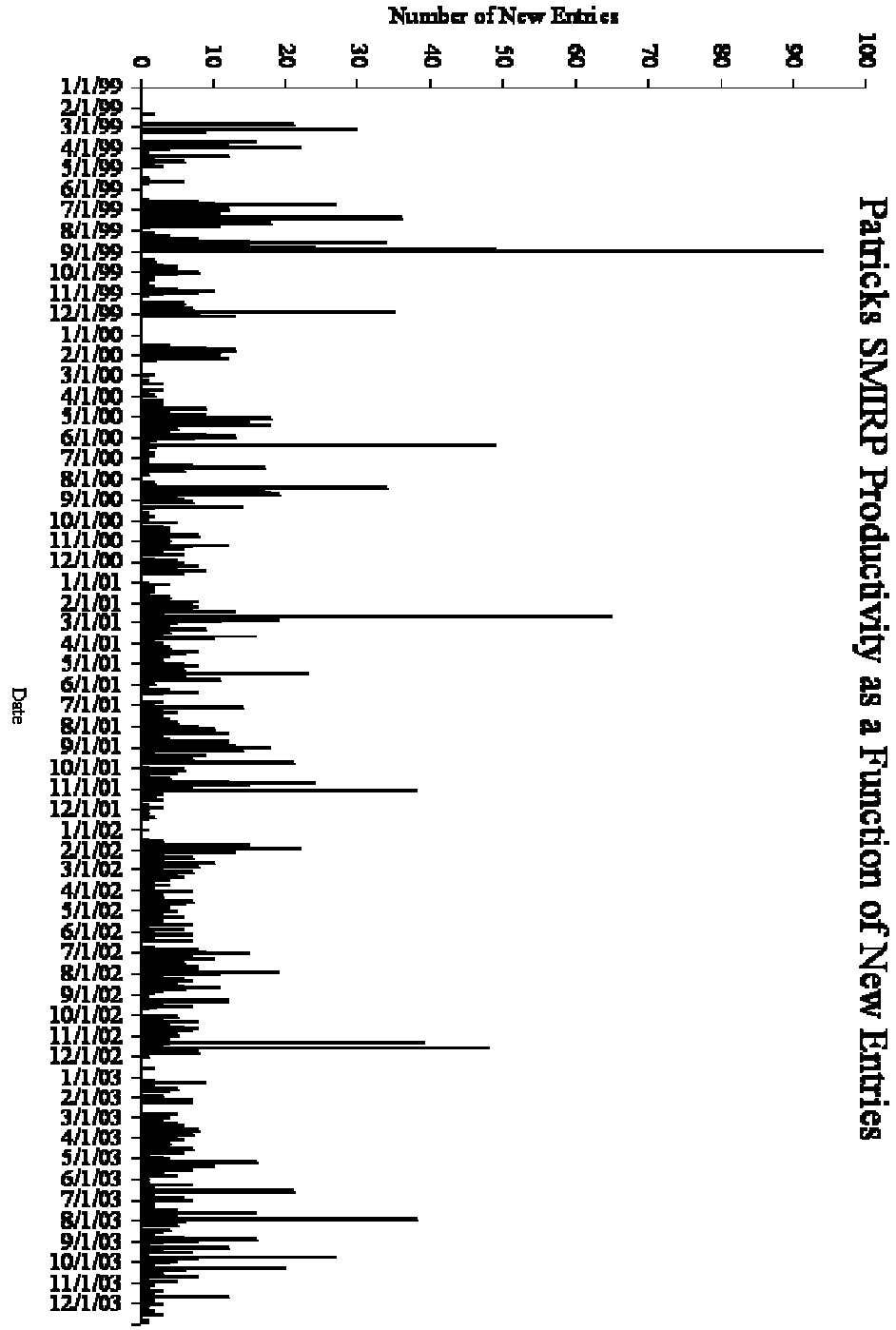

Figure A1.5. Graph showing Patrick's activity measured as the number of new entries in SMIRP.

From the graph, the work trends follow a general increase right after the Christmas break which reaches a peak, and then drops off and finally the cycle starts again every 4–6 months. This is unexpected because Drexel follows a quarter system thus peaks would be expected between breaks when a graduate student has only to worry about research.

Figure A1.6 shows when the information is categorized into work done on actual experiments (corresponds to full working modules), literature-related work (mainly article archive, knowledge filters), lab management (e.g. productivity tracking, ordering material), other (modules that do not fit any category), and prototypes; a different pattern emerges. In any year, the majority of work is done on fully developed modules i.e. experiments. This is followed by literature-related work. Prototype work varies from year to year and does not necessarily seem to result in a greater amount of work in full modules i.e. experiments.

The amount of literature work done as a whole remains relatively constant from year to year. Lab management saw significant increases in 2001 and 2002. This is due to the influx of undergraduate students during the summer months of those years.

A1.8 SMIRP Pros and Cons

The ability to organize experimental data in a digital format is one significant advantage of working with SMIRP. This has been useful, especially in this lab since electron micrographs can be presented with the experimental parameters. I see this as "a quick and dirty poster" available twenty four hours a day. Flexibility inherent within SMIRP means that modules can be created as needed, modified as needed, and evolve with the researcher's needs. A good example is protocol prototyping.

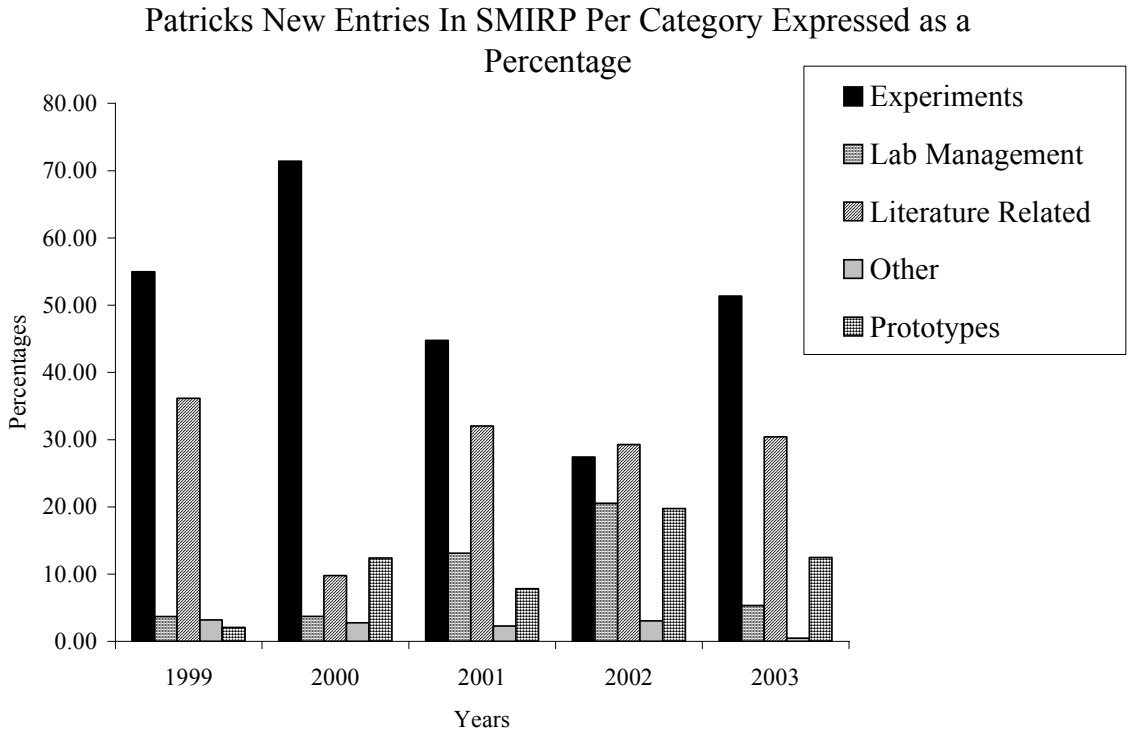

Figure A1.6. A column graph displaying new entries in SMIRP by Patrick; the data was first organized in to specific categories for each year, and then percentages were calculated.

SMIRP provides a way to organize and, if necessary, obtain literature references. References are available through a specific module (Article Archive), and through a separate module, articles containing information of interest can be linked in one record.

Data can be retrieved and examined with relative ease. Since all the information is already in a digital format, it can be easily downloaded and manipulated using conventional commercial software.

The main issue with SMIRP has been the need to enter the data after writing it down in a conventional lab notebook. But this only comes up when prototypes are done (need to give procedure and any results), otherwise for a full module this is not an issue. One point about the data entry issue that I immediately realized is that in today's modern world, the data eventually has to be digitized some way. Thus SMIRP actually provides a way to do half the work by providing a medium for a researcher to store experimental data in a digital format. With the SMIRP excel tool, the manipulation of data is extremely easy.

A1.9 Summary

SMIRP is a web based highly dynamic and interactive database system. From the point of view of a frequent user SMIRP has been an extremely useful way to maintain and organize literature references, digitization and presentation of data, and a way to increase productivity.

References

1. http://smirp.drexel.edu/

2. Bradley, J.-C.; Samuel, B. SMIRP-A Systems Approach to Laboratory Automation. *JALA*. **2000**, 5, 48-53.

3. Bradley, J.-C.; McEachron, D.; Dorsey, D.; Samuel, B.; Babu, S.; Boecker, J.; Haghkar, M.; Bhatt, J. The use of SMIRP for the rapid design and implementation of pedagogical constructs: Case study of a question-answer-reference framework. *Educational Technology & Society* **2003**, *6*, 74-82.

Vita

Patrick Gathura Ndungu was born on December 23rd 1975 in Nairobi Kenya. He attended Hillcrest preparatory school, and Hillcrest Secondary school, one of Kenya's premier and internationally renowned private schools. While attending Hillcrest Secondary school he represented the school as a member of the first 15 rugby squad two years in a row. In 1993 he completed his secondary school education.

In 1994 he began his undergraduate studies at the University of Tennessee at Martin, where he pursed dual bachelor's degrees in chemistry and biology. In 1998 he graduated cum laude.

Patrick Ndungu's graduate school education began in 1998 at the chemistry department in Drexel University. He joined Dr Jean-Claude Bradley's research group in the winter of 1999. During this time he has co-authored one paper, several pre-prints, and presented posters at various society meetings.